EXTINCTION OF NEAR INFRARED SOLAR RADIATION AS A MEANS FOR REMOTE DETERMINATION OF ATMOSPHERIC WATER VAPOR

by

Larry Willis Thomason

A Dissertation Submitted to the Faculty of the

DEPARTMENT OF ATMOSPHERIC SCIENCE

In Partial Fulfillment of the Requirements
For the Degree of

DOCTOR OF PHILOSOPHY

In the Graduate College

THE UNIVERSITY OF ARIZONA

1 9 8 5

8529410

Thomason, Larry Willis

EXTINCTION OF NEAR INFRARED SOLAR RADIATION AS A MEANS FOR REMOTE DETERMINATION OF ATMOSPHERIC WATER VAPOR

The University of Arizona PH.D. 1985

University
Microfilms
International 300 N. Zeeb Road, Ann Arbor, MI 48106

EXTINCTION OF NEAR INFRARED SOLAR RADIATION AS A MEANS FOR REMOTE DETERMINATION OF ATMOSPHERIC WATER VAPOR

by

Larry Willis Thomason

A Dissertation Submitted to the Faculty of the

DEPARTMENT OF ATMOSPHERIC SCIENCE

In Partial Fulfillment of the Requirements
For the Degree of

DOCTOR OF PHILOSOPHY

In the Graduate College

THE UNIVERSITY OF ARIZONA

1 9 8 5

THE UNIVERSITY OF ARIZONA
GRADUATE COLLEGE

As members of the Final Examination Committee, we certify that we have read

the dissertation prepared by Larry Willis Thomason

entitled Extinction of Near Infrared Solar Radiation as a Means for

Remote Determination of Atmospheric Water Vapor

and recommend that it be accepted as fulfilling the dissertation requirement

for the Degree of Doctor of Philosophy.

John A. Reagan — Oct. 3, 1985
Date

B. Roy Frieden — Oct. 3, 1985
Date

Benjamin M. Herman — Oct 3, 1985
Date

Lance J. ... — Oct. 3. 1985
Date

Date

Final approval and acceptance of this dissertation is contingent upon the candidate's submission of the final copy of the dissertation to the Graduate College.

I hereby certify that I have read this dissertation prepared under my direction and recommend that it be accepted as fulfilling the dissertation requirement.

Benjamin M. Herman — Oct 3, 1985
Dissertation Director — Date

STATEMENT BY AUTHOR

This dissertation has been submitted in partial fulfillment of requirements for an advanced degree at The University of Arizona and is deposited in the University Library to be made available to borrowers under rules of the Library.

Brief quotations from this dissertation are allowable without special permission, provided that accurate acknowledgment of source is made. Requests for permission for extended quotation from or reproduction of this manuscript in whole or in part may be granted by the head of the major department or the Dean of the Graduate College when in his or her judgment the proposed use of the material is in the interests of scholarship. In all other instances, however, permission must be obtained from the author.

SIGNED: Larry Thomason

ACKNOWLEDGMENTS

I wish to thank Dr. Ben Herman for his encouragement and guidance in conduct of the research leading to this dissertation. I also wish to thank Bill Chu of NASA-Langley for providing some of the data used in Chapter IV.

I especially wish to acknowledge the patience and support that my wife, Diane, has generously bestowed upon me over the last eight years.

This research was supported by a grant from NOAA under contract number NA80 RAD00065.

TABLE OF CONTENTS

LIST OF ILLUSTRATIONS

LIST OF ILLUSTRATIONS--Continued

LIST OF ILLUSTRATIONS--Continued

LIST OF ILLUSTRATIONS--Continued

LIST OF TABLES

ABSTRACT

A computationally efficient and accurate model is derived for the calculation of the atmospheric transmittance along inhomogeneous paths and within spectral bands dominated by molecular line absorption. It is a Stieltjes integration of transmission weighted by the frequency of occurrence of absorption coefficient within the band. Path inhomogeneitites are accounted for by assuming that the rank of absorption coefficient at any wavenumber is independent of temperature and pressure.

The technique is then applied to the ground based radiometric determination of precipitable water. It is found that the technique predicts the behavior of the $\rho\sigma\tau$ water vapor absorption band very well. An RMS disagreement of 11% is found when the model predictions are compared to radiosonde determinations of precipitable water.

The model is also applied to the determination of vertical water vapor distributions in the stratosphere given measured effective optical depths as a function of tangent height from a limb scanning satelitte. A new iterative reduction technique is introduced which incorporates the transmission model and it is shown to be both numerically stable and rapidly convergent. A comparison of the results with an independent reduction technique shows good overall agreement with a small systematic difference above 20km. The uncertainty in the

measurements, which yields solution uncertainties on the order of 30%, renders this systematic difference unimportant.

CHAPTER 1

INTRODUCTION

Trace gas constituents in the terrestrial atmosphere frequently assume a greater importance than their relative abundances would imply due to their role in one or more of the physical processes occuring within the atmosphere. The hydroxyl radical is of great importance in atmospheric chemical reactions yet has an abundance of only about 10^7 molecules/cm^{+3} (Heicklen, 1976, p. 293). Carbon dioxide with an abundance of little more than 300ppm is of great importance in radiative heat transport. But of all of the trace gases, it is water vapor that assumes the greatest importance because of the major role it plays in many of the physical processes in the atmosphere. Beyond it's obvious and extraordinary role in precipitation, water vapor also plays a significant role in atmospheric chemical processes (Heicklen, 1976, pp. 83-97), radiative heat transport (Rodgers and Walshaw, 1966) and latent heat transport (Chou and Atlas, 1982).

Because of water vapor's importance, it has long been considered critical to a complete description of the state of the atmosphere that the amount of water vapor to be specified. The in situ measurement of water vapor also known as hygrometry has a long history and may be traced to 1500 when Leonardo DaVinci experimented with a simple hygrometer. A complete discussion of the theory of hygrometry may be found in Spencer-Gregory and Rourke (1957) including a discussion of most of the common instruments in use today.

One of the major difficulties with in situ measurements is that water vapor is not well mixed in the atmosphere and may vary rapidly both horizontally and vertically. Radiosondes may be used to determine the vertical distribution of water vapor above a release site and with data from a network of such sites, it is possible to derive an approximate three-dimensional distribution of water vapor, but the density of the launch sites and frequency of the releases are limited by cost considerations. Furthermore, such launch sites are virtually nonexistant over vast oceanic areas covering about three quarters of the globe. Water vapor amounts as determined by radiosondes have a reasonable degree of reliability over the bulk of the troposphere. At higher altitudes, however, where the water vapor density is low, the reliability of the simple hygrometer used in the radiosonde decreases significantly and above the tropopause usually no useful data is retrieved. In this work, two problems will be considered for which the radiosonde and the radiosonde network are not adequate.

The first problem is the real time monitoring of precipitable water which is the total mass of water vapor in a unit, vertically oriented, column of the atmosphere. The reason that this is of interest is because the probability of summer airmass thunderstorms in the Tucson area is closely related to the precipitable water. The mesoscale dynamics of the summer monsoon permit the rapid fluctuation of precipitable water during the course of the day. Therefore the precipitable water inferred from the morning radiosonde sounding, launched at 0500 MST, may not be valid by afternoon when thunderstorm activity would be expected. So by monitoring precipitable water, it may be possible to improve the predictability of afternoon thunderstorms.

The second problem is the determination of stratospheric vertical water vapor profiles and ultimately the construction of three dimensional distributions of water vapor within the stratosphere. There is interest in this because little is known about the climatology of the distribution of water vapor in the stratosphere. It is also possible, given histories of the three dimensional distribution of water vapor, to infer stratospheric circulation patterns and the rate of production of H_2O in the upper stratosphere associated with methane photodisassociation.

A technique which may be employed to solve these problems is passive remote sensing. Remote sensing is the determination of some property of the atmosphere via a signal, measured some distance from the source of the signal. Passive remote sensing makes use of naturally occurring radiative fields, that is, ones which are not anthrpogenic. Among the approaches that have been used to passively determine atmospheric water vapor amounts are multichannel microwave and infrared radiometers which make use of the dependence of the emissivity of water vapor on frequency and temperature to determine water vapor profiles (Staelin et al., 1976; Russell et al., 1984). Another technique, and the one of interest here, is the use of a single spectral determination of the transmission of solar radiation to infer the water vapor amount along a path from the sun to a radiometer that is directly observing the sun. The assertion in this technique is that if a spectral channel is chosen to lie within a region in which attenuation is dominated by water vapor absorption lines then it is possible to infer the path water vapor amount given a measured water vapor optical depth.

While the problem of equating water vapor optical depth with water vapor amount initially seems to be a straight forward problem, it turns out to be quite complicated. The main problem in solving this equivalency is that the mass absorption coefficient is a highly complicated function of wavenumber within an absorption band and it is also a strong function of temperature and pressure thus making it difficult to adequately determine the expected water vapor transmission for a given set of conditions. Various approximate techniques have been developed and used over the past ten or twenty years and among these are numerically fitting point determinations of transmission as a function of absorber amount (Liou, 1974), laboratory calibration of the radiometer (Tomasi et al., 1983), and the fourier transform method (Mankin, 1979). Herein, a new approach to this problem is developed which satisfactorily meets the requirements placed upon it, that is, it must be computationally efficient and accurate to the degree that compared to measurement errors it does not itself represent a significant degradation in the water vapor retrieval. Past experience indicates that the basic physics and engineering of the problem prohibit determining water vapor density to an accuracy of much better than 5 to 10%.

The technique, which is developed in Chapter 2, is a Stieltjes integration of transmission weighted by the frequency of occurrence of absorption coefficient within the water vapor channel. Temperature and pressure variations along the path are accounted for by employing the correlated absorption coefficient method as discussed in Hansen et al. (1983). An advantage of this approach is that it closely approximates a line by line solution allowing, first of all, an exact solution under optimum conditions and, secondly, a thorough error analysis of the technique and the problem in general. This technique is then applied, in Chapter 3, to the determination of precipitable water from transmission measurements made by a ground based radiometer. The radiometer operates in the $\rho\sigma\tau$ water vapor absorption band, which extends from about 0.9μm to 1.0μm. A thorough error analysis of the technique as applied to this problem is performed and a comparison of radiosonde determinations of precipitable water with radiometric determinations is presented in overall confirmation of the technique.

In Chapter 4, the technique is applied to the determination of vertical water vapor profiles in the stratosphere. The water vapor optical depth is determined by a limb scanning satellite, SAGE II, as a function of the height of the tangent point of the path followed by the rays of the sun intercepted by the satellite.

A new iterative inversion of the water vapor optical depths to water vapor mixing ratio as a function of height is developed and is shown to be both numerically stable and rapidly convergent. A complete error analysis of the inversion technique and comparisons with an independent reduction technique are presented and show that the precision of the approach is significantly better than the quality of the data provided by SAGE II.

Chapter 5 presents some general discussion and conclusions about the overall utility of the technique and its applicability to the problems presented within this dissertation. Also included are some suggestions for improving the technique, particularly for stratospheric applications.

CHAPTER 2

FORMULATION OF THE PROBLEM

The transport of radiant energy through a medium in thermocynamic equilibrium is governed by the Equation of Radiative Transfer which is most fundamentally a statement of the conservation of energy. Solutions to this equation can be either for a single wavelength, as is common when studying light scattering by aerosols, or for a band, or interval of wavelength, as is most often of interest when considering radiative transfer in spectral regions dominated by molecular line absorption.

In this chapter, starting from the Equation of Radiative Transfer, a general form of the band transmission function will be derived that is valid for an attenuating atmosphere with no internal sources of radiant energy. Limiting consideration to attenuation by molecular line absorption, the general band transmission function is transformed to a Stieltjes integral. The steps necessary to incorporate the correlated absorption coefficient assumption for paths along which temperature and pressure are allowed to freely vary, are also shown.

The General Band Transmission Function

Most solutions to radiative transport problems begin with the Equation of Radiative Transfer because it expresses the fundamental property of the conservation of radiant energy. It has been derived and thoroughly discussed by, among others, Chandrasekhar (1960) and therefore that will not be repeated here. In differential form, it may be expressed as

$$\frac{dI_\nu}{K_{\nu T} ds} = J_\nu - I_\nu \tag{2.1}$$

where I_ν is the radiance associated with wavenumber ν, J_ν is the source function representing the contribution from all sources to the radiance, ds is the differential path length, as shown in Figure 2.1, and $K_{\nu T}$ is the total volume extinction coefficient for the medium.

Equation 2.1 may be simplified by considering the special conditions under which we will be applying it. First, because of the relatively cool temperature of the atmosphere, the energy emitted by the spectral region we are considering (about 1μm) may be neglected. Secondly, since the scattering efficiency of the atmosphere is normally low within the ρστ band and since consideration is limited to the case of a radiometer directly observing the sun, the contribution to the measured radiance by scattering processes can be neglected (Box, 1981). Thus for the stated limitations, the source term, J_ν can be eliminated. The formal solution to 2.1 may then be easily seen to be

$$I_\nu(s) = I_\nu(0)e^{-\tau_\nu(s)} \tag{2.2}$$

where $\tau_\nu(s)$ is the monochromatic optical depth between a point 0 in the attenuating medium and the point s for the particular path

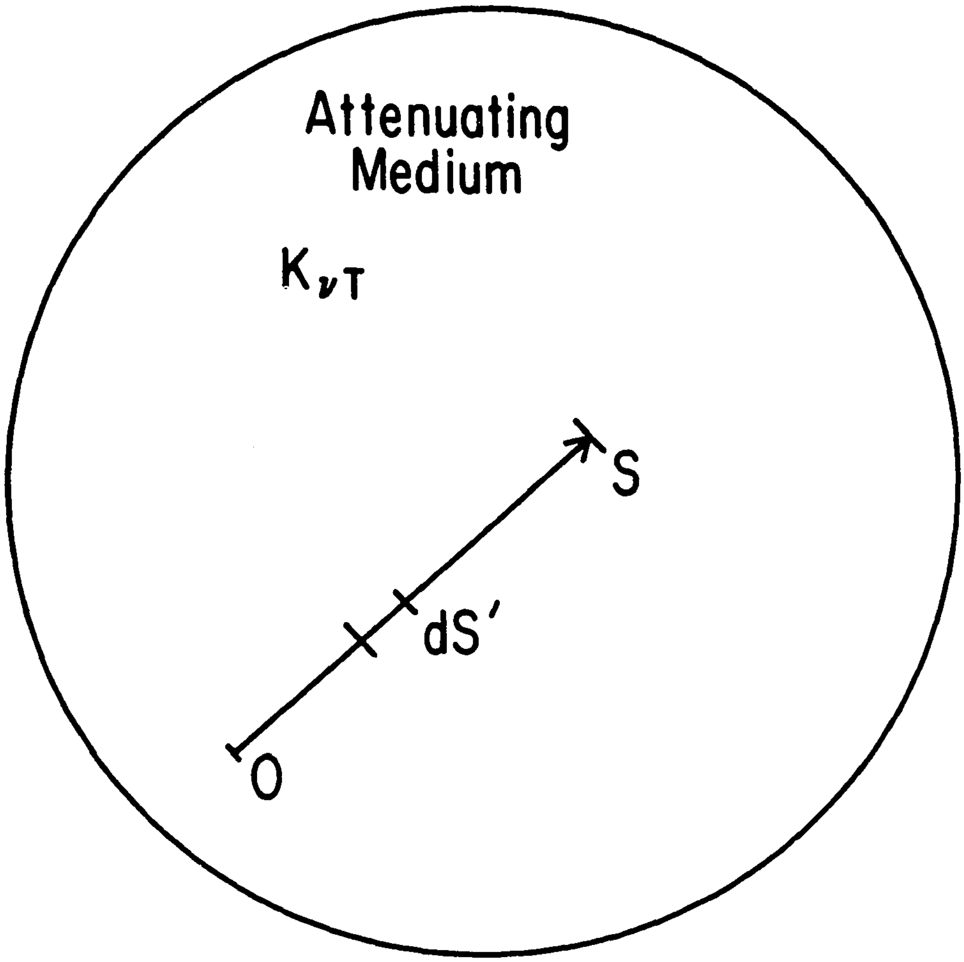

Figure 2.1. The differential path length for a path from 0 to S within a medium of total volume extinction coefficient, $K_{\nu T}$

followed. $I_\nu(0)$ is the radiance of wavenumber incident at the point along the path where s is zero. Formally, the monochromatic optical depth may be expressed as

$$\tau_\nu(s) = \int_0^s K_{\nu T}(s')ds' \tag{2.3}$$

Equation 2.2 is the well known Beer's Law and, physically, it expresses the fact that for the conditions described above, the radiance measured in any direction is equal to the incident radiance in that direction reduced by a factor of $e^{-\tau_\nu(s)}$.

In extending Beer's Law to an interval in wavenumber, there is a temptation to express Equation 2.2 as

$$\bar{I}(s) = \bar{I}(0)^{-\bar{\tau}} \tag{2.4}$$

where the bar superscript is indicative of averaging the quantity over some interval in wavenumber. But, it has been shown (Thomason et al., 1982) that even in cases where the monochromatic optical depth is not a very strong function of wavenumber, this is not a satisfactory approach as it can yield sizeable errors for even fairly narrow intervals. It is necessary, therefore, to consider an integral form of Beer's Law, including a filter spectral response for the radiometer, in order to correctly determine the measured radiance. Equation 2.2 is then expressed as

$$I(s) = \int_{\Delta\nu} I_\nu(0)\Psi(\nu)e^{-\tau\nu(s)}d\nu, \tag{2.5}$$

where $\Delta\nu$ is the band's width in wavenumber, and $\Psi(\nu)$ is the radiometer's spectral filter response. A general transmission function can now be phrased by dividing Equation 2.5 by I(0), which yields

$$T(s) = I(s)/I(0) = \int_{\Delta\nu} I_\nu(0)\Psi(\nu)e^{-\tau_\nu(s)} d\nu / \int_{\Delta\nu} I_\nu(0)\Psi(\nu)d\nu \qquad (2.6)$$

The transmission function, $T(s)$, will have a value of 1.0 when s is zero and decreases monotonically toward zero with increasing s.

Equation 2.6 can be simplified by dividing the interval into small bands within which the product $I_\nu(0)\Psi(\nu)$ may be considered constant resulting in an approximate general transmission function that is the weighted summation of the band transmission functions; that is

$$T(s) = \sum_{b=1}^{B} W_b T_b(s) \qquad (2.7)$$

where B is the number of bands and W_b is the individual band weighting which is given by

$$W_b = \int_{\Delta\nu_b} \Psi(\nu)I_\nu(0)d\nu / \int_{\Delta\nu} \Psi(\nu)I_\nu(0)d\nu \qquad (2.8)$$

where $\Delta\nu_b$ is the band width in wavenumber. $T_b(s)$ is the band transmission function and is formally expressed as

$$T_b(s) = \frac{1}{\Delta\nu_b} \int_{\Delta\nu_b} e^{-\tau_\nu(s)} d\nu \qquad (2.9)$$

In the $\rho\sigma\tau$ band, $I_\nu(0)$ is very nearly constant and the variations in $I_\nu(0)\Psi(\nu)$ are due almost entirely to the variations of the filter function across the band. Figures 2.2 and 2.3 show the approximations for $I_\nu(0)\Psi(\nu)$ that were used in determining the band transmission for the ground based radiometer and the SAGE II radiometer, respectively. Table 2.1 lists the weights that were used for the bands for each radiometer.

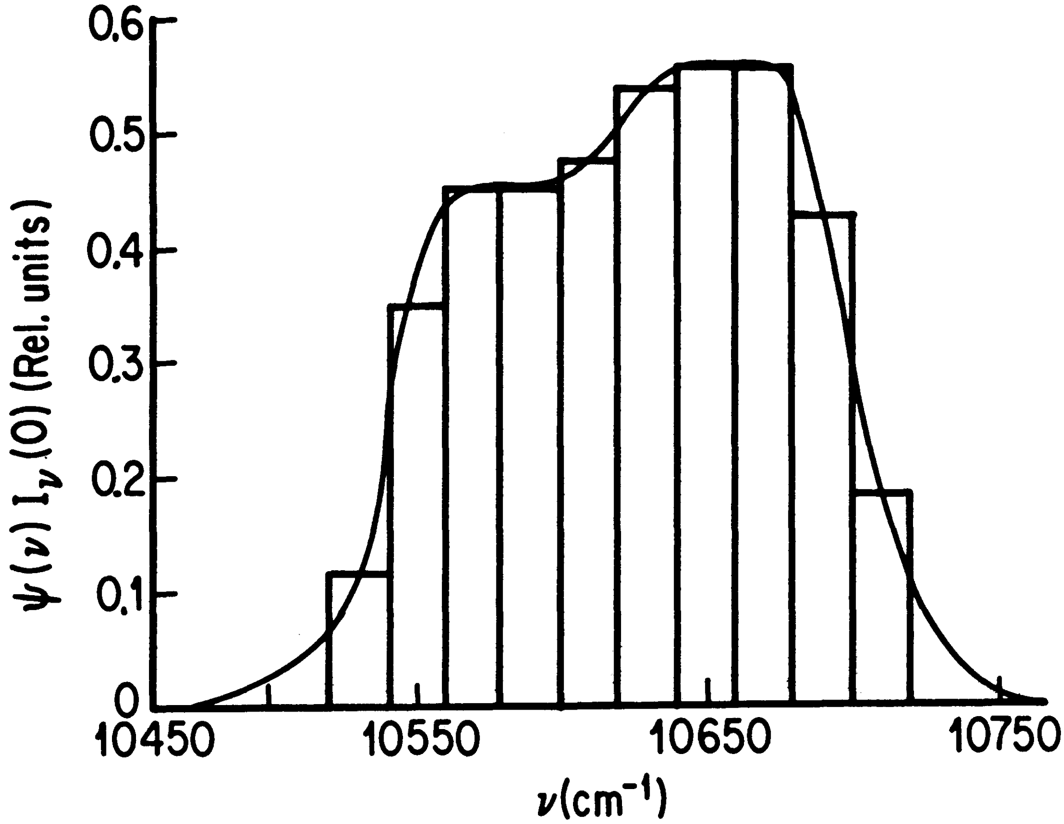

Figure 2.2. The true form (solid curve) and the histrogramic approximation to the product $I_\nu(0)\Psi(\nu)$ for the ground based radiometer's water vapor channel

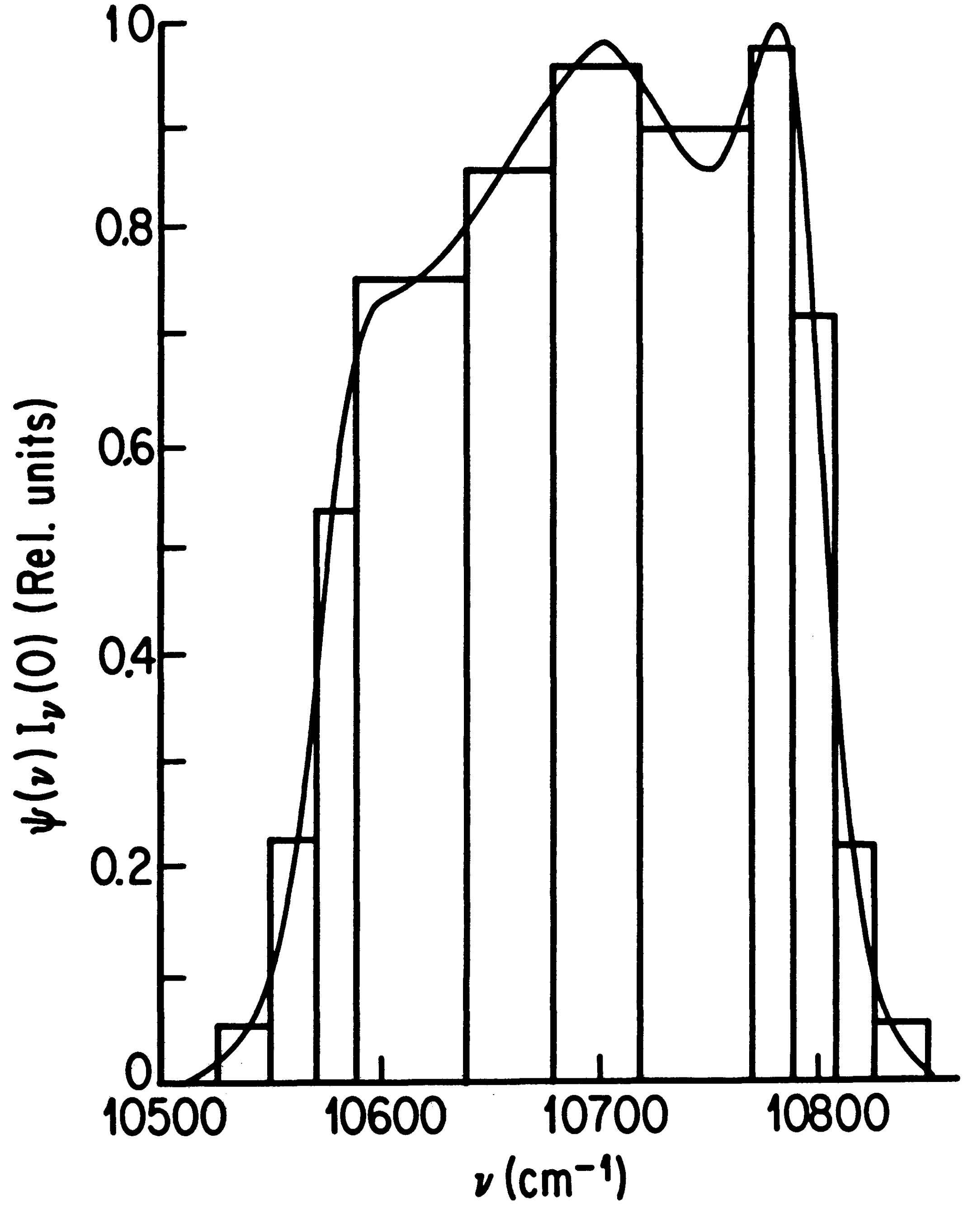

Figure 2.3. The true form (solid curve) and the histogramic approximation to the product $I_\nu(0)\Psi(\nu)$ for the SAGE II radiometer's water vapor channel

Table 2.1. The spectral boundaries and weights of the bands used to approximate the ground-based and SAGE II radiometers' water vapor channels

	Ground Based Radiometer		SAGE II Radiometer	
Band	Band Boundaries*	W_b	Band Boundaries*	W_b
1	10520 - 10540	0.029	10525 - 10550	0.00581
2	10540 - 10560	0.086	10550 - 10570	0.02103
3	10560 - 10580	0.110	10570 - 10590	0.05209
4	10580 - 10600	0.110	10590 - 10640	0.18115
5	10600 - 10620	0.117	10640 - 10680	0.16636
6	10620 - 10640	0.130	10680 - 10720	0.18378
7	10640 - 10660	0.137	10720 - 10770	0.21254
8	10660 - 10680	0.135	10770 - 10790	0.09221
9	10680 - 10700	0.103	10790 - 10800	0.03905
10	10700 - 10720	0.043	10800 - 10810	0.02406
11	-----	--	10810 - 10825	0.01584
12	-----	--	10825 - 10850	0.00608

*band boundaries in cm^{-1}

At most wavenumbers, the monochromatic optical depth has components from aerosol and molecular scattering and absorption by aerosol and various gases. In the $\rho\sigma\tau$ band, in addition to water vapor absorption, there are small but non-negligible contributions to the monochromatic optical depth by scattering, aerosol and molecular, and by absorption due to ozone. In order to determine a water vapor amount from a single transmission measurement it is necessary to be able to remove the effect of the non-water vapor attenuators. There are techniques to permit this and, as they are not of interest herein, it will be assumed they have been performed and limit consideration to the attenuative effects of water vapor only. It is important to remember, however, that errors arising because of the neglect of these non-water vapor attenuation components will have an important effect on the quality of the water vapor determination made from any given measurement.

Based upon the above condition, Equation 2.9 may be written as

$$T_b(u) = \frac{1}{\Delta\nu_b} \int_{\Delta\nu_b} e^{-\tau_\nu(u)} d\nu \qquad (2.10)$$

where u is path water vapor amount as given by

$$u = \int_0^s \rho_\nu(s')ds' \qquad (2.11)$$

where $\rho_\nu(s')$ is the water vapor density at point s'. The monochromatic optical depth may be rewritten as

$$\tau_\nu(u) = \int_0^s k_\nu(s')\rho_\nu(s')ds' \tag{2.12}$$

where $k_\nu(s')$ is the water vapor mass extinction coefficient at wavenumber ν and at point s' along the path.

Transformation to Stieltjes Integral

Given the rather simple form of the band transmission function of Equation 2.10 it is a natural assumption that it would not be difficult to evaluate. However given the exordinarily complicated form of the monochromatic water vapor optical depth throughout the $\rho\sigma\tau$ absorption band, as can be seen in part in Figure 2.4, it becomes apparent that accurate solutions will be very difficult to obtain.

It is possible to integrate numerically Equation 2.10 via the trapezoidal method but the large number of points required to accurately evaluate the integral makes such an approach an anathema to the stated goals of the project, specifically that the method be computationally efficient. Therefore, a different approach is called for in evaluating the integral.

Consider a homogenous path through the atmosphere, that is, a path along which temperature, pressure and water vapor density are constant, and consider a single absorption band, b, within which the water vapor mass absorption coefficient varies as shown in Figure 2.5. Instead of dividing the independent axis, the ν-axis, into small increments and integrating by the trapezoidal method, the dependent axis, the k-axis, is divided into J increments assigning

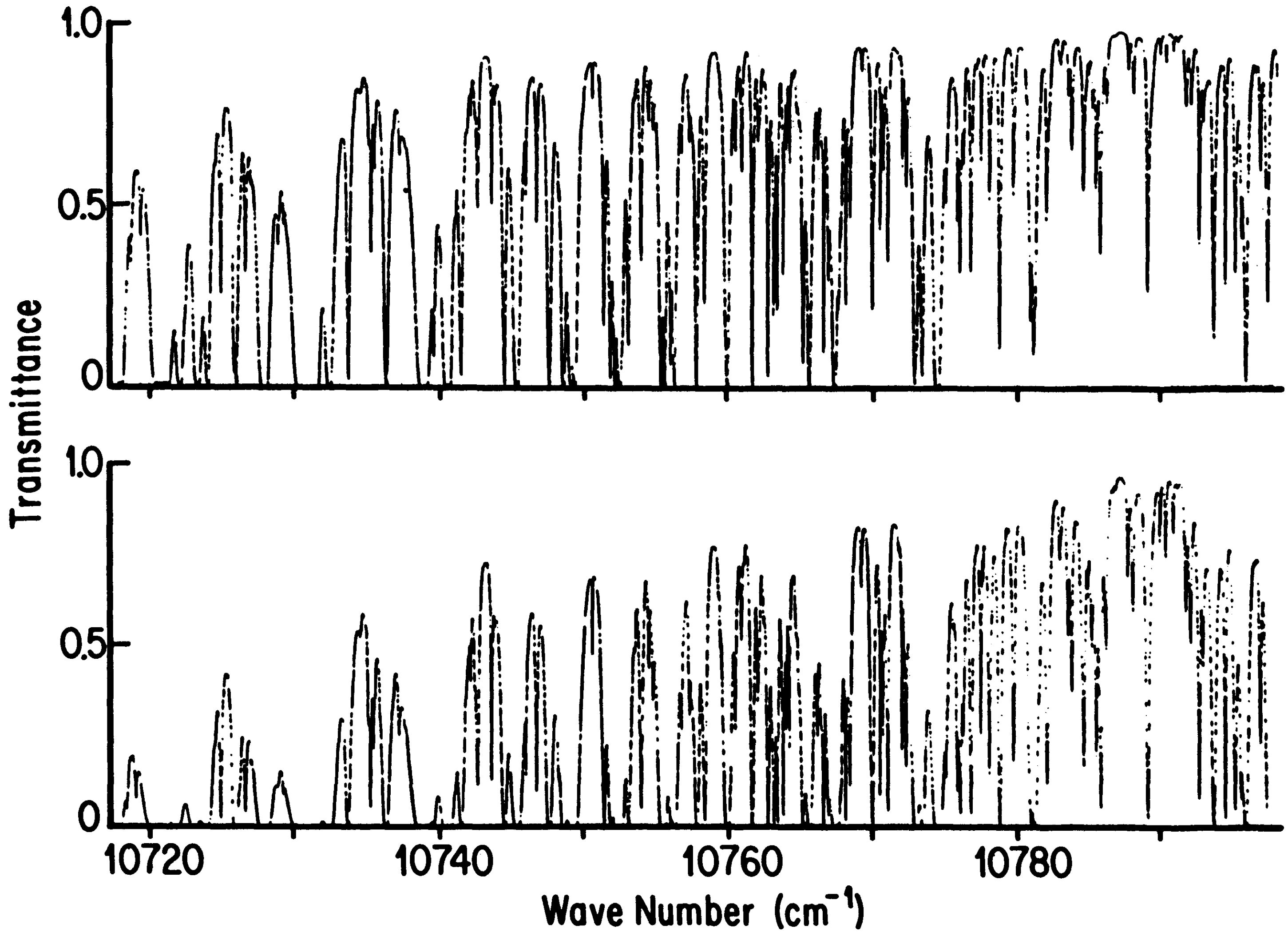

Figure 2.4. Two samples of the monochramatic transmittance of the full atmosphere through a portion of the ρστ water vapor absorption band

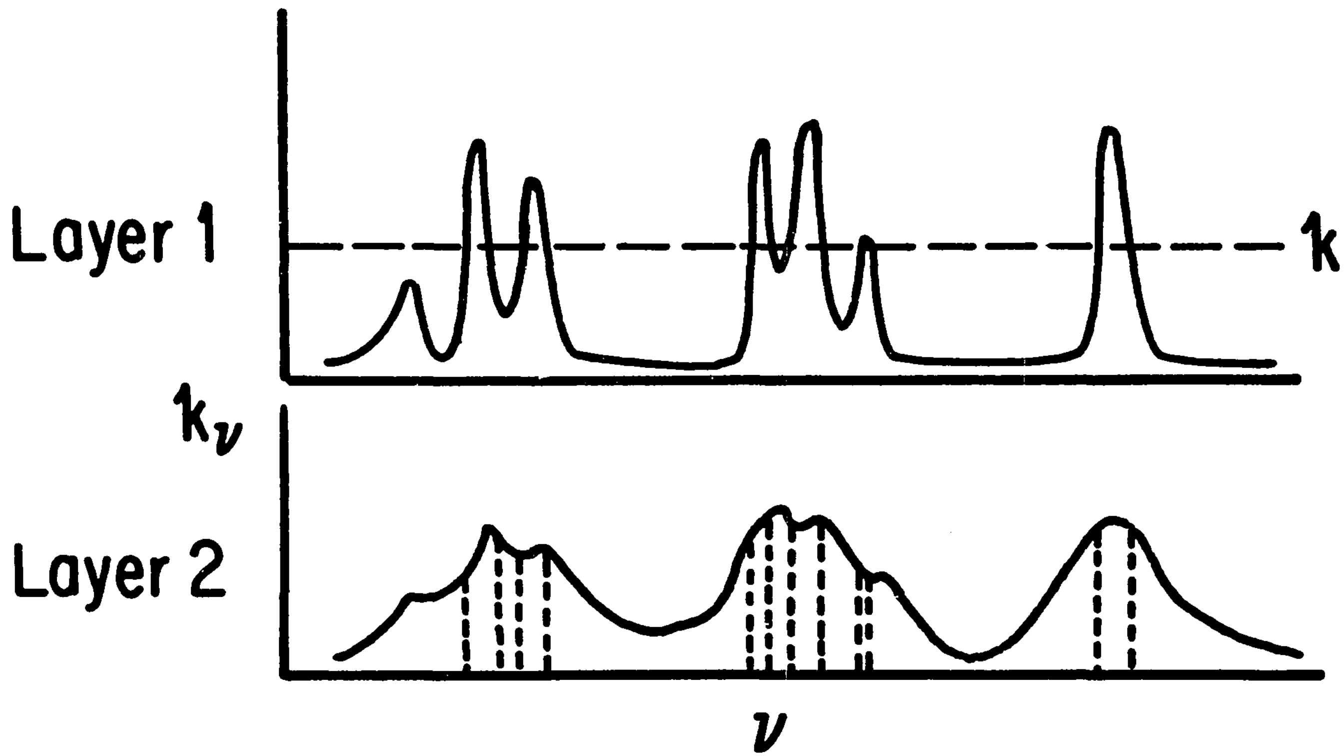

Figure 2.5. A model absorption band and an example of the incrementing of the absorption coefficient axis.

characteristic values of water vapor absorption coefficient to each increment, as shown in Figure 2.5. Now if Equation 2.10 is integrated only over the domain of wavenumbers within the band with water vapor mass absorption coefficients lying within the jth increment, $\Delta\nu(j)$ and the homogeneity condition previously stated is invoked, Equation 2.10 may be rewritten as

$$T_j(u) = \frac{1}{\Delta\nu_b} \int_{\Delta\nu(j)} e^{-k_j u} \, d\nu \tag{2.13}$$

or

$$T_j(u) = \frac{e^{-k_j u}}{\Delta_{\nu b}} \int_{\Delta\nu(j)} d\nu \tag{2.14}$$

In this equation, $T_j(u)$ is the transmissivity associated with an absorption of value k_j and absorber amount u weighted by the "probability" of any wavenumber within the band being associated with the jth increment in absorption coefficient. The band transmission function may then be expressed as the summation of the transmissivity associated with each increment weighted by its frequency of occurrence. This may be expressed as

$$T_b(u) = p_1 e^{-k_1 u} + p_2 e^{-k_2 u} + \ldots + p_j e^{-k_j u} \ldots + p_j e^{-k_j u} \tag{2.15}$$

where

$$p_j = \frac{1}{\Delta\nu_b} \int_{\Delta\nu(j)} d\nu = \frac{\Delta\nu(j)}{\Delta\nu_b} \tag{2.16}$$

and

$$\sum_{j=1}^{J} p_j = 1.0 \tag{2.17}$$

If the size of the increments is allowed to become infintesimal then Equation 2.15 may be written as

$$T_b(u) = \int_0^\infty p(k)e^{-ku}dk \tag{2.18}$$

where $p(k)dk$ is the frequency of occurrence of absorption coefficient between k and k + dk within the band. Expressed in this form it is easy to see that the band transmission function, $T_b(u)$, represents the expected or average value of transmissivity, e^{-ku}, for the band given some density function, $p(k)$, for the absorption coefficient distribution within the band. If $p(k)$ is known exactly, then $T(u)$ may be exactly produced.

The function $p(k)$ is a density function of absorption coefficient and a cumulative absorption coefficient distribution function, $g(k)$, may be defined by

$$g(k) = \int_0^k p(k')dk' \tag{2.19a}$$

or

$$dg(k) = p(k)dk$$

where $g(0)$ is zero and $g(\infty)$ is one. Substituting Equation 2.19b into Equation 2.18 yields

$$T_b(u) = \int_0^{\infty} e^{-ku} dg(k) \tag{2.20}$$

which has the mathematical form of a Stieltjes Integral. Taylor and Mann (1972, pp. 592-597) discuss the form and nature of Stieltjes Integrals. Equation 2.20 may be transformed, in what is primarily a bookkeeping change to

$$T_b(u) = \int_0^1 e^{-k(g)u} dg, \tag{2.21}$$

where $k(g)$ is simply the inverse of $g(k)$. This approach to band transmission determination, at least in the more empirical form of Equation 2.15, dates back to a paper by Kondrat'yev in 1947 (Kondrat'yev, 1969). So far as I am aware the Stieltjes integral approach has been limited to the substantially less sensitive problem of flux divergence and has never been applied to a remote sensing problem.

Extension to Inhomogeneous Atmospheres

The form of band transmission function that has been derived so far is only valid for homogeneous atmospheres as the value of the mass absorption coefficient across the $\rho\sigma\tau$ band is a strong function of temperature and pressure. This dependence is reflected in a strong dependence of $g(k)$ on temperature and pressure. In order to calculate transmission along an inhomogeneous path, that is, one along which temperature and pressure are not constant, a different technique must be employed.

This technique makes use of the correlated absorption coefficient method which has been described for flux divergence applications in Lacis and Hansen (1979) and Wang and Ryan (1983). In this method, the atmosphere is divided into N layers within each one of which the spectrum of absorption coefficient is assumed constant (no pressure or temperature induced variations) and a cumulative absorption coefficient distribution function, $g_n(k)$, is determined for each layer n. A layer transmission can be determined via Equation 2.20 by allowing u to be the water vapor along the path in layer n only. However, a simple product of layer transmissions will yield an inaccurate value of transmission for the full atmosphere. This error is a result of the highly correlated nature of the spectral distribution of absorption coefficient between the various layers.

In derivation of the correlated absorption method, an atmosphere consisting of two homogeneous layers will be considered. Also a spectral band will be considered within which the absorption lines are equally spaced and of equal intensity as shown in Figure 2.6. The difference is k_ν between the two layers are due to the pressure and temperature differences only. In this idealized case, at the wavenumbers in layer 1 which are associated with an absorption coefficient, k, there is exactly one value of absorption coefficient, k', associated with those wavenumbers in layer 2. Therefore, between the domain of absorption coefficient of layer 1 and the domain of absorption coefficient of layer 2 there exists a one-to-one mapping and, in fact, there is a complete correlation. Also, the fraction of

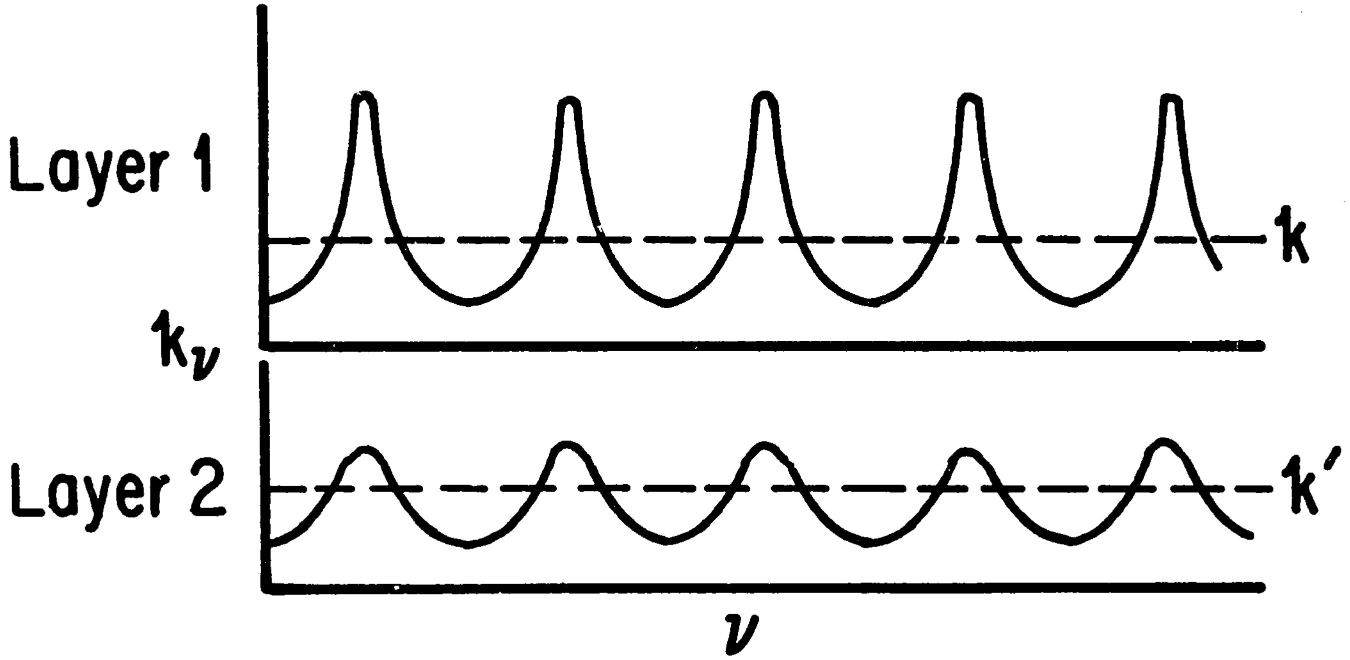

Figure 2.6. An idealized absorption band for a two layer atmosphere where lines are of equal strength and equally spaced; k and k' are particular values of absorption coefficient within layers 1 and 2 respectively

wavenumbers with absorption coefficients less than k in layer 1 is the same as the fraction of wavenumbers in layer 2 with absorption coefficients less than k' or $g_1(k) = g_2(k')$. For all wavenumbers within the band the percentile rank of absorption coefficient is independent of temperature and pressure. These are the basic assumptions of the correlated absorption coefficient method and they allow the construction of a cumulative distribution of optical depth for a homogeneous path by simply adding the optical depths from each layer as a function of rank, g. For the two layer case this may be written

$$T_b(u) = \int_0^1 \exp(-(k_1(g)u + k_2(g)u))dg \tag{2.22}$$

where the subscript is indicative of the association with a particular layer. This treatment is analogous to solving $(dg)^{-1}$ monochromatic transmission problems but much more computationally efficient.

If a two layer atmosphere is examined in which the distribution of line location and strengths within the band is more physically plausible, as the one shown in Figure 2.7, it is found that the assumptions used in deriving Equation 2.22 are not completely valid. This is demonstrated by the fact that for wavenumbers associated with an absorption coefficient of k in layer 1, there is, contrary to the idealized case, a range of values of absorption coefficients associated with the wavenumbers in layer 2. This is a manifestation of a certain degree of lack of correlation and represents a departure from the transmission model that has been formulated. A discussion of the significance of this departure will be presented in Chapter 3.

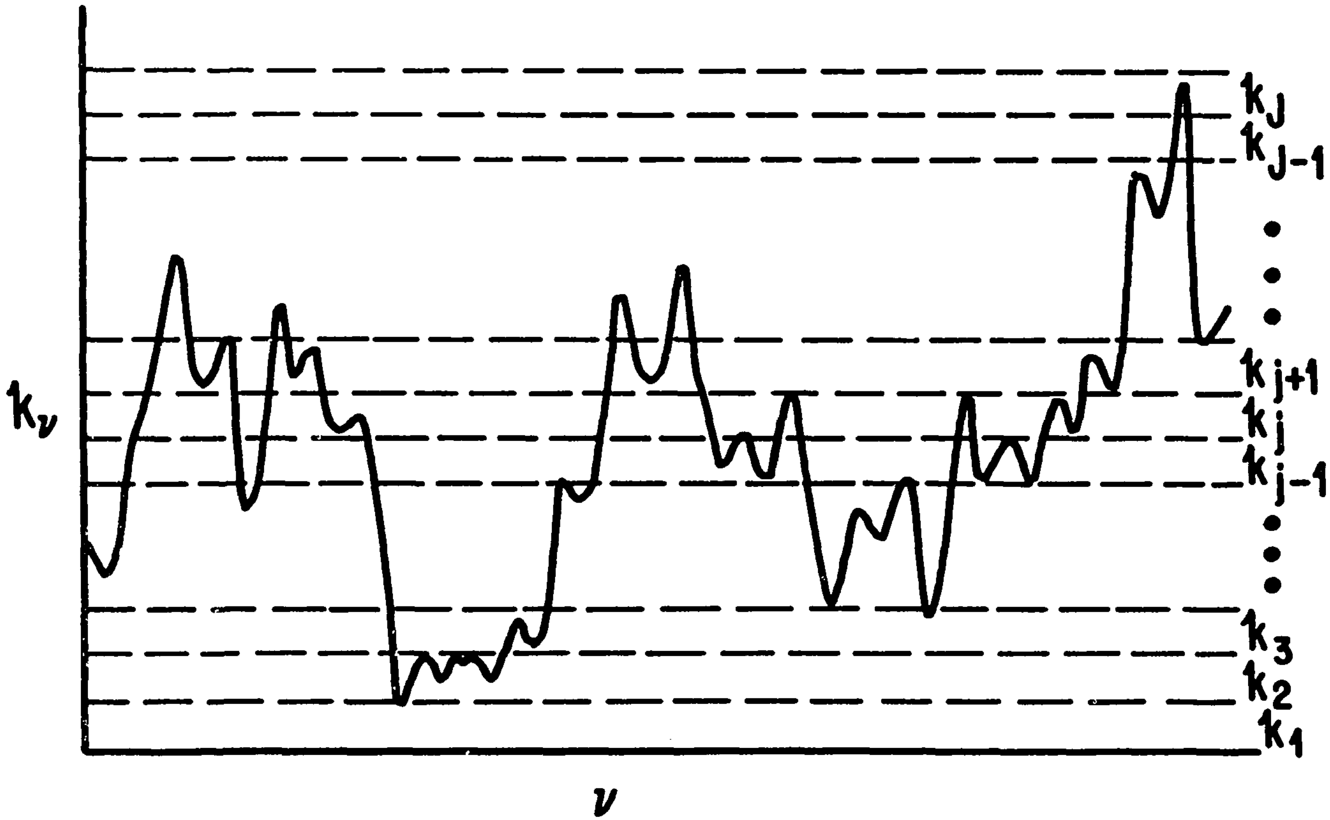

Figure 2.7. A more plausible absorption band for a two layer atmosphere where lines have varying strengths and random locations within the band, the vertical dashed lines in layer 2 are the wavenumbers which in layer 1 had an absorption coefficient of k

Extending the transmission function for an inhomogeneous path to N layers, it is found that

$$T_b(u) = \int_0^1 \exp(-\sum_{n=1}^{N} k_n(g)u_n)dg, \tag{2.23}$$

where $k_n(g)$ is the value of absorption coefficient of rank g within the homogeneous layer n. In it's most general form, for a continuous medium, it may be expressed

$$T_b(u) = \int_0^1 \exp\ (-\int_0^s k(g,s')\rho_\nu(s')ds')dg \tag{2.24}$$

where k(g,s') is the value of absorption coefficient associated with rank g and location along the path s'. Once $k_n(g)$ and u_n are known for each layer, the transmission for the full interval may be determined by evaluating Equation 2.23 for each band and then combining them via Equation 2.7.

In summary, a general transmission function has been derived that is applicable to spectral intervals dominated by molecular line absorption. It is valid for inhomogeneous atmospheres subject only to the validity of the correlated absorption coefficient assumption and the subdivision of the spectral interval into smaller bands. It retains many of the characteristics of a line by line calculation of transmission, but is computationally much more efficient.

CHAPTER 3

THE RADIOMETRIC DETERMINATION OF PRECIPITABLE WATER

An application in which there is considerable interest is the determination of precipitable water using a ground based radiometer and in this chapter that problem is addressed. First a general form for the function $k_n(g)$ is derived that may be adapted to fit the behavior of the absorption bands for normal tropospheric temperatures and pressures. Next, details of the evaluation of the band transmission integral are discussed as are the sources and natures of the systematic errors within the model. The effect of random measurement errors on the precipitable water estimate is discussed and finally a comparison of the precipitable water determined from the radiometric measurements and radiosonde measurements is performed.

The Determination of k_ν

In order to construct $k_n(g)$, it is necessary to know the dependence of the mass absorption coefficient on wave number within the band. Therefore in this section, the determination of the mass absorption coefficient at a given wavenumber will be discussed. Also the dependence of the line parameters, line strength, width, and shape, on temperature and pressure will be addressed.

The absorption coefficient at wavenumber ν, k_ν may be expressed as the summation of the values of absorption coefficient of all the individual absorption lines within the local spectral region at wavenumber ν. This may be expressed by

$$k_\nu = \sum_{j=1}^{J} S(j) f(\nu, \nu_0(j), \alpha_L(j), \alpha_0(j)) \qquad (3.1)$$

where S(j) is the line strength of the jth line, $\nu_0(j)$ is its line center, $\alpha_L(j)$ is its Lorentz line width, and $\alpha_0(j)$ is its Doppler line width. The function $f(\nu, \nu_0, \alpha_L, \alpha_0)$ is the line shape function and it is most generally given by the Voight line shape (Gille and Ellingson, 1968). The Voight line shape combines the effects of both pressure and Doppler broadening.

The Voight line shape is given by the convolution of the Lorentz line shape and the Doppler line shape. The Lorentz line is Cauchy in form and given by

$$f(\nu) = \alpha_L/\pi \ / \ ((\nu - \nu_0)^2 + \alpha_L^2) \qquad (3.2)$$

for some unspecified line. The Doppler line is gaussian in form and it is given by

$$f(\nu) = (2\pi\alpha_0^2)^{-\frac{1}{2}} e^{-(\nu-\nu_0)^2/2\alpha_0^2} \qquad (3.3)$$

The Doppler half width is given by

$$\alpha_0 = \nu_0 (RT/M_0 C^2)^{\frac{1}{2}}. \qquad (3.4)$$

Here R is the universal gas constant, M_0 is the molecular weight of the absorbing species and C is the speed of light.

The convolution of the Loretnz and Doppler line shape functions as given in Equations 3.2 and 3.3 will yield the Voight line shape function. By applying the Fourier transform theorem and Faltung's Theorem a convenient integral form for the Voight line can be shown to be

$$f(\nu) = \frac{1}{\pi} \int_0^\infty \exp(-\alpha_L \xi - \alpha_0^2 \xi^2/2) \cos\xi\nu d\xi. \tag{3.5}$$

Integration leads to

$$f(\nu) = (8\pi\alpha_0^2)^{-\frac{1}{2}} \left[\exp\left(\frac{(\alpha_L - i\nu)^2}{2\alpha_0^2}\right) \left(1 - \phi\left(\frac{\alpha_L - i\nu}{\sqrt{2}\alpha_0}\right)\right)\right.$$

$$\left. + \exp\left(\frac{(\alpha_L + i\nu)^2}{2\alpha_0^2}\right) \cdot \left(1 - \phi\left(\frac{\alpha_L + i\nu}{\sqrt{2}\alpha_0}\right)\right)\right], \tag{3.6}$$

where i is $\sqrt{-1}$ and ϕ is the probability function. The Voight line shape as given by Equation 3.6 is not exceptionally useful as it is rather difficult to evaluate. Since Equation 3.5 may be efficiently evaluated for wide ranges of values of ν, α_L, and α_0, it will be used when it is necessary to evaluate the Voight line shape function.

In this chapter the transmission model will be applied to a ground based measurement of transmission for the purpose of determining precipitable water. Consideration, therefore, will be limited to the Lorentz line shape except where otherwise stated, as throughout the troposphere pressure broadening dominates the Doppler effect, so that the latter may be neglected. With this limitation, Equation 3.1 may be written

$$k_\nu = \sum_{j=1}^{J} S(j)\alpha_L(j)/\pi/((\nu - \nu_0(j))^2 + \alpha_L^2(j)) \tag{3.7}$$

where the Lorentz line shape function has been substituted for the general line shape function.

The line strength is dependent on temperature only and it can be expressed, for water vapor, by

$$S(j) = S_0(j) \left(\frac{T_0}{T}\right)^{3/2} \exp\left(-\frac{E(j)}{K}\left(\frac{1}{T} - \frac{1}{T_0}\right)\right) \tag{3.8}$$

where $S_0(j)$ is the line strength of jth line at temperature T_0, E(j) is the energy of the ground state of the molecule and K is the Boltzman constant.

The line width has been shown to exhibit a dependence on temperature and pressure of the form

$$\alpha_L(j) = \alpha_{L0}(j) \left(\frac{P}{P_0}\right)\left(\frac{T_0}{T}\right)^{1/2} \tag{3.9}$$

where $\alpha_{L0}(j)$ is the Lorentz half width for a standard temperature T_0 and standard pressure P_0. The values of $\alpha_{L0}(j)$, $S_0(j)$, $\nu_0(j)$, and ρστ E(j) have been compiled on magnetic tape (McClatchy et al., 1973) for most molecular species with absorption lines in the ultraviolet to the far infrared. The water vapor absorption line parameters for the band were taken from this compilation this study noting that $S_0(j)$ and $\alpha_{L0}(j)$ were defined for P_0 = 1 atm and T_0 = 296K.

The Determination of $k_n(g)$

In this section the determination of a model form of $k_n(g)$ will be begun. Starting with an assumed line shape and line strength distribution, model forms of band transmission functions are developed;

the relationship between the model band transmission functions and $k_n(g)$ will be shown to be dependent only on S_0', the equivalent line strength, and α'_L, the equivalent line width. A new technique for the determination of these parameters will be developed that is based on the moments of the distribution of mass absorption coefficient within a specified spectral band and at a given temperature and pressure.

The most intuitive approach to constructing $g_n(k)$, and therefore $k_n(g)$, is to randomly select a wavenumber within the band and determine via Equation 3.7 the value of k_ν for that wavenumber. By repeating this a large number of times, it is possible to construct a histogram of the frequency of occurrence of incremental values of absorption coefficient. This is the optimal approach in terms of computational accuracy as with sufficient sampling it is possible to determine $g_n(k)$ to any desired precision. Unfortunately, this technique is extremely time consuming as a very large sampling of wavenumbers is required to adequately define $g_n(k)$ particularly for values of k near zero or infinity which are important when the transmission is either low or high respectively.

Since one of the goals of this research was to develop a technique that is computationally efficient and the facilities were not available to execute the sampling approach, use was made of a less computationally demanding procedure at the cost of surrendering some degree of accuracy. A model of the distribution of line centers and line strengths within the band was constructed and from this a model form for $g_n(k)$ was developed. Then by forcing some characteristics of the model $g_n(k)$ to correctly reproduce some characteristics of the true k_ν, it may be possible to force the model $g_n(k)$ to satisfactorily reproduce the true $g_n(k)$. The derivation of $g_n(k)$ will be for a general layer and band and so the n and b subscripts, as shown in Equations 2.7 and 2.23, will be dropped until it is necessary to distinguish between layers and/or bands.

For the homogeneous path, the band transmission function, as given by Equation 2.18, can be expressed as the Laplace Transform of the mass absorption coefficient distribution function, p(k). This is a convenient behavior because it is very difficult to derive a model for either p(k) or g(k) directly, but many model forms of transmission have been developed. Therefore given an analytic model transmission function, it is possible to determine an analytic form of p(k) via

$$p(k) = \mathcal{L}^{-1}(T(u);k) \tag{3.10}$$

where $\mathcal{L}^{-1}(;)$ is the inverse Laplace transform. The mathematical forms and properties of Laplace and inverse Laplace Transforms are discussed in Kreyszig (1979, Chapter 5).

Most of the model band transmission functions are derived by defining an equivalent line width, W, which represents the width of an equivalent rectangular line. The rectangular line has the property of being completely absorbing within the width W and completely transmitting outside of it. This width has been shown (Goody, 1964), to be given by

$$W = \int_{-\infty}^{\infty} [1 - \exp(Suf(\nu)]d\nu \tag{3.11}$$

where $f(\nu)$ is the line shape function for a band of lines with equal strength or by

$$W = \int_{-\infty}^{\infty} \int_{0}^{\infty} [1 - \exp(S'uf(\nu))]p(S')dS'd\nu \tag{3.12}$$

when there is a distribution of line strengths within the band (Goody, 1964). The value of $p(S)dS$ is the fraction of lines with strengths between S and $S + dS$.

Two forms for $p(S)$ are commonly used in the derivation of transmission functions, the exponential distribution and a Malkmus distribution in which $p(S)$ is proportional to $S^{-1}e^{-S/S_0}$, where S_0 is the mean line strength. These are chosen since they at least in a broad sense reproduce the distribution of line strengths observed in most real absorption bands. Neither reproduces the exact distribution of line strengths but neither is usually grossly wrong. In Figure 3.1 is given a comparison of the exponential distribution, the Malkmus distribution, and the observed distribution for band 7 of SAGE II radiometer water vapor filter as given in Table 2.1. In this comparison the Malkmus' distribution agrees well with the observed distribution. For the line strength distributions of the $\rho\sigma\tau$ band it is usually found that the Malkmus distribution is in better agreement with the observed distribution than is the exponential distribution.

At a given wavenumber, the probability that an absorption line of width W is present is given by $W/\Delta\nu$, where $\Delta\nu$ is the width of the

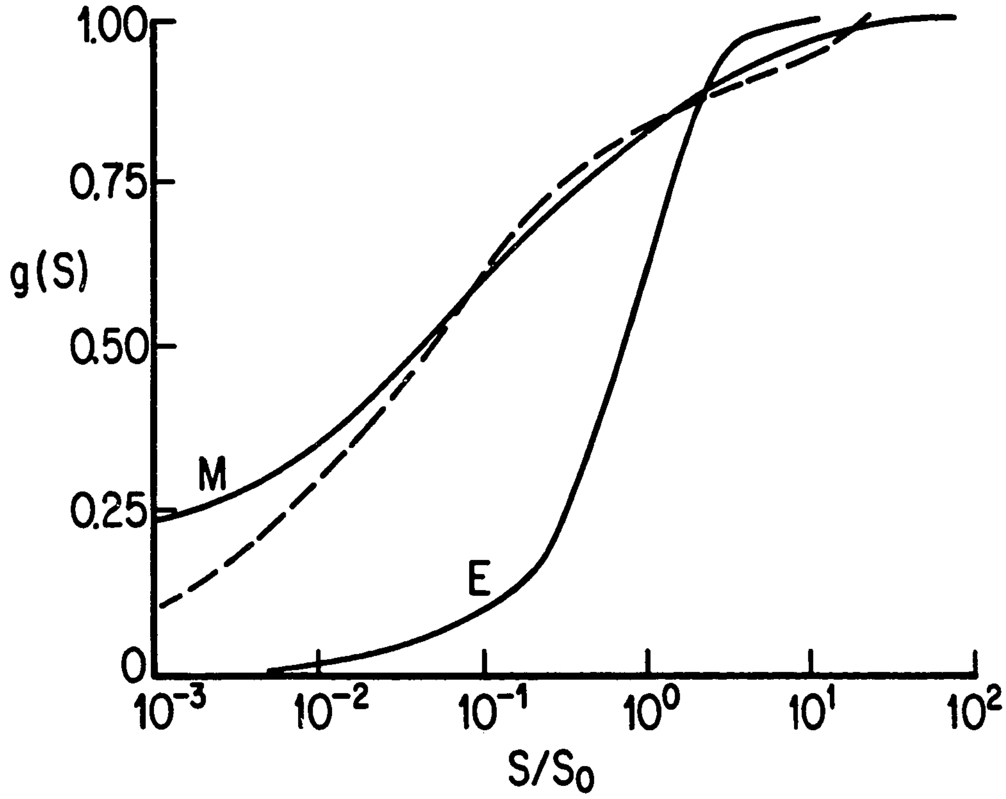

Figure 3.1. A comparison of the line strength distributions given by the Malkmus distribution (M), the exponential distribution (E), and the observed line strength distribution (dashed) for band 7 of the SAGE II radiometer's water vapor channel and mean surface conditions

band. If there are N lines randomly located within the band, the probability that n lines are present at any given wavenumber is given by the Poison probability law in the form

$$P_n = e^{-\frac{WN}{\Delta\nu}} \left(\frac{WN}{\Delta\nu}\right)^n / n! \tag{3.13}$$

where the expression $WN/\Delta\nu$ represents the expected number of lines present at a given wavenumber. Since the transmission function for these equivalent rectangular absorption lines would be equal to the fraction of wavenumbers within the band at which no lines are present, the band transmission function may be expressed as the value of Equation 3.13 for n = 0 or

$$T(u) = e^{-W/\delta} \tag{3.14}$$

where δ is the mean spacing between line centers and is defined by

$$\delta = \Delta\nu/N. \tag{3.15}$$

The expression W/δ is frequently referred to as the equivalent optical depth of the band.

For an exponential distribution of line strength the equivalent line width has been shown (Gille and Ellingson, 1968) to have the form

$$W_{exp} = \int_{-\infty}^{\infty} (S_0 u f(\nu)/1 + S_0 u f(\nu)))d\nu \tag{3.16}$$

where S_0 is the mean line strength. Goody (1952) has shown that for a Lorentz line shape W_{exp} has the form

$$W_{exp} = S_0 u/(1 + \frac{S_0 u}{\pi\alpha_L})^{1/2} \quad . \tag{3.17}$$

If a distribution of line strengths proportional to $S^{-1}e^{-S/S_0}$ is assumed, it can be shown that the equivalent line width has the form

$$W_M = \frac{1}{4}\int_{-\infty}^{\infty} \ln(1 + 4\, S_0 u f(\nu))\, d\nu. \tag{3.18}$$

For Lorentz line shape, Malkmus (1967) has shown that the equivalent line width, W_M, is given by

$$W_M = \frac{\pi\alpha_L}{2}\left(\left(1 + \frac{4S_0 u}{\pi\alpha_L}\right)^{\frac{1}{2}} - 1\right). \tag{3.19}$$

An interesting and valuable distinction of the relationship between T(u) and p(k) is that in many ways, T(u) fulfills the role of a characteristic function of p(k). Since, according to the model, p(k) is a unique representation of T(u) via the inverse Laplace transform, either p(k) or T(u) is sufficient to describe completely the variations of k. Taking successive derivatives with respect to u of Equation 2.18 and evaluating for an argument of u = 0 we find that

$$T^{(n)}(u)\Big|_{u=0} = \frac{d^n T(u)}{du^n}\Big|_{u=0} = \int_0^{\infty} (-k)^n p(k)\, dk \tag{3.20}$$

or

$$T^{(n)}(0) = -1^n \langle k^n \rangle = -1^n M_n \tag{3.21}$$

where M_n is the nth moment. So the moments of the distribution, p(k), are characterized by the behavior of the transmission function about the origin. This is a very convenient relationship as the integral of Equation 3.20 is usually difficult to evaluate whereas the left hand side is usually not.

From Equations 3.17 and 3.19 it can be seen that the equivalent line width, W, is a function not only of absorber amount but also of the parameters S_0 and α_L. The proficiency with which T(u) and therefore p(k) describes the actual behavior of the band is in large part dependent on the suitability of values taken for S_0 and α_L. The standard means of defining these parameters is based upon forcing the model equivalent optical depth at strong line and weak line absorption to agree with the true behavior.

The concept of strong or weak line absorption by a gas is based upon the observed behavior of the transmission for limitingly wide or narrow line widths. When the absorption lines are narrow, for instance, both Equations 3.17 and 3.19 may be approximated by the strong line or square-root approximation for the equivalent optical depth, where W/δ is given by

$$\frac{W}{\delta} = (\pi\alpha_L S_0 u)^{\frac{1}{2}}. \qquad (3.22)$$

When the lines are wide, both Equations 3.17 and 3.19 are given by the so-called weak line or linear approximation, where W/δ is given by

$$\frac{W}{\delta} = \frac{S_0 u}{\delta}. \qquad (3.23)$$

A more general condition for the occurrence of these special cases is based upon the magnitude of the parameter $S_0 u/\pi\alpha_L$ which shall be called x. When x is much greater than one, W/δ approaches the strong line approximation, whereas when it is much less than one the equivalent optical depth is approximately given by the weak line form.

It has been shown (Godson, 1955a) that for the standard approach S_0 and α_L are given by

$$S'_0 = \frac{S_0}{\delta} = \frac{1}{\Delta\nu}\sum_{j=1}^{J} S(j) \tag{3.24}$$

and

$$\alpha'_L = \frac{\alpha_L}{\delta} = \left[\frac{1}{\Delta\nu}\sum_{j=1}^{J}(S(j)\alpha_L(j))^{\frac{1}{2}}\right]^2 / S'_0 \tag{3.25}$$

where the j subscript indicates the jth line within the band. The equivalent line strength S'_0 is equal to the mean value of the absorption coefficient in the band. However the equivalent line width, α'_L, is not necessarily the mean line width scaled by the mean line spacing. These definitions for S'_0 and α'_L serve to force the transmission function to produce the correct transmission as the value of the parameter x approaches either zero or infinity. Unfortunately, since the band model of transmission is not a perfect representation of the actual behavior of a band, it is observed that the value of α'_L required to make the model form of the equivalent optical depth agree with the observed value is a weak but significant function of the absorber amount. Godson (1955b) has shown that the error in determining W/δ caused by using α'_L as defined by Equation 3.25 can be as large as 5% in the vicinity of a transmission of 0.50. This behavior is at least in part due to the fact that α'_L has no recollection of the true line structure, that is, the true placement of lines of differing strengths relative to one another. This is unfortunate for the applications considered here as the transmission will nearly always lie between 1.0 and 0.30. It is not feasible to carry the functional dependence of α'_L on u throughout the calculative process, instead it is preferred to determine a value for α'_L which is more indicative of a mid-range value of transmission.

One way to do this is by invoking the moment generating property of transmission functions shown in Equation 3.21. From this it can be shown that the moments of the exponential and the Malkmus transmission models are functions of S'_0 and α'_L only. For the exponential line strength distribution, the first three moments of the absorption coefficient distribution can be shown by Equation 3.21 to be

$$M_0 = 1.0 \tag{3.26a}$$

$$M_1 = S'_0 \tag{3.26b}$$

and

$$M_2 = S'^2_0 \left(1 + \frac{1}{\pi\alpha'_L}\right) \tag{3.26c}$$

The moments of the p(k) for the Malkmus distribution of line strengths can be shown to be

$$M_0 = 1.0 \tag{3.27a}$$

$$M_1 = S'_0 \tag{3.27b}$$

and

$$M_2 = S'^2_0 \left(1 + \frac{2}{\pi\alpha'_L}\right) \tag{3.27c}$$

The lth moment can be shown to be given by

$$M_l = S'^l_0 \sum_{k=0}^{l-1} \frac{(l - 1 + k)!}{k!\,(l - 1 - k)!} (\pi\alpha'_L)^{-k} \tag{3.28}$$

for $l \geq 1$.

The moments of k_ν can also be found directly by averaging the proper power of k_ν across the band interval. Thus

$$M_l = \frac{1}{\Delta\nu} \int_{\Delta\nu} k^l{}_\nu d\nu = \frac{1}{\Delta\nu} \int_{\Delta\nu} [\sum_{j=1}^{J} k_\nu(j)]^l d\nu \tag{3.29}$$

The evaluation of this equation appears at first to be quite difficult, but when considering Lorentz line shapes, Equation 3.29 can be solved for lower orders of moments both efficiently and accurately. The zeroth order moment is obviously equal to one in agreement with Equation 3.26a and 3.27a. For $l = 1$, Equation 3.29 may be simplified to

$$M_1 = \frac{1}{\Delta\nu} \sum_{j=1}^{J} \int_{\Delta\nu} k_\nu(j) d\nu \tag{3.30}$$

and, for Lorentz line shapes, this is equal to

$$M_1 = \frac{1}{\Delta\nu} \sum_{j=1}^{J} \frac{S(j)}{\pi} [\mathrm{Atan}(\frac{\nu_2 - \nu_0(j)}{\alpha_L(j)}) - \mathrm{Atan}(\frac{\nu_1 - \nu_0(j)}{\alpha_L(j)})] \tag{3.31}$$

where wavenumbers ν_1 and ν_2 represent the upper and lower bounds of the band. Reasonable simplification reduces Equation 3.31 to

$$M_1 = \frac{1}{\Delta\nu} \sum_{j=1}^{J} S(j). \tag{3.32}$$

The second moment, $l = 2$, may be expressed via Equation 3.29 as

$$M_2 = \frac{1}{\Delta\nu} [\sum_{j=1}^{J} \int_{\Delta\nu} k^2{}_\nu(j) d\nu + 2 \sum_{j=1}^{J-1} \sum_{m=j+1}^{J} \int_{\Delta\nu} k_\nu(j) k_\nu(m) d\nu] \tag{3.33}$$

which for Lorentz lines may be approximately expressed as

$$M_2 = \frac{1}{\Delta\nu} \left[\sum_{j=1}^{J} \frac{S^2(j)}{2\pi\alpha_L(j)} + 2 \sum_{j=1}^{J-1} \sum_{m=j+1}^{J} \frac{S(j)S(m)}{\pi} \right.$$

$$\left. \cdot \frac{\alpha_L(j) + \alpha_L(m)}{((\nu_0(j) - \nu_0(m))^2 + (\alpha_L(j) + \alpha_L(m))^2} \right] \tag{3.34}$$

where it is assumed that no line is in the immediate vicinity of the borders of the band. This assumption has been examined and shown to have a negligible effect on the determination of the moments and on α'_L.

The value of S'_0 and α'_L may now be found by taking the numerical values for the first and second moments as determined by Equations 3.32 and 3.34, respectively, and solving via Equations 3.26b or 3.27b and Equations 3.26c or 3.27c for S'_0 and α'_L, respectively. In both cases S'_0 is equal to the first moment but α'_L for the exponential model is given by

$$\alpha'_L = (m_2/m_1^2 - 1)^{-1}/\pi \tag{3.35}$$

while in the Malkmus band model α'_L is equal to

$$\alpha'_L = 2(m_2/m_1^2 - 1)^{-2}/\pi \tag{3.36}$$

which results in an equivalent Lorentz half width twice the magnitude of the former case.

There are some advantages in defining S'_0 and α'_L using the moments. First of all, since the calculation of the second moment includes some dependence on the true line structure, the value of α'_L calculated in this manner has some information on the actual line structure. Secondly, since Equation 2.18 may be rewritten as

$$T(u) = \sum_{l=0}^{\infty} (-1)^l m_l u^2/l! \tag{3.37}$$

by expanding the exponential into its Taylor series and integrating, high values of transmission will be determined very accurately. This occurs because for high transmissions Equation 3.37 may be accurately approximated as a summation involving only the lowest order moments, that is

$$T(u) \simeq 1 - m_1 u + m_2 u^2/2 \tag{3.38}$$

since u is very small and the summation may be truncated.

Another means of selecting the preferred method to define S'_0 and α'_L is to select the method which minimizes the effect of the assumed line strength distribution. Under optimum circumstances the equivalent line widths predicted by the exponential and Malkmus models would be identical. However, this is not observed to be the case. In Figure 3.2 the ratio of equivalent line widths for the exponential model and the Malkmus model are shown as a function of x which is equal to $S'_0 u/\pi\alpha'_L$ for both methods of defining S'_0 and α'_L. For the standard method, the ratio approaches 1 for very small and very large values of x and has a maximum value of 1.16 for $x = 2.0$. For the moment method, the ratio is nearly 1 for $x < 1$ and then approaches $\sqrt{0.5}$ as x becomes large. Since x usually is between 0.5 and 20.0 for the ground based radiometer case, it is apparent that neither method is superior in this regard. However, for the SAGE II problem, where

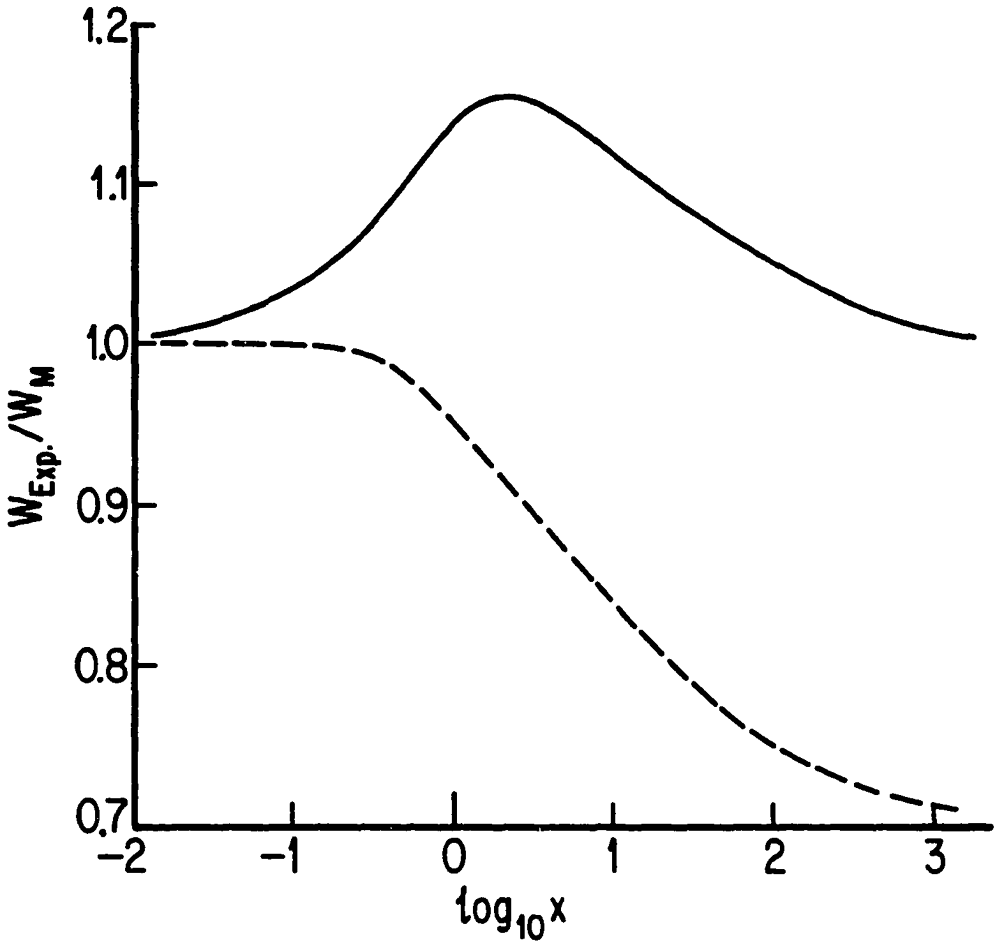

Figure 3.2. The ratio W_{exp}/W_M as a function of x for the standard method (solid) and moment method (dashed) of defining S'_0 and α'_L

x is almost always less than 1, the moment method nearly eliminates the effect of the assumed line strength distribution.

Tables of S'_0 and α'_L are now constructed for each band and for a range of values of temperature and pressure, by employing Equation 3.32 and Equations 3.34 and 3.36 respectively. Values of S'_0 and α'_L for a particular band and a particular temperature and pressure may accurately be obtained by interpolating across the appropriate table.

The Determination of $\mathcal{L}^{-1}$ [T(u);u]

In this section, the derivation of k(g) will be completed by evaluating the inverse Laplace transform of the model band transmission functions. The limiting cases of strong and weak line absorption will be examined first. The inverse Laplace transforms of the Malkmus and exponential band transmission functions will be derived in some detail.

In Equation 2.18, it was shown that the relationship between the mass absorption coefficient distributionfor a homogeneous path is related to the band transmission function for that path by a Laplace transform. It therefore follows that if the inverse Laplace transform may be found for the transmission function that p(k) and ultimately k(g) may be found.

The complexity of the inverse Laplace transform of the transmission function defined by Equation 3.10 is dependent upon the functional dependence of the equivalent line width on u. The simplest inverse occurs for the weak line absorption case where the transmission function is given by

$$T(u) = \exp(-S'_0 u) \tag{3.39}$$

The inverse Laplace transform for this expression may easily be found to be

$$p(k) = \delta(k - S'_0) \tag{3.40}$$

where $\delta(\;)$ is the delta function. From the latter expression, it can be seen that the weak line case is equivalent to a grey body assumption where the value of absorption coefficient is independent of wavenumber. The function $k(g)$ may be expressed as

$$k(g) = S'_0 \tag{3.41}$$

for all values of g.

The transmission function for the strong line approximation is given by

$$T(u) = \exp(-(\pi\alpha'_L\, S'_0\, u)^{1/2}) \tag{3.42}$$

and its inverse Laplace transform is found to be

$$p(k) = \frac{1}{2}\,(S'_0\alpha'_L)^{1/2}\, k^{-3/2}\, \exp\left(\frac{-\pi\alpha'_L S'_0}{4k}\right). \tag{3.43}$$

By solving for $g(k)$ using Equation 2.19a and inverting the function it is found that

$$k(g) = (\mathrm{erf}^{-1}(1 = g))^{-2}\, \frac{\pi\alpha'_L S'_0}{4} \tag{3.44}$$

where $\mathrm{erf}(x)$ is the error function which is of the form

$$\mathrm{erf}(x) = \frac{2}{\sqrt{\pi}} \int_0^x e^{-t^2}\, dt. \tag{3.45}$$

The Malkmus transmission function may be expressed as

$$T(u) = \exp[-\frac{\pi\alpha'_L}{2}((1 + \frac{4S'_0 u}{\pi\alpha'_L})^{\frac{1}{2}} - 1)] \tag{3.46}$$

and its inverse Laplace transform may be found using a simple substitution. In integral form p(k) may be expressed as

$$p(k) = \frac{1}{2\pi i}\int_{\gamma-i\infty}^{\gamma+i\infty} \exp[-\frac{\pi\alpha'_L}{2}((1 + \frac{4S'_0 u}{\pi\alpha'_L})^{\frac{1}{2}} - 1] e^{ku}\, du. \tag{3.47}$$

Substituting $w = u + \pi\alpha'_L/4S'_0$ and $dw = du$ it is found that

$$p(k) = \frac{e^{\pi\alpha'_L/2}}{2\pi i}\int_{\gamma-i\infty}^{\gamma+i\infty} \exp(-(\pi S'_0\alpha'_L w)^{\frac{1}{2}})\exp(kw - \frac{\pi\alpha'_L k}{4S'_0})dw. \tag{3.48}$$

This may be written as

$$p(k) = \exp(\frac{\pi\alpha'_L}{4}(2 - \frac{k}{S'_0}))\, \mathcal{L}^{-1}(\exp(-(\pi S'_0\alpha'_L w)^{\frac{1}{2}});\ k) \tag{3.49}$$

then by similarity with the inverse of Equation 3.42, it can be seen that the mass absorption coefficient distribution is given by

$$p(k) = \frac{1}{2}(S'_0\alpha'_L)^{1/2}\, k^{-3/2} \exp[\frac{\pi\alpha'_L}{4}(2 - \frac{k}{S'_0} - \frac{S'_0}{k})] \tag{3.50}$$

While no analytic form for k(g) has been found, the function g(k) has been shown (Domoto, 1974) to be

$$g(k) = \frac{1}{2}[e^{\pi\alpha'_L}\mathrm{erfc}[\sqrt{\frac{\pi\alpha'_L S'_0}{4k}} + \sqrt{\frac{\pi\alpha'_L k}{4S'_0}}] + \mathrm{erfc}[\sqrt{\frac{\pi\alpha'_L S'_0}{4k}} - \sqrt{\frac{\pi\alpha'_L k}{4S'_0}}]] \tag{3.51}$$

where erfc( ) is the complementary error function which is usually available as an intrinsic function on most main frame computers. It is interesting to note that in the limit of strong line absorption Equation 3.50 approaches the functional form of Equation 3.43 as would be expected.

The last transmission function to be considered is the exponential band model which may be expressed

$$T(u) = \exp\left[- S'_0 u/\left(1 + \frac{S'_0 u}{\pi\alpha'_L}\right)^{\frac{1}{2}}\right] \tag{3.52}$$

In integral form p(k) may be expressed as

$$p(k) = \frac{1}{2\pi i}\int_{\gamma-i\infty}^{\gamma+i\infty} \exp\left[-S'_0 u/\left(1 + \frac{S'_0 u}{\pi\alpha'_L}\right)^{\frac{1}{2}}\right] e^{ku}\, du \tag{3.53}$$

substituting $w = \frac{S'_0 u}{\pi\alpha'_L} + 1$, this may be written as

$$p(k) = \frac{1}{2\pi i}\int_{\gamma-i\infty}^{\gamma+i\infty} \frac{\pi\alpha'_L}{S'_0} \exp[-\pi\alpha'_L(w^{\frac{1}{2}} - w^{-\frac{1}{2}})] \exp\left[\frac{\pi\alpha'_L kw}{S'_0} - \frac{\pi\alpha'_L k}{S'_0}\right] dw. \tag{3.54}$$

This may be reexpressed by invoking Faltung's theorem, as

$$p(k) = \frac{\pi\alpha'_L}{S'_0} e^{-\pi\alpha'_L k/S'_0} \left[\mathcal{L}^{-1}\left(e^{-\pi\alpha'_L w^{\frac{1}{2}}} ; \frac{\pi\alpha'_L k}{S'_0}\right) * \mathcal{L}^{-1}\left(e^{\pi\alpha'_L w^{-\frac{1}{2}}} ; \frac{\pi\alpha'_L k}{S'_0}\right)\right] \tag{3.55}$$

where the * operator indicates a convolution. After some further manipulation, a final form for p(k) is found to be

$$p(k) = \frac{(\alpha'_L S'_0)^{\frac{1}{2}}}{2} e^{-\pi\alpha'_L k/S'_0} [k^{-3/2} e^{-\pi\alpha'_L S'_0/4k}$$

$$+ \sum_{n=1}^{\infty} [\frac{(\pi\alpha'_L)^{3n/2}}{n!\ S'^{n/2}_0} 2^{(n-1)/2} (\frac{\pi\alpha'_L S'_0}{4})^{-\frac{1}{2}} k^{\frac{n}{2}-1}$$

$$\cdot \exp(\frac{-\pi\alpha'_L S'_0}{8k}) D_{1-n}((\frac{\pi\alpha'_L S'_0}{2k})^{\frac{1}{2}})]] \qquad (3.56)$$

where $D_p(x)$ is the parabolic cylinder function of the order p. $D_p(x)$ is defined (Gradshteyn and Ryzhik, 1980, pg. 1064) by the integral

$$D_p(x) = \frac{e^{-x^2/4}}{\Gamma(-p)} \int_0^{\infty} e^{-xt-t^2/2} t^{-p-1} dt. \qquad (3.57)$$

This is not a particularly convenient form for p(k) since at least twenty terms of the summation are required for reasonable convergence and values for the parabolic cylinder function are not readily available.

Figure 3.3 shows a comparison of g(k) for band 2 of the ground based radiometer for mid tropospheric conditions for the exponential model, the Malkmus model and the observed absorption coefficient distribution. It can be seen that for k/S'_0 greater than about 0.2 both models produced reasonable agreement through the Malkmus model is somewhat better. For k/S'_0 less than 0.2 both models tend to under estimate the value of g probably as a result of over predicting the presence of very strong lines. While this tendency does not have a strong effect when k is large, the tails of such lines may contribute significantly to an over estimation of k when k is fairly small.

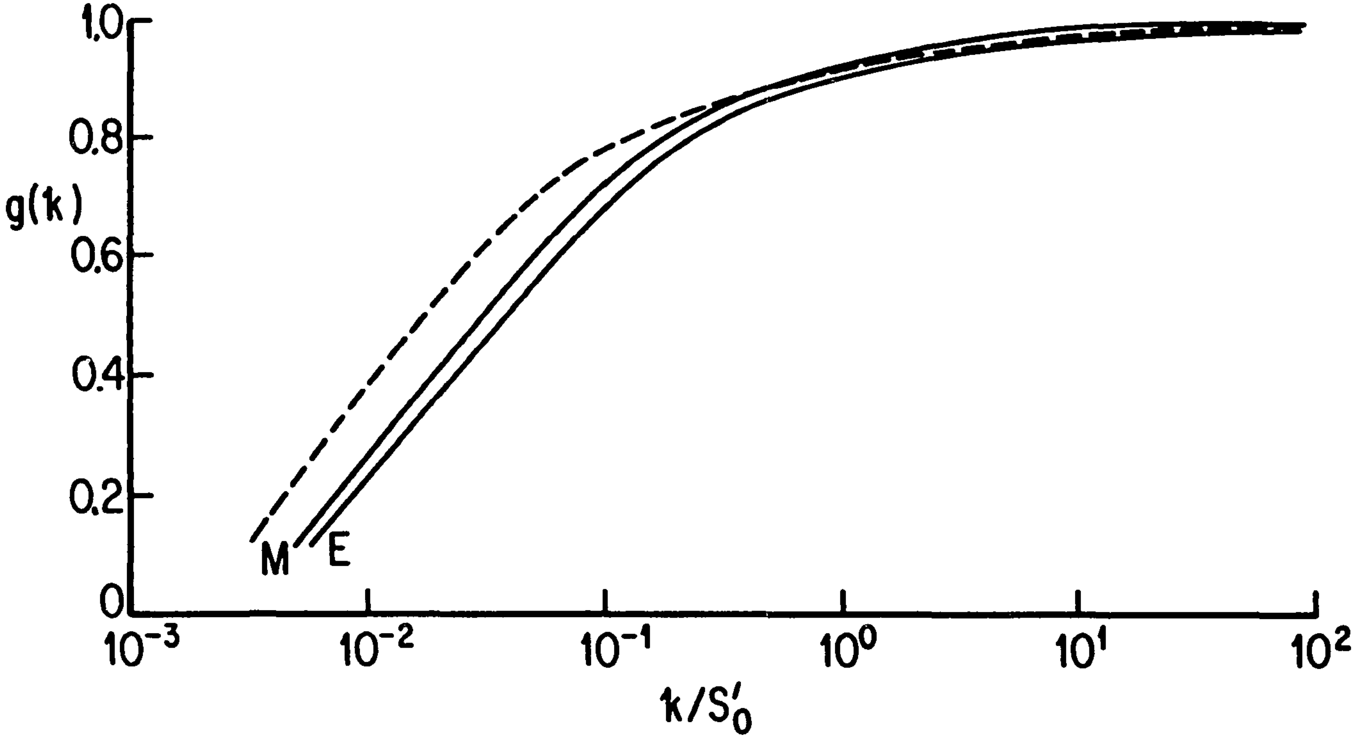

Figure 3.3. A comparison of the cumulative absorption coefficient distribution observed in band 2 in the ground based radiometer's water vapor channel for mid-tropospheric conditions (dashed) with that predicted by the exponential model (E) and the Malkmus model (M)

At this point, rather than continue consideration of the exponential model for the mass absorption coefficient distribution function, attention will be limited to the Malkmus model because both models will yield similar results and the Malkmus model is the most computationally convenient.

The Computation of Transmission

In this section the details of the evaluation of the integral of Equation 2.23 and the problem of determining precipitable water from a measured effective optical depth will be addressed. The correlated absorption coefficient assumption will be evaluated and all other sources of error in the transmission calculation will be discussed. A comparison of precipitable water determinations by radiosonde with those determined radiometrically will also be presented.

The computation of transmission for an individual band for a given distribution of atmospheric temperature, pressure and water vapor density is now possible by employing the transmission function for inhomogeneous paths, as given in Equation 2.23. The value of $k_n(g)$ is given by numerically finding the inverse of the mass absorption coefficient dumulative distribution function as given in Equation 3.51 by defining α'_L and S'_0 using Equations 3.36 and 3.32 respectively, for the line parameters of the band in question and the temperature and pressure of the layer in question.

In executing this integration, a final few simplifying alterations have been made. By defining a new variable, h, as the ratio k/S'_0, Equations 2.23 and 3.51 may be changed to

$$T_b(u) = \int_0^1 \exp[-\sum_{n=1}^{N} h_n(g)\ S'_{0n}\ u_n]\ dg \tag{3.58}$$

and

$$g_n(h) = \frac{1}{2}\ [e^{\pi\alpha'_{Ln}}\ \mathrm{erfc}[\sqrt{\frac{\pi\alpha'_{Ln}}{4h}} + \sqrt{\frac{\pi\alpha'_{Ln}h}{4}}] + \mathrm{erfc}[\sqrt{\frac{\pi\alpha'_{Ln}}{4h}} - \sqrt{\frac{\pi\alpha'_{Ln}h}{4}}]] \tag{3.59}$$

respectively. This has the favorable effect of reducing $g_n(h)$ to a function of α'_L only. Since the integral of either Equation 2.23 or 3.58 must be solved numerically, it is most efficient to tabulate $h_n(g)$ as functions of its independent variables and then interpolate to the relevant values of h_n. By using the transmission function in the form of Equation 3.58, we may eliminate S'_0 as a variable in the above table and thus eliminate the need for one interpolation with a resulting improvement in accuracy and speed and a reduction in the volume of computer memory required to store the table. The value of hn has been tabulated, for the ground based radiometer problem, for 65 values of g between 0.0000 and 1.0000 and for 15 values of α'_L between 0.01 and 0.35. The values chosen for α'_L bracket all values characteristic of any of the 10 bands for the full range of midlatitude tropospheric conditions.

The geometry of the ground based radiometer problem is given in Figure 3.4. The lowest 10km of the atmosphere is divided into ten 1km thick layers or twenty 0.5km thick layers. A temperature and pressure for each layer was assigned based upon a surface pressure

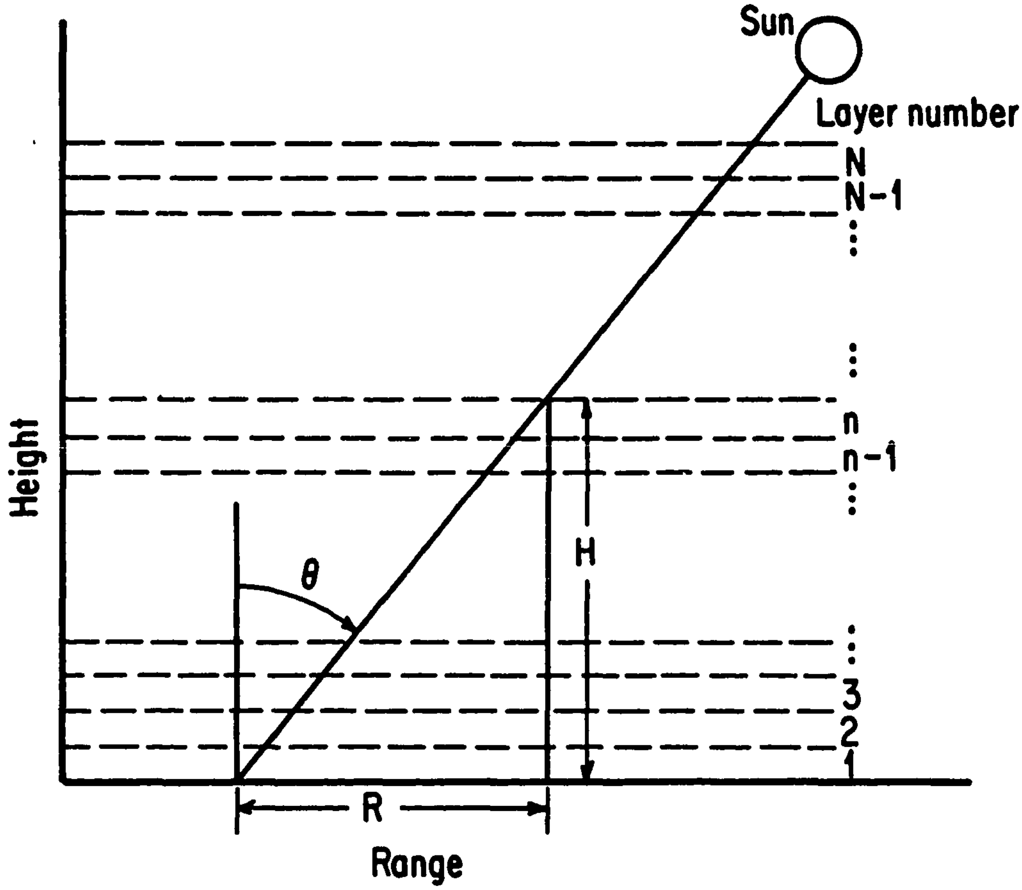

Figure 3.4. The geometry of the ground based radiometer problem where H is a height with an associated horizontal range R for the sun-radiometer line of sight

and temperature and an average lapse rate through the troposphere. A value for u_n was determined based upon the above information and upon an assumed distribution of atmospheric water vapor mixing ratio (U.S. Standard Atmosphere, 1976). Values for α'_{Ln} and S'_{0n} were interpolated for each band and layer from the previously constructed standard tables for each. The value of $h_n(g)$ for each band and layer may be determined by interpolating through α'_{Ln} for each of the 65 tabulated values of g.

The transmission for each band may now be determined by numerically integrating Equation 3.58, employing an 8th order Romberg integration. A Romberg integration of the 8th order makes use of 64 intervals in g or 65 points but yields a precision most analogous to a 256 interval trapezoidal integration; a discussion of the form of the Romberg integration is given in Stark (1970). For a homogeneous atmosphere, transmissions calculated via Equation 3.58 should agree exactly with transmissions determined via the analytic transmission function given by Equation 3.46. Comparisons conducted for a wide range of temperatures, pressures and total precipitable water show that for the full range of transmissions, from 0.0 to 1.0, the agreement is never worse than 4 significant figures and usually at least 5 digits. For inhomogeneous atmospheres comparisons of the transmission calculated for the ten layer atmosphere with the twenty layer atmosphere show agreement to 4 significant figures. On the basis of these two comparisons it is possible to assert that integration errors of Equation 3.58 do not significantly contribute to the uncertainty in transmission determination and therefore to the determination of the precipitable water. A full interval transmission may now be calculated by combining the transmissions for each band via Equation 2.7.

Discussion

The ultimate goal of this project is not the determination of the transmission of the $\rho\sigma\tau$ water vapor absorption band for a given set of atmospheric conditions but rather the goal is to determine the precipitable water given a measured water vapor absorption and a minimum of other a priori information.

The type of a priori information that is required seems to be limited to knowing the surface temperature and pressure. This effect can be seen in Figure 3.5 in which the negative of the log of the full interval transmission, called the effective optical depth, τ_e, is plotted against the square root of the vertical precipitable water, u, times the airmass, m. The airmass is approximately given by the secant of the solar zenith angle. In this figure there is a curve for average conditions in Tucson, Arizona (288K, 940mb) and two curves that yield the most extreme values of transmission for a given amount of precipitable water for conditions that commonly occur in Tucson. For a given effective optical depth these curves indicate that there is a wide range of $\pm 6\%$ in the implied precipitable water depending on the particular surface conditions. This indicates that for precipitable water determinations at least some accommodation for the ambient conditions needs to be made.

The three curves of Figure 3.5 were determined for an atmosphere within which the lapse rate is a constant 6.5K/km and the ratio u_n/u_1 is held constant for all n. These two assumptions do not have a great effect on the calculated transmissions because, since most of the water vapor in the atmosphere is located near the ground, the response to even fairly large variations from the above assumptions is quite small. This can be seen in Figure 3.6 which shows that about 75% of the precipitable water under average conditions lies below 3km and about 75% of the effective optical depth originates below 4km. Transmission calculations for lapse rates of 5°K/km and 10°K/km show an overall difference of 2% in the effective optical depth and therefore this effect is not of great importance.

The amount of water inferred from a radiometric measurement is not the vertical precipitable water but it represents a line of sight vapor amount, being the total amount of water vapor along the path from the sun to the radiometer. If, as is usually the case, a value for the vertical precipitable water is desired then it must be assumed that the atmosphere is horizontally homogeneous for some range about the radiometer location. The horizontal range, R, is associated with a height, H, below which a sizeable fraction of the water vapor exists. A reasonable value for H, from the previous discussion, is about 4km and since measurements are made for solar zenith angles of 30 degrees to 80 degrees, this implies the necessary horizontal range is on the order of 10 to 20km. This is a reasonable assumption and it will not

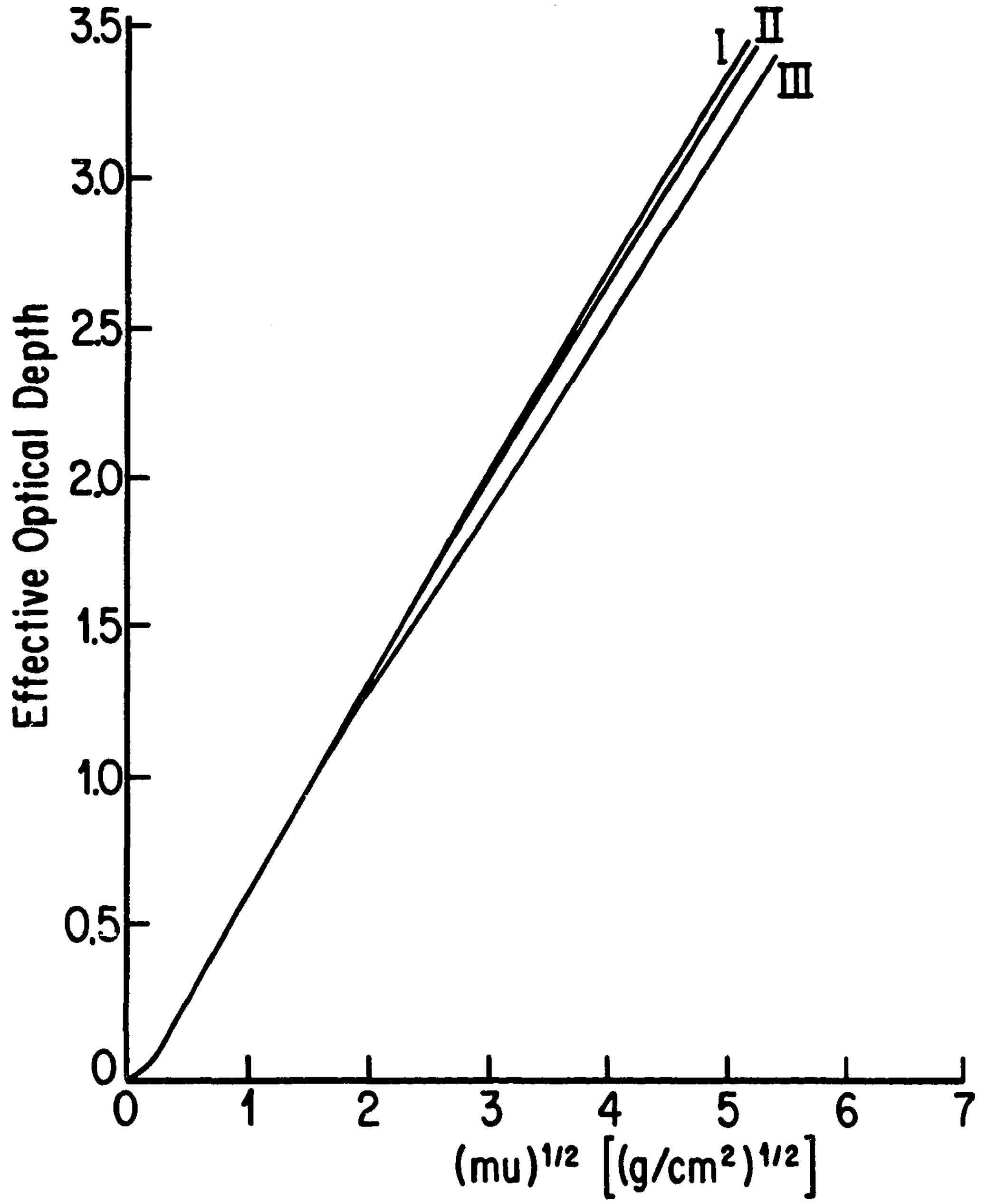

Figure 3.5. Effective optical depth as a function of mu for surface conditions of 280°K and 950mb (I), 288°K and 940mb (II), and 305°K and 920mb (III)

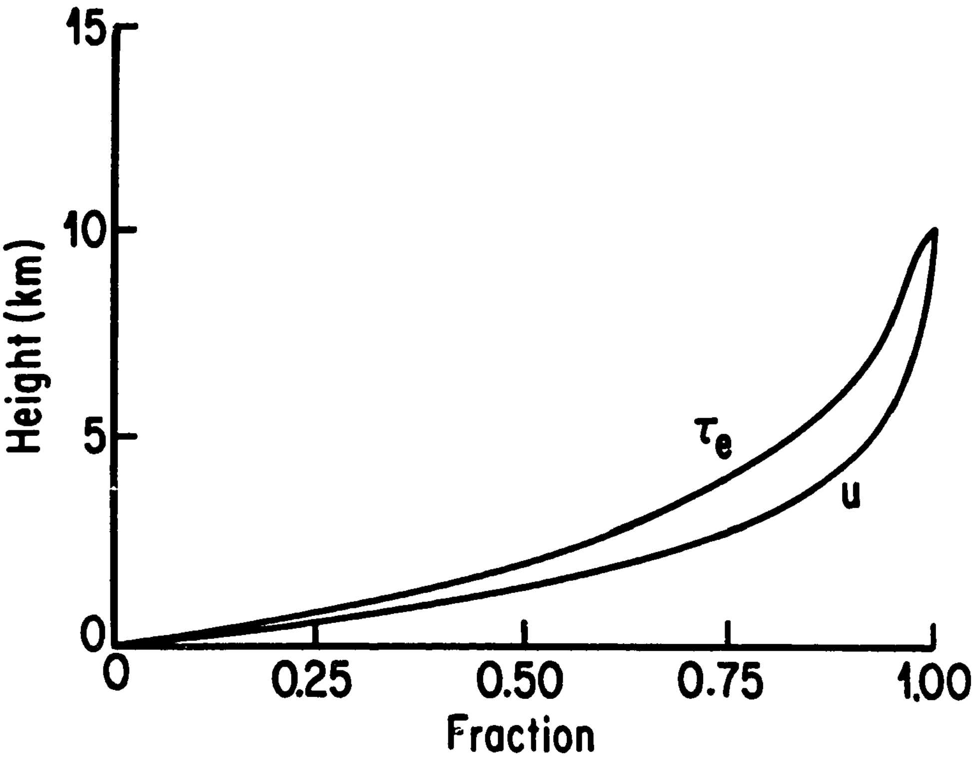

Figure 3.6. The fraction of effective optical depth, τ_e, one precipitable water originating below a given height for mean atmospheric conditions

normally add significantly to the uncertainty in determination of the local precipitable water.

Given a measured water vapor transmission and the surface temperature and pressure there are factors which contribute to uncertainties in the implied amount of atmospheric water vapor along the path. Among the more important of these factors are the specification of the equivalent Lorentz width α'_L, the effect of any failure in the correlated absorption coefficient assumption, and any random errors in the water vapor transmission value due to instrument error and/or to errors in the removal of the effect of attenuation by aerosols and molecular scatterers.

It is difficult to quantify the effect of the uncertainty in specifying α'_L because of the difficulty in separating the error from different sources. It is possible, however, to estimate a relative uncertainty in α'_L by defining the parameter in several different but appropriate ways and comparing the values that are determined. The variations in the α'_L ought to be indicative of the overall uncertainty in it.

As an alternative method of defining α'_L, it is possible to determine a value by using the first moment in conjunction with moments higher than the second. If the true band and the model band exactly coincided, then the value of α'_L would be independent of the moments used to define it. However, it is observed that α'_L is a weak function of the moments chosen to define it. In Table 3.1 for band 3 of the ground based radiometer, α'_L is given as determined via the

Table 3.1. Comparison of equivalent Lorentz line widths as determined from the moments of the absorption coefficient distribution for band 3 of the ground based radiometer and mean surface conditions

Order of Moment	Moment	α'_L
0	1.0	--
1	2.8027	--
2	68.687	0.0822
3	7,852.4	0.0854
4	140,080.0	0.0887

first and second through fourth moments, respectively, and it shows an overall variation of about 7%. Another method would be to simply use the standard method of defining α'_L as previously described. This approach yields values of α'_L that tend to be somewhat smaller than the moment defined method being from 20% smaller to 10% larger. This behavior is indicative of the inability of the model to correctly predict the full range of possible outcomes with a single value of α'_L.

The magnification of an error in a parameter y into an error in an effective optical depth estimate may be determined by defining the effective optical depth, τ_e, to be a function of the parameter to a power times a constant, or

$$\tau_e = ay^P \tag{3.60}$$

over a narrow interval in y. For a fractional error in the parameter y or $\pm\varepsilon_y$ the rectangular error in τ_e, ε_τ, is given by

$$\pm\varepsilon_\tau = (1 \pm \varepsilon_y)^P - 1. \tag{3.61}$$

This local power law may be expressed for an infinitesimal interval in y as

$$P = \frac{y}{\tau_e}\frac{d\tau_e}{dy}. \tag{3.62}$$

Choosing y to be absorber amount u, the local power law for the band equivalent optical depth given in Equation 3.19 is given by

$$P_u(x) = 2x(1 + 4x)^{-\frac{1}{2}}\,((1 + 4x)^{\frac{1}{2}} -1), \tag{3.63}$$

where x, as usual, is equal to $S'_0 u/\pi\alpha'_L$. For y equal to the equivalent Lorentz half width, α'_L, the local power law can be shown to be given by

$$P_\alpha(x) = 1. - P_u(x) \tag{3.64}$$

The functional forms of $P_\alpha(x)$ and $P_u(x)$ are given in Figure 3.7 and in the limit of small and large x, both functions exhibit the behavior expected from strong and weak line absorption considerations.

The variations in α'_L resulting from the different definitions of the parameter are on the order of 10% for the total spectral interval and this uncertainty is reflected in a corresponding uncertainty in the predicted value for the precipitable water. The error in the estimate of u due to an uncertainty in the effective optical depth is given by

$$\pm\varepsilon_u = (1. \pm \varepsilon_\tau)^{1/P_u(x)} - 1. \tag{3.65}$$

and, therefore, the error in u resulting from some uncertainty in α'_L can be expressed as

$$\pm\varepsilon_u = (1. \pm \varepsilon_\alpha)^{P_\alpha(x)/P_u(x)} - 1. \tag{3.66}$$

and for small values of ε_α, this can approximately be given by

$$\varepsilon_u = \varepsilon_\alpha \, P_\alpha(x)/P_u(x) \tag{3.67}$$

The functional form of $P_\alpha(x)/P_u(x)$ is given in Figure 3.7 from which it is apparent that for values of x normally encountered in the ground based radiometer problem, a consistent 10% uncertainty in α'_L for all the bands results in a 5 to 8% uncertainty in the prediction for u.

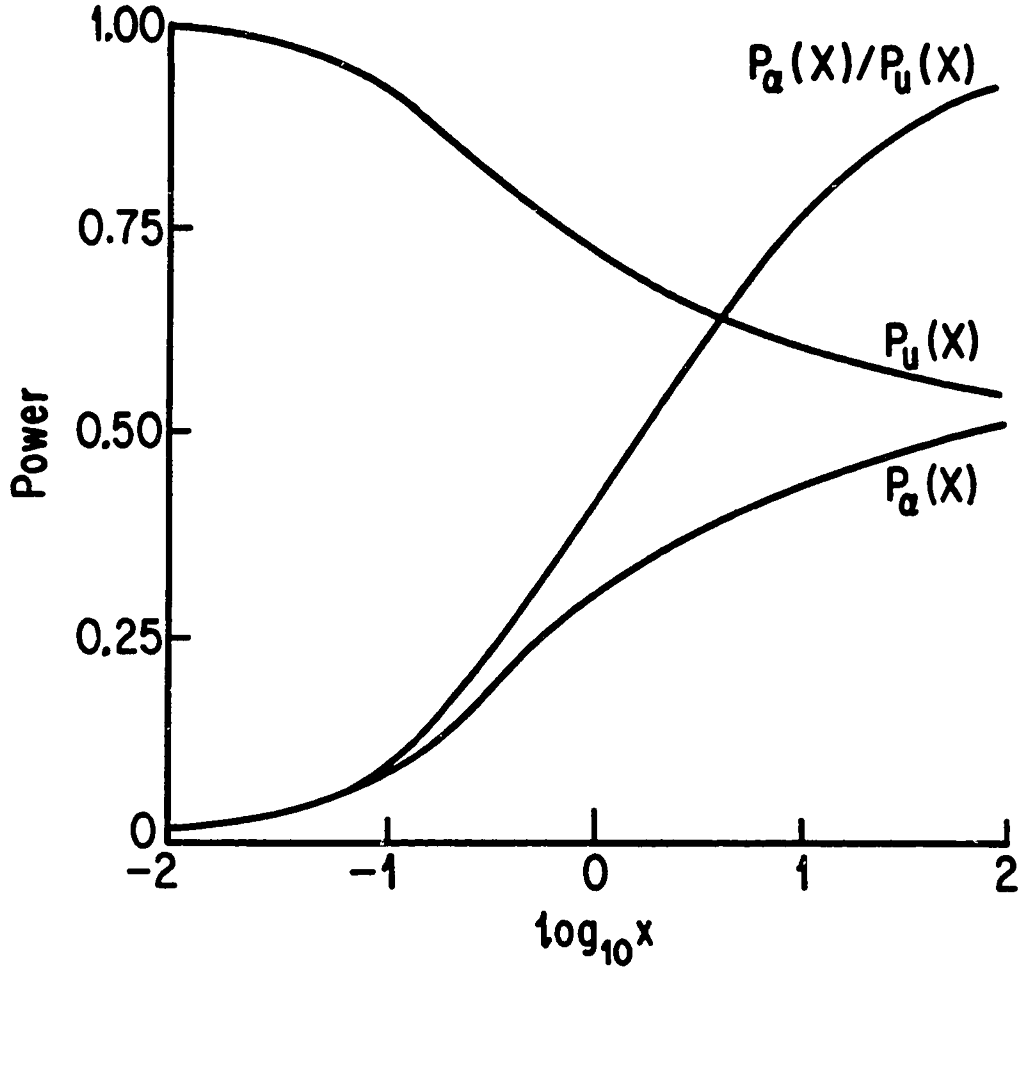

Figure 3.7. The local powers $P_\alpha(x)$, $P_u(x)$, and $P_\alpha(x)/P_u(x)$ as functions of x

This uncertainty is not random in nature but takes the form of biasing causing the predicted value for u to be consistently either too large or too small. Note that ε_u is defined such that it represents a 95% confidence level.

Random errors in the determination of the precipitable water are a result of random errors in the determination of the water vapor absorption either due to measurement errors or due to errors in the removal of the effects of the other attenuators. The effect of these random errors is given by Equations 3.65 or, for small ε_τ, it may be given by

$$\varepsilon_u = \varepsilon_\tau / P_u(x) \tag{3.68}$$

Therefore, random errors in the effective water vapor optical depth result in a random error in the precipitable water estimates whose magnitudes are from 1.3 to 1.8 times greater for dry and moist cases, respectively.

The final source of error in the determination of precipitable water is the effect of the assumption that the rank of the mass absorption coefficient at a given wavenumber is preserved from one layer in the atmosphere to any other. Another way of stating this is that the percentile rank of the absorption coefficient at any wavenumber within the band is assumed to be independent of temperature and pressure. The application of this assumption is usually called the correlated absorption coefficient method.

The correlation coefficient, ρ, between the mass absorption coefficient functions, $k(\nu)$, for two different layers in the atmosphere or equivalently between the functions at two sets of temperature and pressure is given by

$$\rho = \frac{<k_1(\nu)\ k_2(\nu)> - <k_1(\nu)> <k_2(\nu)>}{<(k_1(\nu) - <k_1(\nu)>)^2>^{\frac{1}{2}} <(k_2(\nu) - <k_2(\nu)>)^2>^{\frac{1}{2}}} \tag{3.69}$$

where the 1 and 2 subscripts indicate different layers. This equation may be evaluated relatively easily for both the Lorentz and Voight line shapes. In Figure 3.8, results showing the correlation between the $k(\nu)$ function for certain reference layers with the $k(\nu)$ function for layers above the reference layer are exhibited, for a temperature and pressure distribution as given by the 1976 U.S. Standard Atmosphere. The value of ρ decreases rapidly with the distance between the layers and has dropped below 0.9 for separations of only 6km. It is difficult to determine from a value of the correlation coefficient a measure of the uncertainty in determining the correct effective optical depth, τ_e, and therefore we will define a new test of the correlation assumption. To do this a new function, $g(\nu)$, is defined such that it represents the rank of absorption coefficient as a function of wavenumber for a given temperature and pressure. Then a significant determinator of appropriateness of the model would be the root mean squared difference between the $g(\nu)$ functions for different layers. This quantity, G, is defined by

$$G = <(g_1(\nu) - g_2(\nu))^2>^{\frac{1}{2}} \tag{3.70}$$

Under optimal circumstances the value of G would be zero whereas under the worst circumstances where $g_1(\nu)$ and $g_2(\nu)$ were independent of each

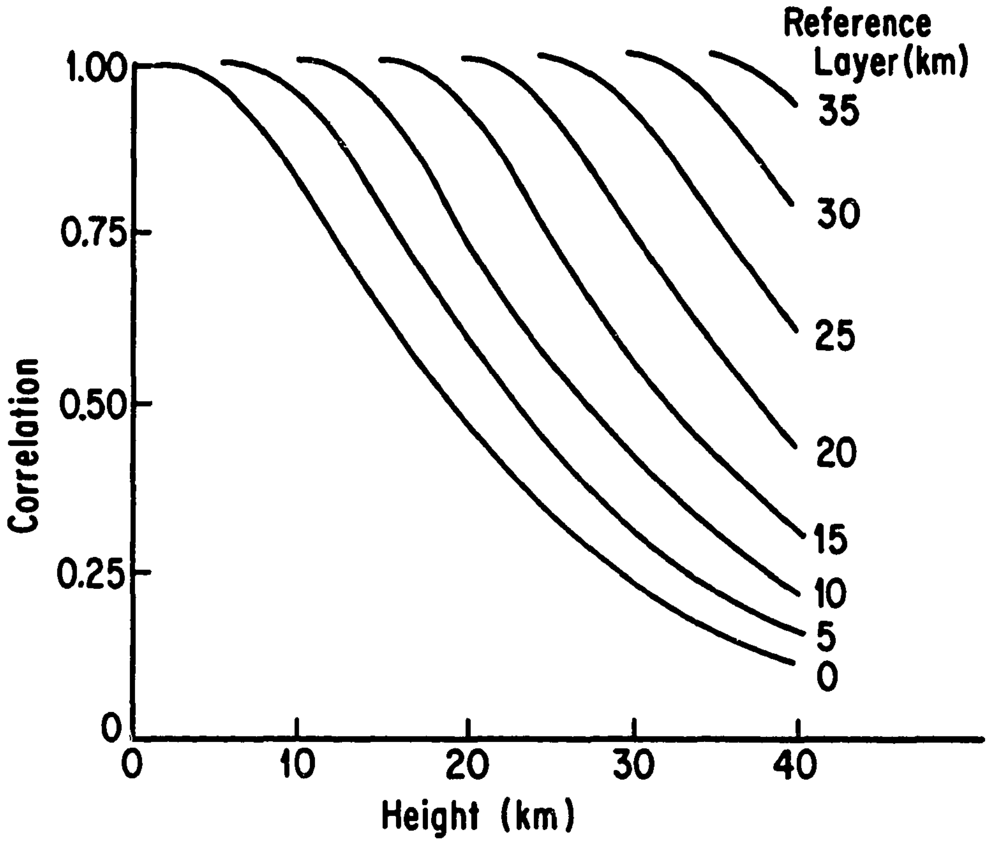

Figure 3.8. The correlation, ρ, of the k(ν) function for certain reference layers with the k(ν) for the layers above the reference layer; the calculation was performed for band 3 of the ground based radiometer's water vapor channel and standard atmospheric conditions

other then G would approach 0.408. This is a more appropriate test than the correlation coefficient since the model is more based on the preservation of rank with height than on correlation. The value of G for selected reference layers, 1, as a function of companion layer 2 is given in Figures 3.9a and 3.9b for band 2 of the ground based radiometer and band 7 of the SAGE II radiometer, respectively. It can be seen that G for a separation between the layers of 5km varies from 0.01 to 0.05. For greater separations G increases but the significance of the higher layer decreases rapidly since the water vapor density decreases rapidly with height.

It is now possible to estimate the error in determining the effective optical depth due to a partial failure in the assumption of complete rank preservation. To do this a two layer atmosphere is considered where one layer is at 300K and 1atm and the other is at 230K and 0.3atm and each layer has the same water vapor amount, u/2. In the model's ideal case, the band transmission would be evaluated via

$$T_b(u) = \int_0^1 e^{-(k_1(g)+k_2(g))u/2}\, dg, \tag{3.71}$$

and the total interval transmission, T(u), could be determined via Equation 2.7. From the evaluation of G, it can be seen that, for wavenumbers that in one layer all have absorption coefficient of rank g, rather than have an absorption coefficient of rank g in any other layer, exhibit a spreading of g that increases in width as the separation of the layers increases. This can be modeled by letting the absorption coefficient of rank g in layer 1 be associated with

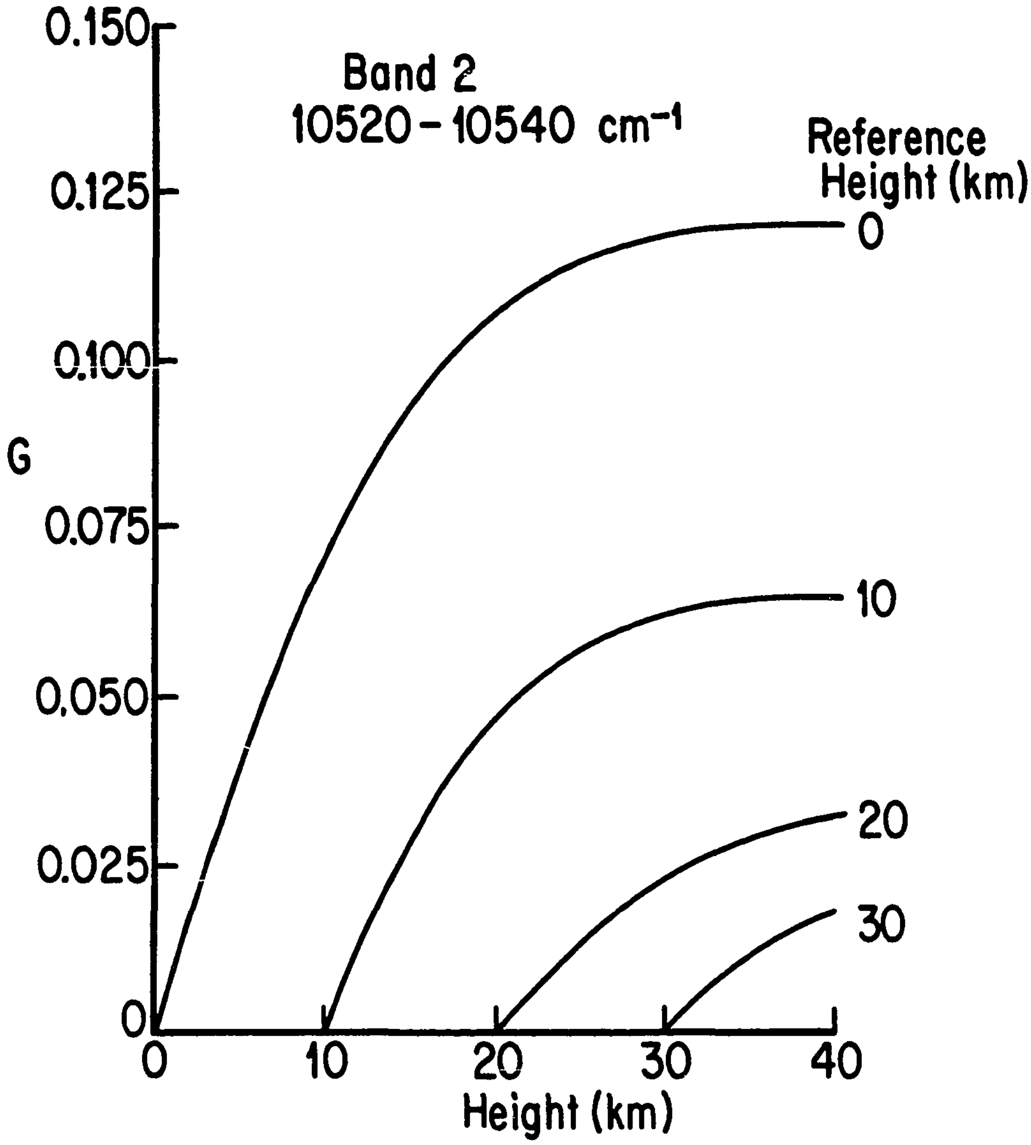

Figure 3.9a. The value of G for selected reference layers as a function of the companion layer for band 2 of the ground based radiometer's water vapor channel and standard atmospheric conditions

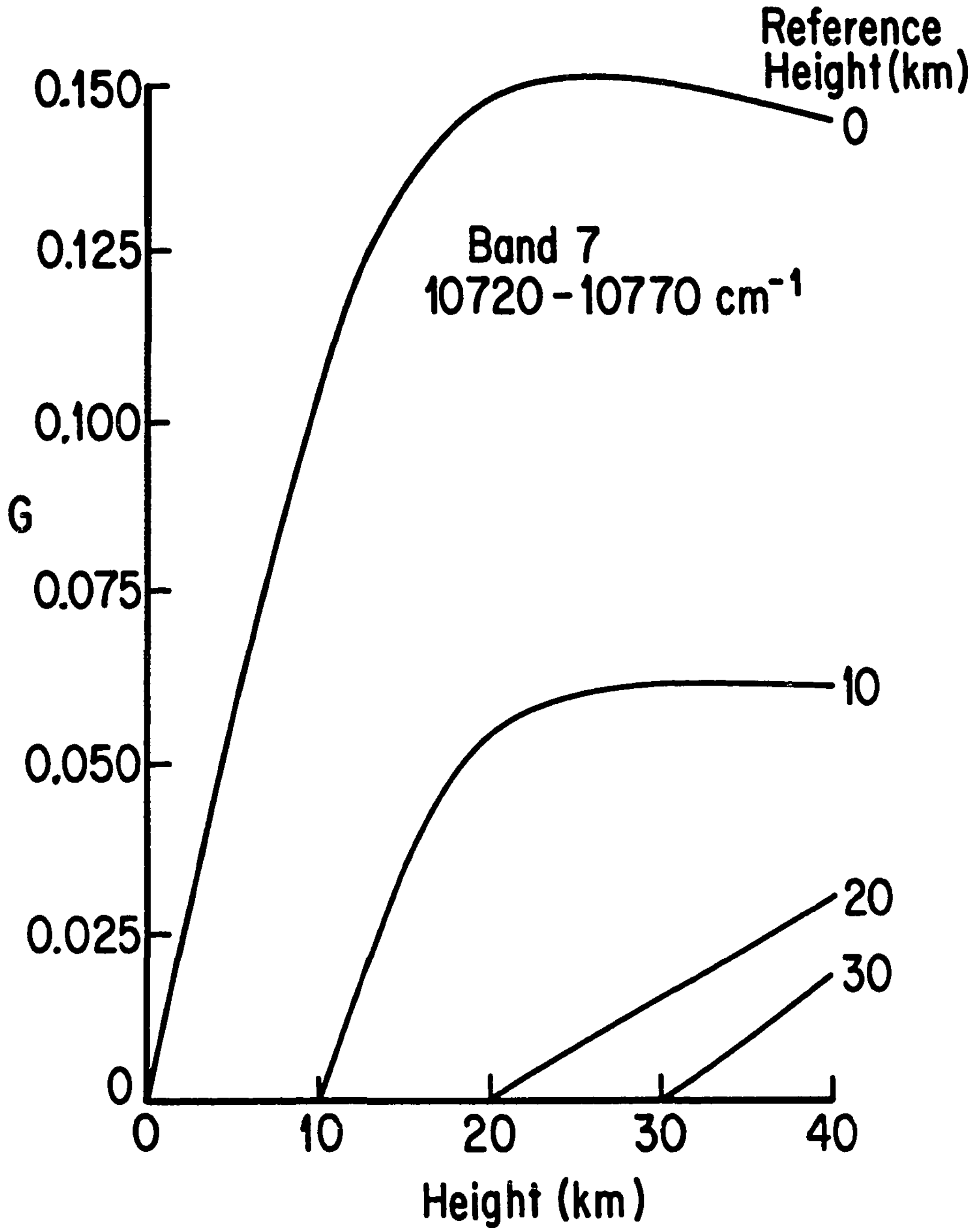

Figure 3.9b. The value of G for selected reference layers as a function of the companion layer for band 7 of the SAGE II radiometer's water vapor channel and standard atmospheric conditions

absorption coefficients of rank g - G, g, and g + G weighted by 0.2, 0.6, and 0.2, respectively. This yields a band transmission function of the form

$$\hat{T}_b(u) = \int_0^1 \exp[-(k_1(g) + 0.2k_2(g - G) + 0.6k_2(g)$$

$$+ 0.2k_2(g + G))\frac{u}{2}] \tag{3.72}$$

A total interval transmission function, $\hat{T}(u)$, can be determined via Equation 2.7. The error in determining the effective optical depth is expressed by

$$\text{Error} = -100. \cdot (\ln\hat{T}(u) - \ln T(u))/\ln\hat{T}(u) \tag{3.73}$$

and is shown in Figure 3.10 as a function of u and G. For Tucson, u is normally between $0.5 g/cm^2$ and $5.0 g/cm^2$ indicating that, as G is between 0.02 and 0.05, the correlation assumption leads to a 1 to 3% underestimation of the effective optical depth for a given water vapor amount. In terms of translating a measured water vapor τ_e into a precipitable water, this would mean a 2 to 6% overestimation. This is a rather severe test and this degree of error represents an upper limit estimate.

The most important test of any model is its ability to successfully predict from real data the parameter of interest. For the ground based radiometer the parameter of interest is precipitable water produced from a measured water vapor optical depth. In Figure 3.11 is displayed the result of such a test using data taken in the spring of 1984. In this test, radiometrically measured values of the water vapor

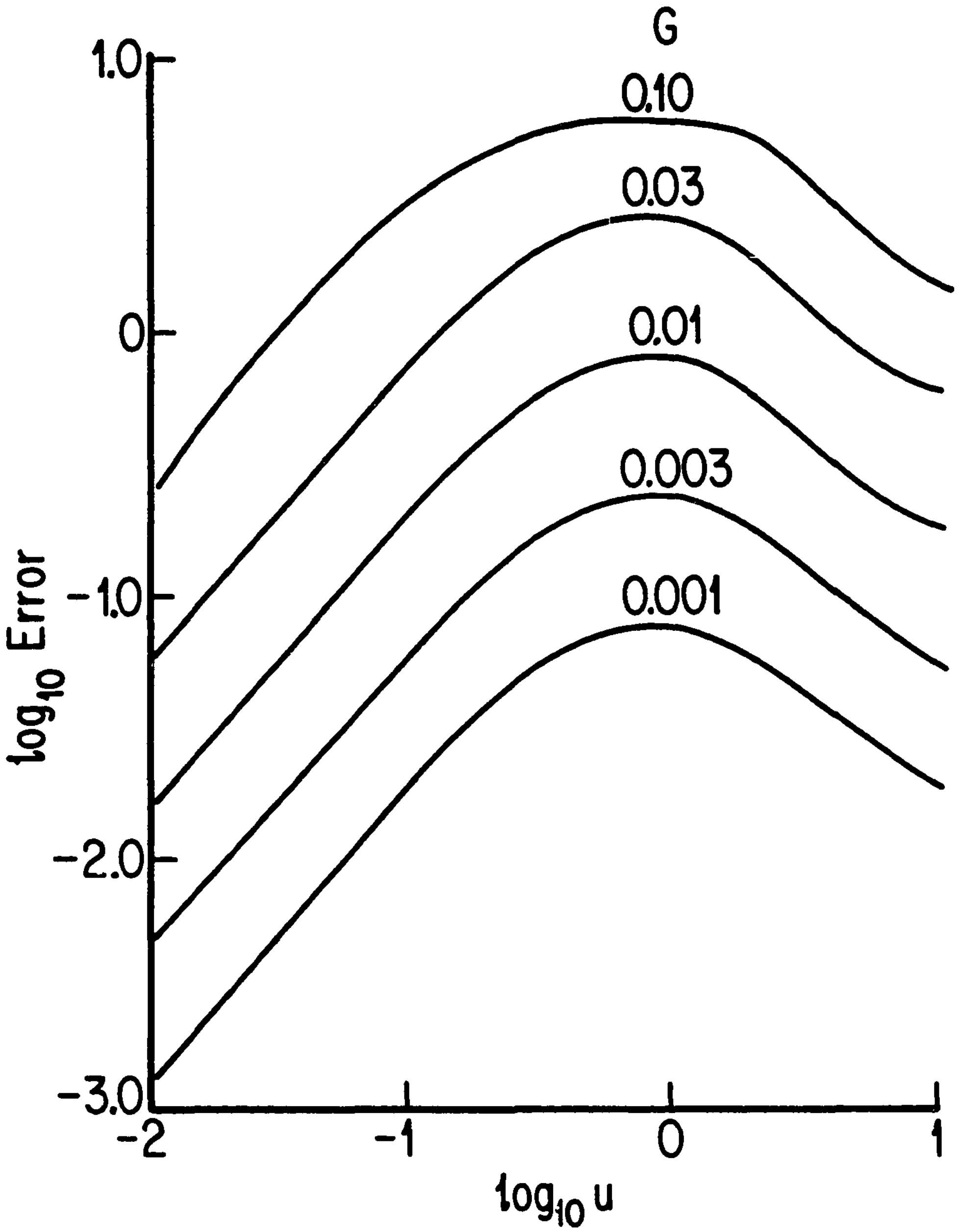

Figure 3.10. The dependence of the error introduced by the assumption of complete rank preservation on u and G

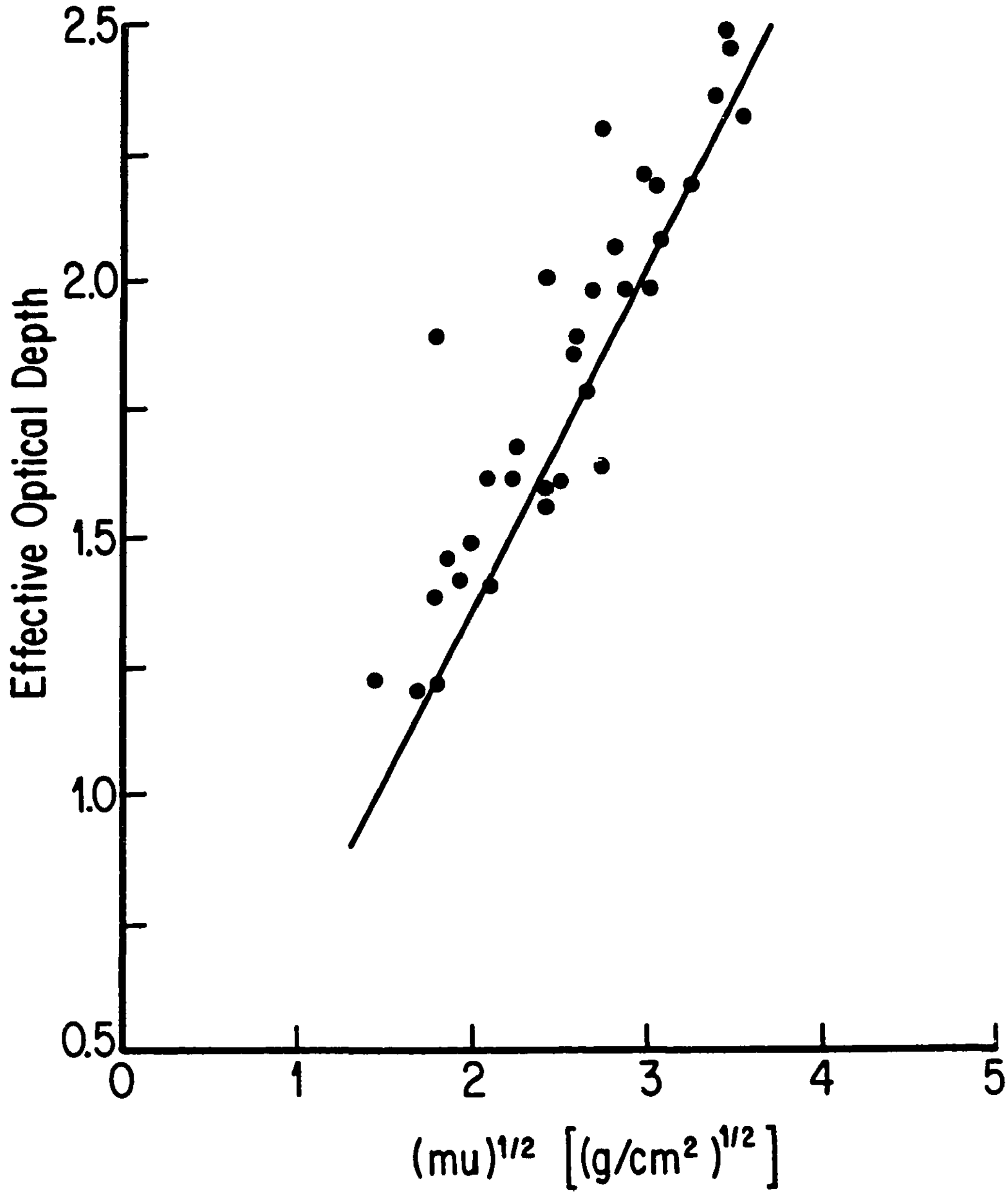

Figure 3.11. A comparison of radiometric and radiosonde determinations of precipitable water; the solid line is curve II from Figure 3.5 and the data points are measured water vapor effective optical depth versus radiosonde precipitable water times the airmass of the radiometer measurement

optical depth taken at an air mass of m were plotted against a precipitable water measurement as inferred from radiosonde measurements made by the NWS weather station located at Tucson International Airport. For convenience, the precipitable water was multiplied by the air mass associated with the radiometric measurement and then taken to the power of ½ as this made the figure somewhat easier to interpret. It should also be noted that the radiometer which is located at the University of Arizona campus and the airport are separated by about 10 miles and the times of measurements by the radiosonde and the radiometer were frequently separated by several hours. This leads to some increase in the scatter of the data points in Figure 3.11 due simply to natural geographic and temporal variations in the precipitable water.

The transmission model prediction of water vapor effective optical depth, τ_e, versus total absorber amount, mu, for average Tucson conditions, as previously shown in Figure 3.5 is also shown in Figure 3.11. The curve seems to predict the behavior quite well with an RMS disagreement with data points of 11%. This level of agreement is quite good since it is the product of errors from not only the model but also the radiometric determination of the water vapor optical depth and the radiosonde determination of precipitable water. The radiometric precipitable water systematically tends to overestimate the radiosonde precipitable water by about 4%. This biasing may originate in the model but the value thereof is not particularly worrisome and certainly does not effect the ability ofthe model to provide a calibration for the radiometric measurement of precipitable water.

In summary, the complete form of the transmission model has now been derived for the case of the ground based radiometric determination of precipitable water. The model can provide inexpensive calibrations for a wide range of atmospheric conditions that produce reasonable agreement with radiosonde determinations of precipitable water. The random difference between the two approaches is a satisfactory 11% with a minimal biasing evident. It is therefore clear that for the stated purpose of the real time monitoring of precipitable water, the method developed here is successful in providing the calibration required by the reduction of the radiometric data.

CHAPTER 4

THE RADIOMETRIC DETERMINATION OF STRATOSPHERIC WATER VAPOR DISTRIBUTIONS

To this point most of the discussion has been limited to the application of the transmission model to the determination of precipitable water from measurements made by a ground-based radiometer. In this chapter the application of the model to the determination of vertical water vapor distributions within the stratosphere from single channel transmission measurements made by a limb scanning satellite will be considered. There are several significant differences between the two problems. First, the geometry of the limb scan is much different from the geometry of the ground-based radiometer case. The Voight line shape must be considered rather than just the Lorentz line shape since in the stratosphere Doppler broadening is significant relative to pressure broadening. The final difference which must be addressed is that of retrieving vertical distributions of water vapor rather than columnar amounts as was previously the case. Thus a technique must be developed that will allow the reduction of measured transmission to water vapor density as a function of height.

In this chapter, these differences will be addressed and a stratospheric limb scan transmission model will be developed. The reliability of the model is discussed in terms of the effect of the model assumptions and an inversion process is defined and tested. Inversion of data taken by SAGE II is performed and compared to results obtained from an independent inversion process.

The Stratospheric Limb Scan Transmission Model

A limb scanning satellite such as SAGE II observed the sun through the earth's atmosphere along paths which do not intersect the surface of the earth. These paths are distinguished from one another by naming them for the height at which the path comes nearest to the earth, the tangent height Z_T. By rapidly scanning the satellite radiometer's field of view across the surface of the sun, as it rises or sets, it is possible to obtain transmission measurements for a wide range of tangent heights. In Figure 4.1, the geometry of a single transmission measurement is shown. The most pronounced difference between this geometry and that of the ground based case as shown in Figure 3.4 is that while in the ground based case the path length through each layer was the same, in the limb scan geometry, the path length is highly dominated by the lowest few layers. The paths would be similar if ground-based measurements were made for zenith angles of 90° but they are rarely made for zenith angles greater than 80°.

The geometric distance, $S_n(Z_T)$, that a path with tangent Z_T follows within a given layer is given by

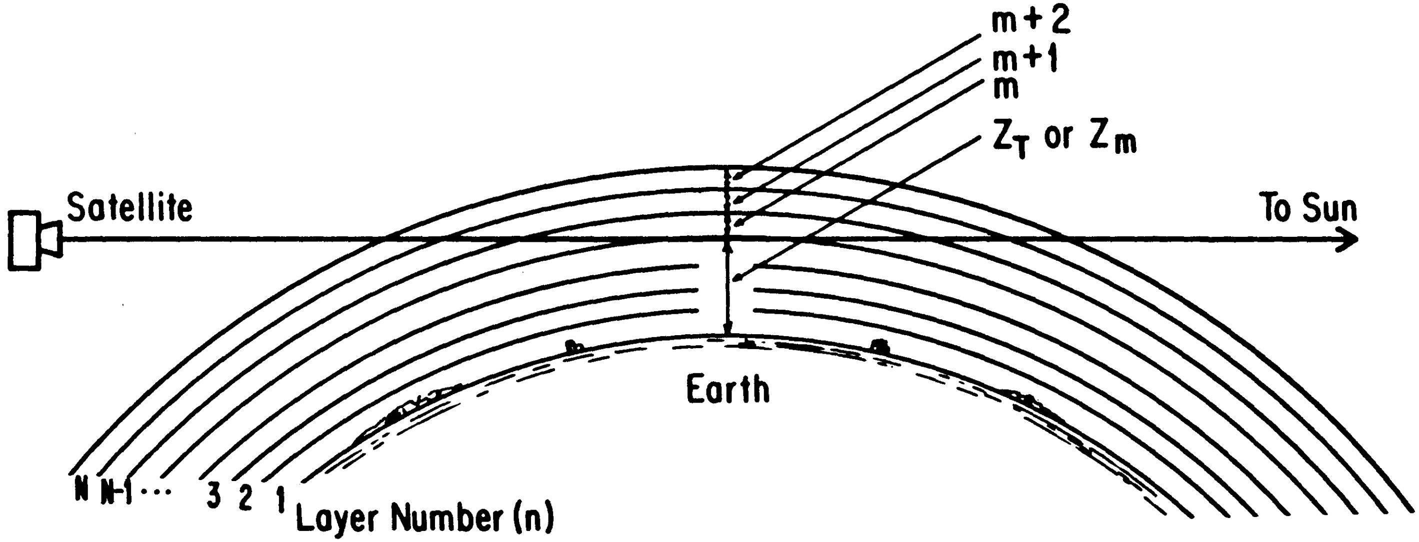

Figure 4.1. The geometry of a SAGE II measurement with a tangent height of Z_m

$$S_n(Z_T) = 2[((R_0 + Z_n)^2 - (R_0 + Z_T)^2)^{1/2} - ((R_0 + Z_{n-1})^2 - (R_0 + Z_T)^2)^{1/2}] \tag{4.1}$$

where Z_n is the height of the top of layer n, R_0 is the radius of the earth, Z_T is the lowest height the path reaches. This formulation neglects refraction which must be considered. Refraction in a spherical atmosphere is a well known process and as such will not be discussed here; the calculation of $S_n(Z_T)$ in a refracting atmosphere is discussed in Chu (1983).

The band transmission equation given in Equation 2.23 may now be written as

$$T_b(u(Z_T)) = \int_0^1 [\exp - \sum_{n=m}^{N} kn(g) q_n \rho_n S_n(Z_T)] \, dg, \tag{4.2}$$

where q_n is the water vapor mixing ratio in layer n, N is the total number of layers, ρ_n is the air density in layer n, and m is the lowest layer traversed by the path. The total path water vapor amount, $u(Z_T)$, is given by

$$u(Z_T) = \sum_{n=m}^{N} q_n \rho_n S_n(Z_T) \tag{4.3}$$

The atmospheric layers are defined so that the base of layer m is at the same altitude as the tangent point as shown in Figure 4.1. Therefore when reference is made to a specific path with a lowest layer of m, the tangent height will be called Z_m. For the SAGE II problem N is equal to 37 and the water vapor mixing ratio can be solved for measurements with tangent heights of 0 to 36km, though usually no useful data is taken for tangent heights below 5km.

The Determination of $k_n(g)$

Equation 4.2 may be evaluated in exactly the same manner as the band transmission function was solved in the ground based radiometer case except the function $k_n(g)$ as previously defined is no longer valid. This is because the absorption line shape throughout the stratosphere takes on considerable Doppler effects due to the low pressure observed there. The change of line shape can be seen in Figure 4.2 in which the height dependence of the Lorentz, Doppler and Voight half widths of a single line are shown. The Voight half widths were calculated using the formula given by Clough et al. (1981). In the line wings the shape is still essentially Lorentzian but near the peaks the line shape is significantly different and neglecting this difference would lead to sizeable errors in the calculation of transmission. Therefore it is necessary to be able to determine a functional form for $k_n(g)$, or at least $g_n(k)$, that is valid for the temperatures and pressures normally observed in the stratosphere and the resultant non-Lorentz line shape. The random frequency sampling technique described in Chapter 3 is the best means to build a valid assumption-free tabular form of $k_n(g)$. But, again as described in Chapter 3, computational considerations as well as storage considerations prohibit the use of this approach as we are seeking a

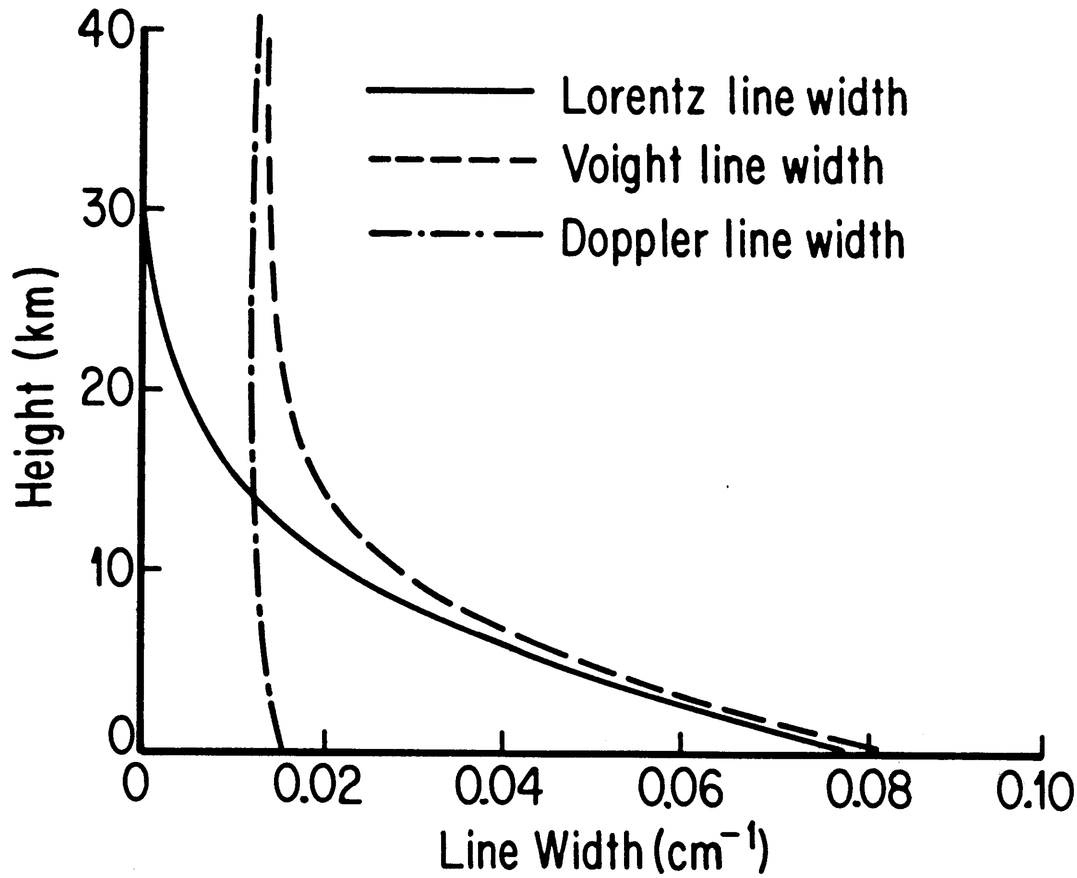

Figure 4.2. The dependence of the Lorentz, Doppler and Voight half widths on height for standard atmospheric conditions

computationally efficient method. Therefore we return to the use of model band transmission functions to allow the construction of our required tables of $k_n(g)$.

It can be shown that for a Malkmus type line strength distribution, the equivalent band optical depth for an arbitrary line shape is given by

$$\frac{W_m}{\delta} = \frac{1}{4\delta} \int_{-\infty}^{\infty} \ln[1 + 4S_o u f(\nu)] d\nu \tag{4.4}$$

where $f(\nu)$ is an arbitrary line shape function. If $f(\nu)$ is chosen to be the Lorentz line shape then W_m/δ can be shown to be given by Equation 3.19. If $f(\nu)$ is chosen to be the Voight line shape as given in Equation 3.5, Equation 4.4 is no longer soluble analytically and it must be solved numerically. By making use of the Voight line behavior of converging rapidly to the Lorentz line shape in the wings, it is possible to simplify the numerical integration by separating the integral into Lorentz and Voight portions in the form

$$\frac{W_{mv}}{\delta} = \frac{1}{2\delta} \int_0^{V_0} \ln(1 + 4S_o u f v(\nu)) d\nu + \frac{1}{2\delta} \int_0^{V_0} \ln(1 + 4S_o u \alpha_L/\pi/(\nu^2 + \alpha_L^2)) d\nu \tag{4.5}$$

where V_0 is the wave number where it is assumed that the line shape has become Lorentzian, α_L is determined by the moment method detailed in Chapter 3, and $f_v(\nu)$ is the Voight line shape. The second integral of Equation 4.5, called ψ, can be integrated analytically to obtain

$$\psi = \frac{\pi\alpha'_L}{2}\left(\left(1 + \frac{4S'_0 u}{\pi\alpha'_L}\right)^{\frac{1}{2}} - 1\right) - \frac{V_0}{2\delta}\ln\left(1 + \frac{4S'_0 u}{\pi\alpha'_L}\Big/\left(\left(\frac{V_0}{\alpha'_L\delta}\right)^2 + 1\right)\right)$$

$$- \alpha'_L\left(1 + \frac{4S'_0 u}{\pi\alpha'_L}\right)^{\frac{1}{2}} \tan^{-1}\left(\frac{V_0/\alpha'_L/\delta}{(1 + 4S'_0 u/\pi\alpha'_L)^{\frac{1}{2}}}\right)$$

$$- \alpha'_L \tan^{-1}(V_0/\alpha'_L/\delta). \qquad (4.6)$$

The parameters α'_L and S'_0 are defined for each band in the manner described in Chapter 3. A value of $0.2\mathrm{cm}^{-1}$ was used for V_0 as this represents an upper limit for the convergence of the Voight line shape into the Lorentz line shape.

The equivalent optical depths calculated for each band with Equation 4.5 are not tremendously different from using the Lorentz form of the equation. Throughout the troposphere the agreement between the two models is better than 1%. But within normal stratospheric conditions the disagreements increase with decreasing pressure until at the lowest pressures to be considered, about 5mb, there is about a factor of 2 difference between the band equivalent optical depths from each model. This verifies the previous assertion, that for tropospheric conditions the line shape may be considered to be the Lorentz line shape. On the other hand the determination of $k_n(g)$ for stratospheric conditions must be based upon the Voight line shape.

One way that $k_n(g)$ may be determined is to calculate the transmission of a particular band for a particular temperature and pressure via Equation 4.5. By examining Equation 2.18, it can be seen that the band transmission function is a Fredholm integral of the first kind and as such p(k) may be found using standard linear inversion techniques (Twomey, 1977). Unfortunately, it is found that the inversion is unstable and that the solution must be constrained to exhibit certain a priori characteristics. This instability takes away from the attractiveness of this approach and when combined with the same storage problems as the random frequency sampling technique, it becomes apparent that the linear inversion approach is not viable for this application.

The approach that will be employed is based upon the observation that while the Voight line shape is different from the Lorentz line shape, both are highly peaked functions which for the conditions we are considering here resemble each other quite a bit. It is assumed, therefore, that the functional form of the equivalent band optical depth is the same for the Voight line shape as for the Lorentz, or

$$\frac{W_{mv}}{\delta} = \frac{\pi\alpha'_v}{2}\left(\left(1 + \frac{4S_0u}{\pi\alpha'_v}\right)^{\frac{1}{2}} - 1\right) \tag{4.7}$$

where α'_v is an equivalent voight line width, which is in general unknown, and W_{mv} is the equivalent line width for a Malkmus line strength distribution and a Voight line shape. Solving this expression for the equivalent Voight line width yields

$$\alpha'_v = \left(\frac{W_{mv}}{\delta}\right)^2 / \pi\left(S'_0u - \frac{W_{mv}}{\delta}\right). \tag{4.8}$$

For a specified band, temperature, pressure and absorber amount, the only unknown on the right hand side of Equation 4.8, W_{mv}, may be found by numerically evaluating Equation 4.5. A numerical value of α'_v may now be determined through the evaluation of Equation 4.8. It is observed that α'_v is a function of u with the strongest variations occurring at the greatest heights. This variation indicates at least some problem in our assumption.

By defining a parameter $\bar{u}$ to be the standard atmospheric water amount associated with the limb path with a tangent point of the given pressure, a standard value of α'_v is chosen to be that given by Equation 4.8 evaluated for an absorber amount of $\bar{u}$. Using a single value of α'_v will cause errors in estimating the absorber amount u when it is not equal to $\bar{u}$. The fractional error may be estimated by the expression

$$\varepsilon_u = -(\alpha'_v(u)/\alpha'_v(\bar{u}) - 1.)\ P_\alpha(x)/P_u(x) \qquad (4.9)$$

where $P_\alpha(x)$ and $P_u(x)$ are the local powers as defined in Chapter 3. In Figure 4.3, the value of ε_u is shown for band 7 of the SAGE II radiometer, as a function of u for selected pressures. Band 7 exhibits the greatest variations of all the bands in α'_v as a function of u. The value of ε_u is greatest for pressures between 50 and 100mb where it is as large as 0.05. The reason for this maximum is that while the variations in α'_v (u) increase with decreasing pressure the value of $P_\alpha(x)/P_u(x)$ decreases with decreasing pressure. In Figure 4.4, the value of ε_u for the entire spectral interval is shown and the peak value again occurs between 50 and 100mb but reaches a maximum amplitude of only about 3%.

The assumption that the equivalent band optical depth, as given in Equation 4.4, can be approximately described by the Lorentz model

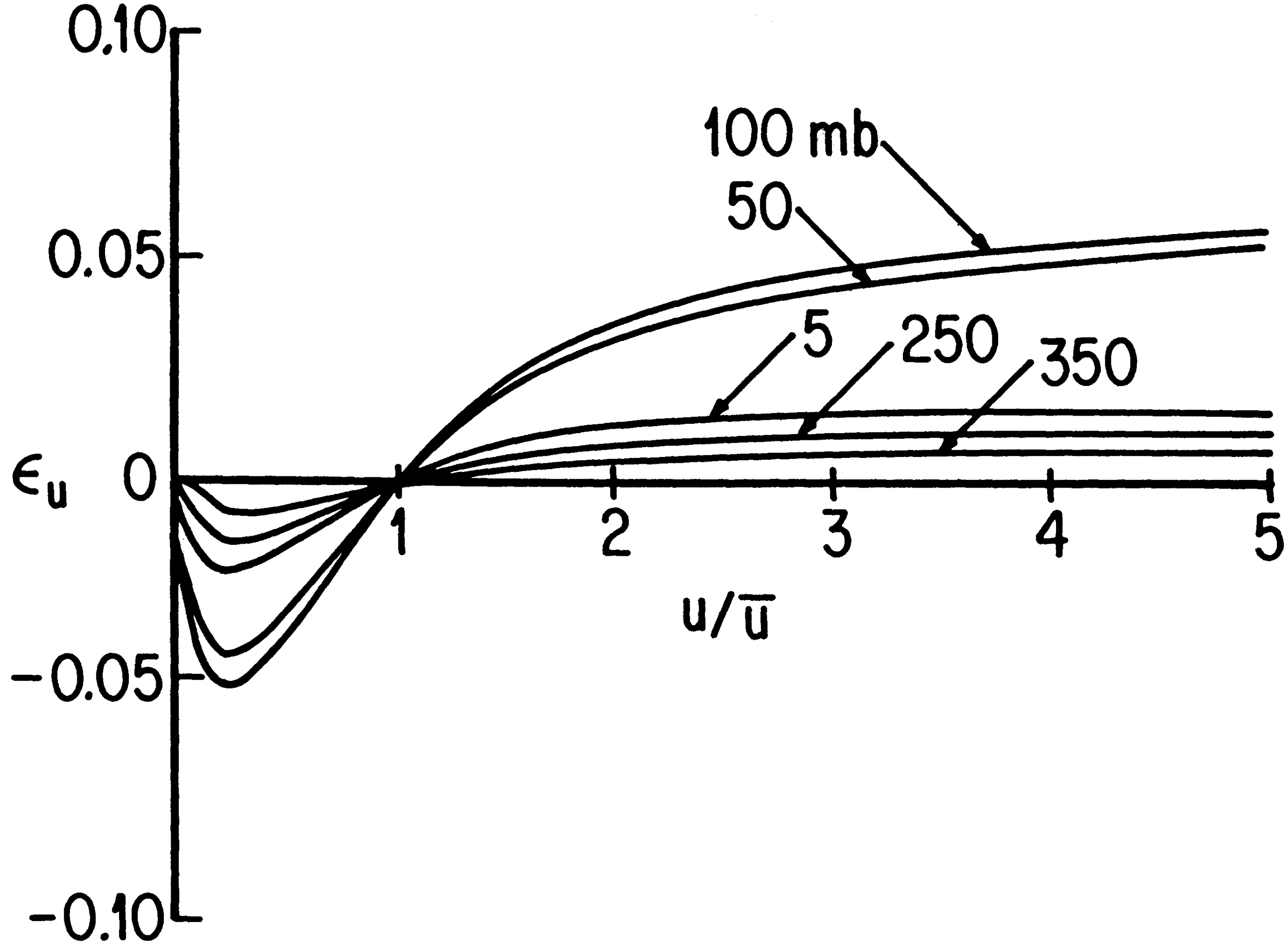

Figure 4.3. The fractional error, ε_u, in the estimation of the path water vapor amount, u, due to the assumption that the Voight transmission function has the same form as the Malkmus transmission function. ε_u is shown for band 7 (10,720-10,770 cm^{-1}) of the SAGE II radiometer and for selected heights

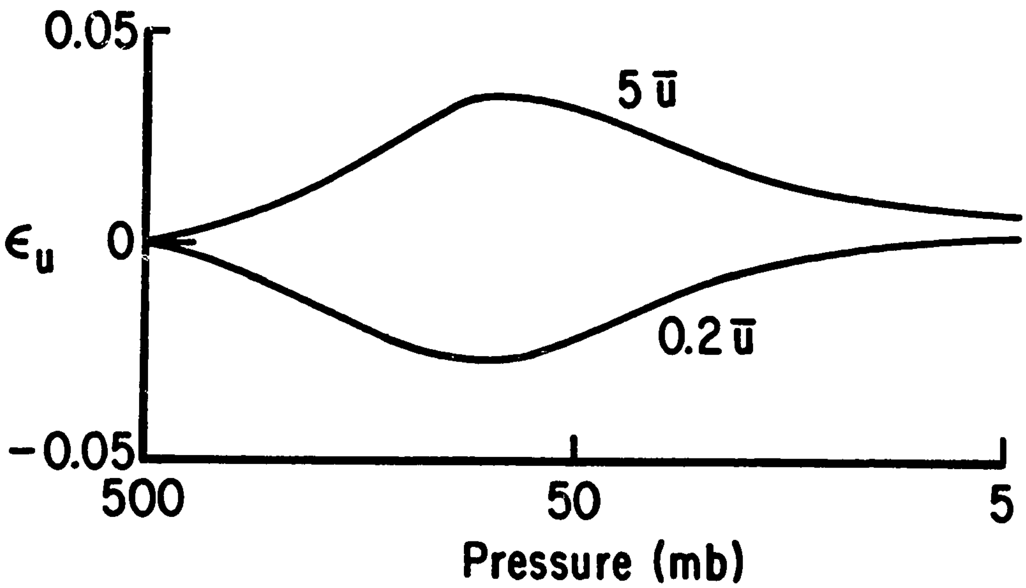

Figure 4.4. The fractional error, ε_u, in the estimation of the path water vapor amount, u, due to the assumption that the Voight transmission function has the same form as the Malkmus transmission function. ε_u is shown as a function of height for the total interval and selected water vapor amounts

where the equivalent Lorentz half width is replaced with an equivalent Voight half width seems to be reasonably sound. The disagreement between the results given by Equations 4.4 and 4.7 is not so large to be of great concern especially in view of the other assumptions inherent in the derivation of Equation 4.5. It is difficult to state whether the disagreement between the two models degrades or improves the overall performance of the transmission model. In fact, the equivalent optical depth given by Equation 4.7 may be considered a true Voight transmission function except for a slightly different line strength distribution than that suggested by Malkmus. From this perspective the model employed herein may be considered to be quasi-Malkmus.

One way to confirm the propriety of the model is to compare a random frequency sampling determination of the cumulative absorption coefficient density function with the model form of it. The model form of g(h) is given by Equation 3.59 with α'_V replacing α'_L. Such a comparison is shown in Figure 4.5 for band 7 and mid-stratospheric conditions. The overall agreement is at least as good as the agreement for tropospheric conditions as shown in Figure 3.3 and is especially good for h greater than 0.9. Since the transmission of the atmosphere is very high throughout the stratosphere, this augurs well for the determination of transmission since larger values of h dominate the calculation when transmission is high.

The limb band transmission function may now be written as

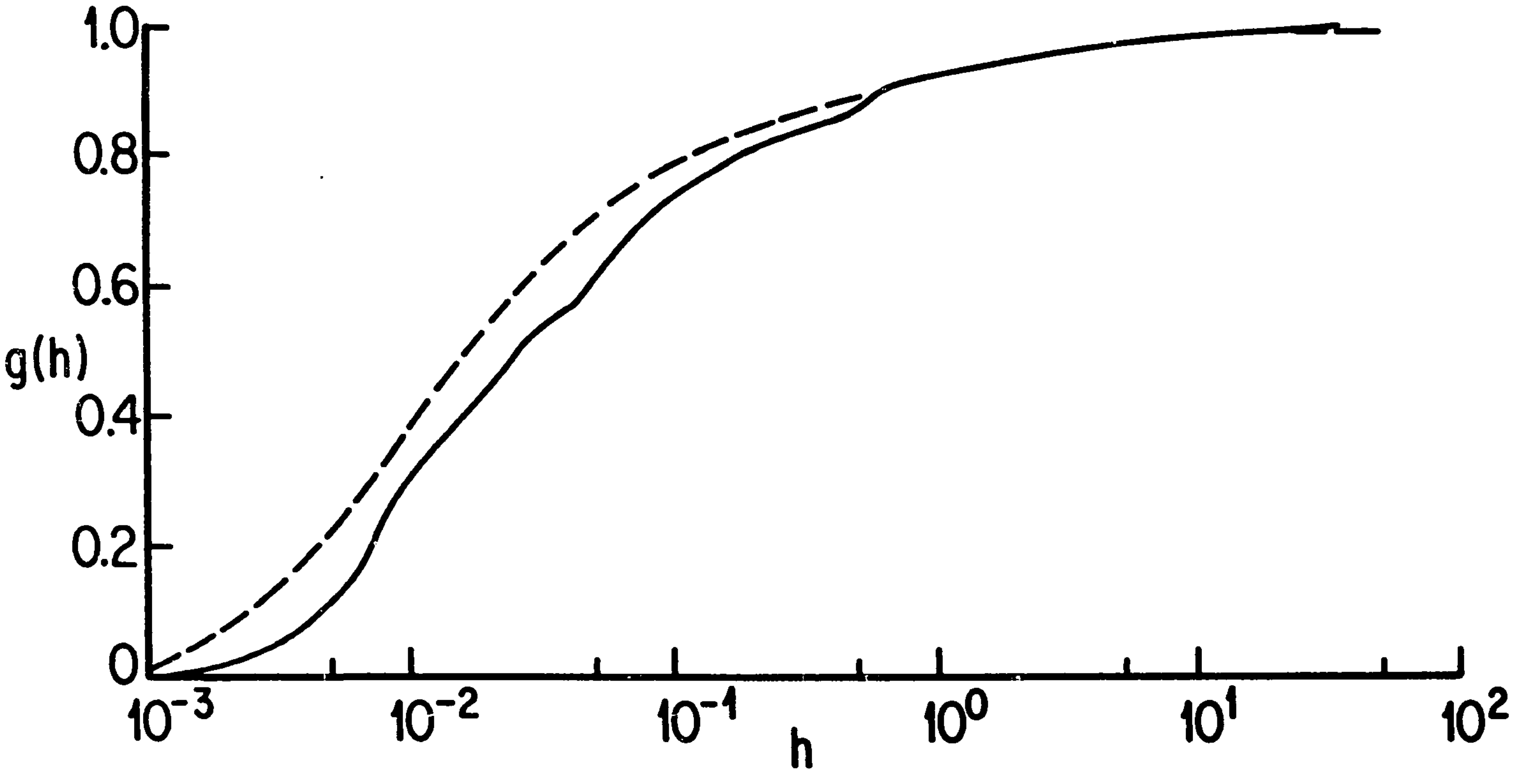

Figure 4.5. The model g(h) (dashed) and the true g(h) (solid) for band 7 of the SAGE II radiometer and mid-stratospheric conditions

$$T_b(u(Z_m)) = \int_0^1 \exp[-\sum_{n=m}^{N} S'_{0n} h_n(g) q_n \rho_n s_n(Z_m)] dg \tag{4.10}$$

where $h_n(g)$ is given by the inverse of

$$g_n(h) = \frac{1}{2} [e^{\pi\alpha'_{vn}} \operatorname{erfc}[\sqrt{\frac{\pi\alpha'_{vn}}{4h}} + \sqrt{\frac{\pi\alpha'_{vn} h}{4}}]$$
$$+ \operatorname{erfc}[\sqrt{\frac{\pi\alpha'_{vn}}{4h}} - \sqrt{\frac{\pi\alpha'_{vn} h}{4}}]]. \tag{4.11}$$

For each band, tables of the values of S'_0 and α'_L for a range of temperatures and pressures were created by previously described processes from which the values of α'_{vn} and S'_{0n} may be interpolated based upon the temperature and pressure of the layer. The value of $h_n(g)$ is tabulated as in the tropospheric case, for 65 values of g and a range of values of α'_v which includes all normally observed values thereof. The value of the band transmission may then be found as a function of tangent height for a given vertical temperature, pressure, and mixing ratio distribution in the same manner as the band transmission function was evaluated in Chapter 3. By employing an 8th order Romberg integration and interpolating to $h_n(g)$ based upon the value of α'_{vn} in the layer, it is found that the numerical integration of Equation 4.10 is accurate to at least four decimal places. Comparison of 0.5km and 1.0km layer thicknesses show no appreciable differences in the calculated value of transmission, indicating that the use of 1km thick layers does not degrade the evaluation of the integral. Therefore, as in the tropospheric case, the evaluation of the integral does not significantly add to the uncertainty in a calculated band transmission for any given set of atmospheric conditions. The transmission for the entire interval may be calculated by evaluating Equation 4.10 for each band and then combining them via Equation 2.7.

The Determination of the Vertical Water Vapor Distribution

The goal of this project is not to determine transmittance for limb paths through the stratosphere but to use measured water vapor transmittances to infer vertical water vapor distributions. Since the relationship between transmission and the vertical water vapor distribution is not linear, the determination of q(z) or rather q_n for all n cannot be directly performed. In this section an iterative reduction technique will be developed that is both numerically stable and rapidly convergent.

The derivation of the reduction technique is started by recalling from Chapter 3 that it is possible to define a local power law relating the dependence of two parameters by the expression

$$P_x = \frac{x}{y}\frac{dy}{dx} \tag{4.12}$$

where $y = ax^{P_x}$ over some interval in x. If y is defined as the effective water vapor optical depth, that is the negative of the natural logarithm of the transmission for the total interval, $\tau_e = -\ln(T(u))$, and x is the absorber amount, then it is possible to determine a local power law for any limb path. This may be expressed as

$$P_u(Z_T) = \frac{u(Z_T)}{\tau_e(Z_T)}\,\frac{d\tau_e(Z_T)}{du(Z_T)}. \tag{4.13}$$

$P_u(Z_T)$ is dependent not only on u and Z_T but also on the temperature and pressure at and above the tangent point. Rather than determining $P_u(Z_T)$ as a function of temperature and pressure, a standard set of $P_u(Z_T)$ curves is determined for standard atmospheric conditions. This is done by first determining a set of curves of $\tau_e(Z_T)$ versus $u(Z_T)$ for standard atmospheric conditions (U.S. Standard Atmosphere, 1976) via Equations 4.10 and 2.7. The value of $u(Z_T)$ was varied in order to include all possible conditions by multiplying the standard distribution of water vapor mixing ratio by a constant whose value was between 10^{-3} and 10^{+3}. The standard curves of $\tau_e(Z_T)$ are shown in Figure 4.6. Standard curves of $P_u(Z_T)$ are found from the information contained in Figure 4.6 and are themselves shown in Figure 4.7.

For the reduction technique, the information of Figure 4.6 was tabulated such that $u(Z_T)$ was given as a function of the effective optical depth and the tangent height. Figure 4.7 was tabulated such that $P_u(Z_T)$ was given as a function of $u(Z_T)$ and tangent height. Given a measured value of effective optical depth for a limb path m with tangent height Z_m, it is now possible to estimate the value of $u(Z_m)$ by interpolating across the tabulated form of Figure 4.6 with respect to effective optical depth and tangent height. For instance, if Z_m is 20km and τ_e(20km) was determined to be 0.1, indicating a total interval transmission of 0.905, u(20km) can be estimated to be 0.36g/cm^2. Therefore for a set of effective optical depth measurements, it is possible to estimate a corresponding set of path water vapor amounts. Note that the measurements are made such that they have

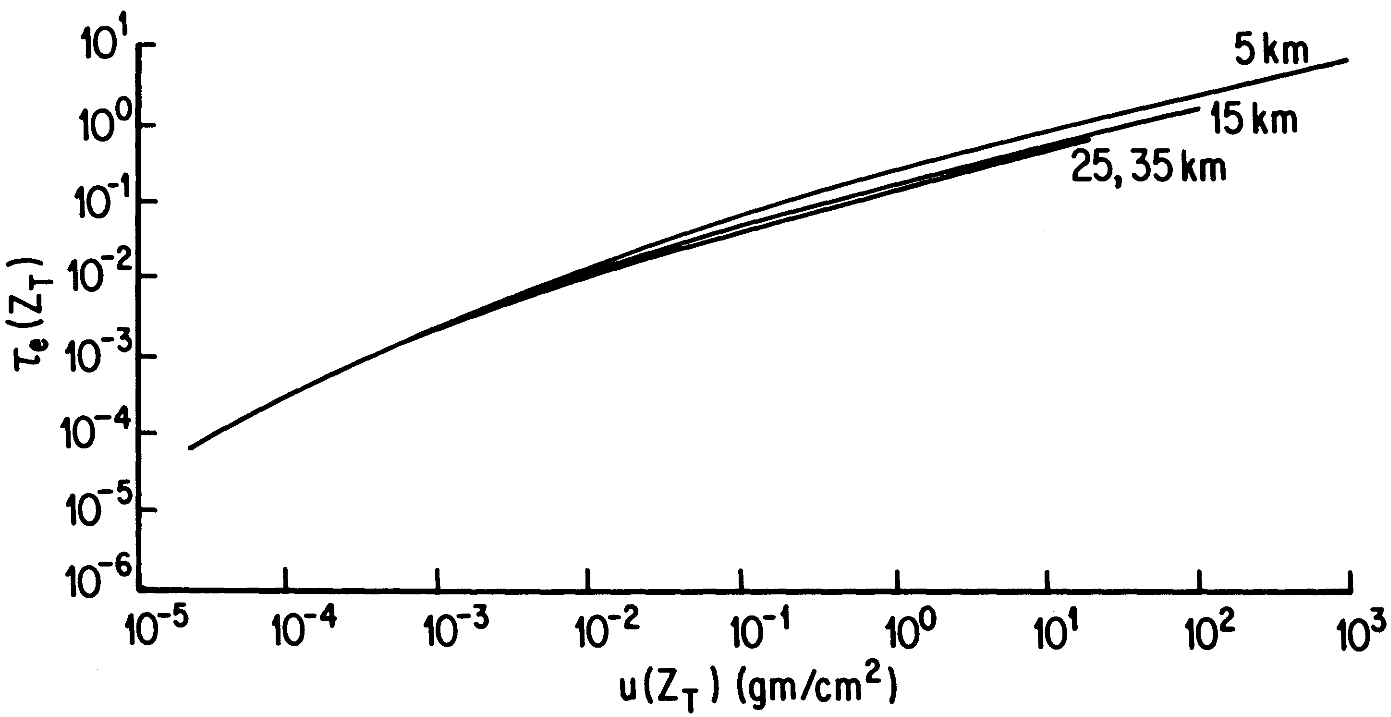

Figure 4.6. The effective optical depth as a function of total path water vapor, $u(Z_T)$, for selected tangent heights and standard atmospheric conditions

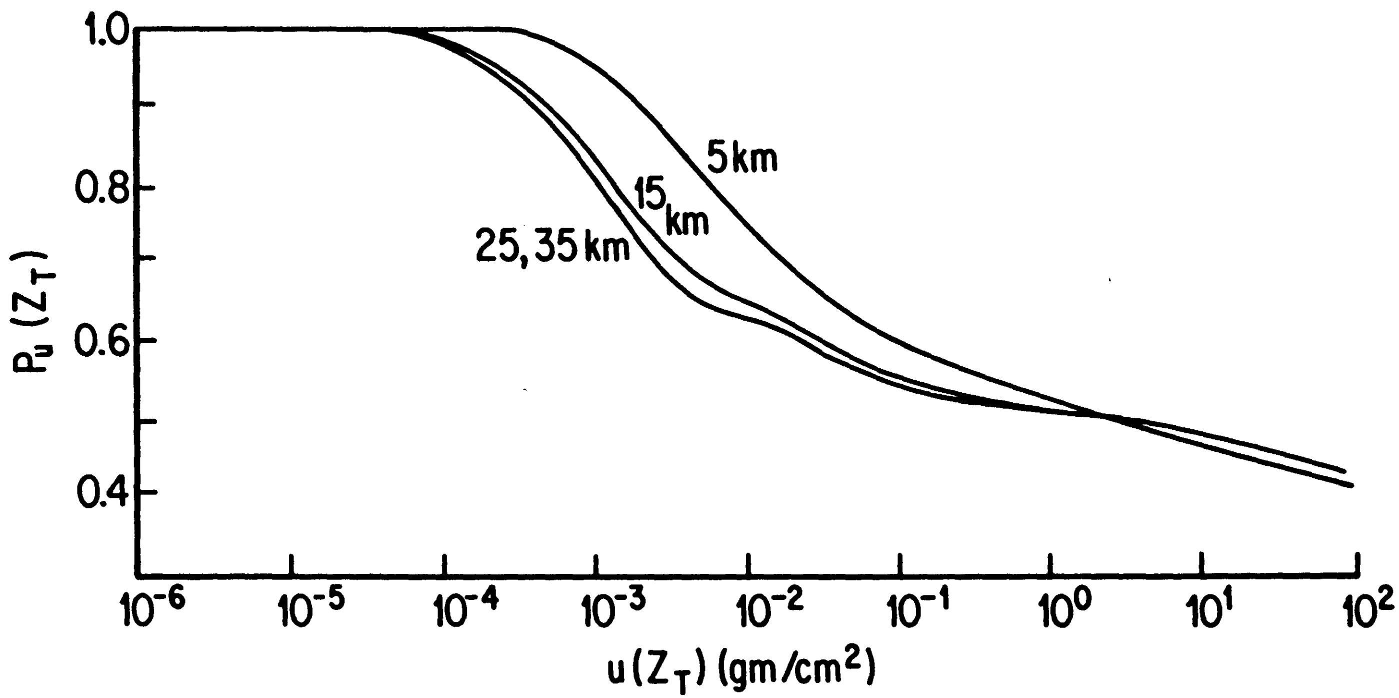

Figure 4.7. The local power $P_u(Z_T)$ as a function of $u(Z_T)$ for selected tangent heights and standard atmospheric conditions

tangent heights spaced 1km apart and are defined such that they end at the base of the last layer in the transmission calculation, usually 36km.

The relationship between $u(Z_m)$ and the water vapor mixing ratio distribution with height is given by Equation 4.3. With the set of $u(Z_m)$ estimates it is possible to record this relationship in matrix form as

$$\underset{\sim}{u} = D\underset{\sim}{q} \tag{4.14}$$

where u_m is $u(Z_m)$, q_n is the mixing ratio in layer n and D_{mn} is given by

$$D_{mn} = \rho_n S_n(Z_m) \tag{4.15}$$

for $n \geq m$ and by

$$D_{mn} = 0. \tag{4.16}$$

when $n < m$. The true pressure and temperature distributions with height are presumed to be known and the air density ρ_n and path length, $S_n(Z_m)$, within layer n for a limb path of tangent height Z_m are computed for the true atmospheric conditions. The so-called onion skin solution for $\underset{\sim}{q}$ is then given by

$$\underset{\sim}{q} = D^{-1}\underset{\sim}{u} \tag{4.17}$$

and a least squares solution for $\underset{\sim}{q}$ is given by

$$\underset{\sim}{q} = (D^T D)^{-1} D^T \underset{\sim}{u} \tag{4.18}$$

where the T superscript indicates a matrix transpose. Solutions for $\underset{\sim}{q}$ from the two above approaches are nearly identical because the determination of q_n is highly dominated by the value of u_n. The reduction employed here uses the least squares solution for $\tilde{q}$.

The vectors $\tilde{u}$ and $\tilde{q}$ represent the first guess solutions for the water vapor distribution and are designated as such by $\tilde{u}^1$ and $\tilde{q}^1$. Since $\tilde{u}^1$ is based upon a model atmosphere whose temperature and pressure distributions may be in significant variance with the true atmosphere, the values of $\tilde{u}^1$ and $\tilde{q}^1$ may be significantly in error. A first guess estimate of the effective optical depth for tangent height Z_m may be determined by employing Equations 4.10 and 2.7 where ρ_n, $S_n(Z_m)$, S'_{0n} and α'_{vn} are determined in accordance with the true atmospheric conditions and q_n is chosen to be equal to $q_n^{\ 1}$; this estimate is designated by $\tau_e^{\ 1}(Z_m)$. Comparisons of $\tau_e^{\ 1}(Z_m)$ with the measured value, $\tau_e(Z_m)$, typically show disagreements of 0 to 50%; the size of which is indicative of the validity of the first guess values of $\tilde{q}$ and $\tilde{u}$. Ideally the iterative technique to be described will reduce these differences to essentially zero.

A second guess of $u(Z_m)$ may be determined by applying the local power law assumption previously used to estimate error magnification. From Equation 4.13, it can be seen that over a narrow range of u that

$$\tau_e(Z_m) = au(Z_m)^{P_u(Z_m)} \tag{4.19}$$

where a is a constant. The second guess value of $u(Z_m)$, $u^2_{\ m}$, is now determined by assuming the difference between the measured effective optical depth, $\tau_e(Z_m)$, and the estimated value, $\tau_e^{\ 1}(Z_m)$, is due strictly to an error in the first guess value of path water vapor $u^1(Z_m)$. The value of $u^2(Z_m)$ is given, therefore, by

$$u^2(Z_m) = u^1(Z_m)(\tau_e(Z_m)/\tau_e^{\,1}(Z_m))^{1/P_u(Z_m)} \tag{4.20}$$

and the second guess value of $\underset{\sim}{q}$ may be found by Equation 4.18 where $\underset{\sim}{u} = \underset{\sim}{u}^2$. The value of $P_u(Z_m)$ is determined from the tabulated form of Figure 4.7 interpolated for the appropriate values of tangent height and absorber amount. For the previous example of u(20km) = 0.36g/cm^{-2} the value of P_u(20km) is found to be 0.56.

A new estimated value of the effective optical depth, $\tau_e^{\,2}(Z_m)$, is then determined again using Equations 4.10 and 2.7 and is found to be in better overall agreement with the measured value than was the first guess, $\tau_e^{\,1}(Z_m)$. By repeating this power law iteration a sufficient number of times very nearly any degree of numerical agreement between the measured set of $\tau_e(Z_m)$ and the estimated set of effective water vapor optical depths is possible. The general form of the jth estimate for the path water vapor amount is given by

$$u^j(Z_m) = u^{j-1}(Z_m)(\tau_e(Z_m)/\tau_e^{\,j-1}(Z_m))^{1/P_u(Z_m)} \tag{4.21}$$

where the ratio $\tau_e(Z_m)/\tau_e^{\,j-1}(Z_m)$ approaches 1 as j increases.

It is in general found that two iterations are sufficient to bring the mean disagreement between the estimated and the measured effective water vapor optical depths to less than 0.5% and three iterations bring the mean disagreement to less than 0.2%. In Figure 4.8, a comparison of $\underset{\sim}{q}^1$, $\underset{\sim}{q}^2$, and $\underset{\sim}{q}^3$ is shown for a set of SAGE II

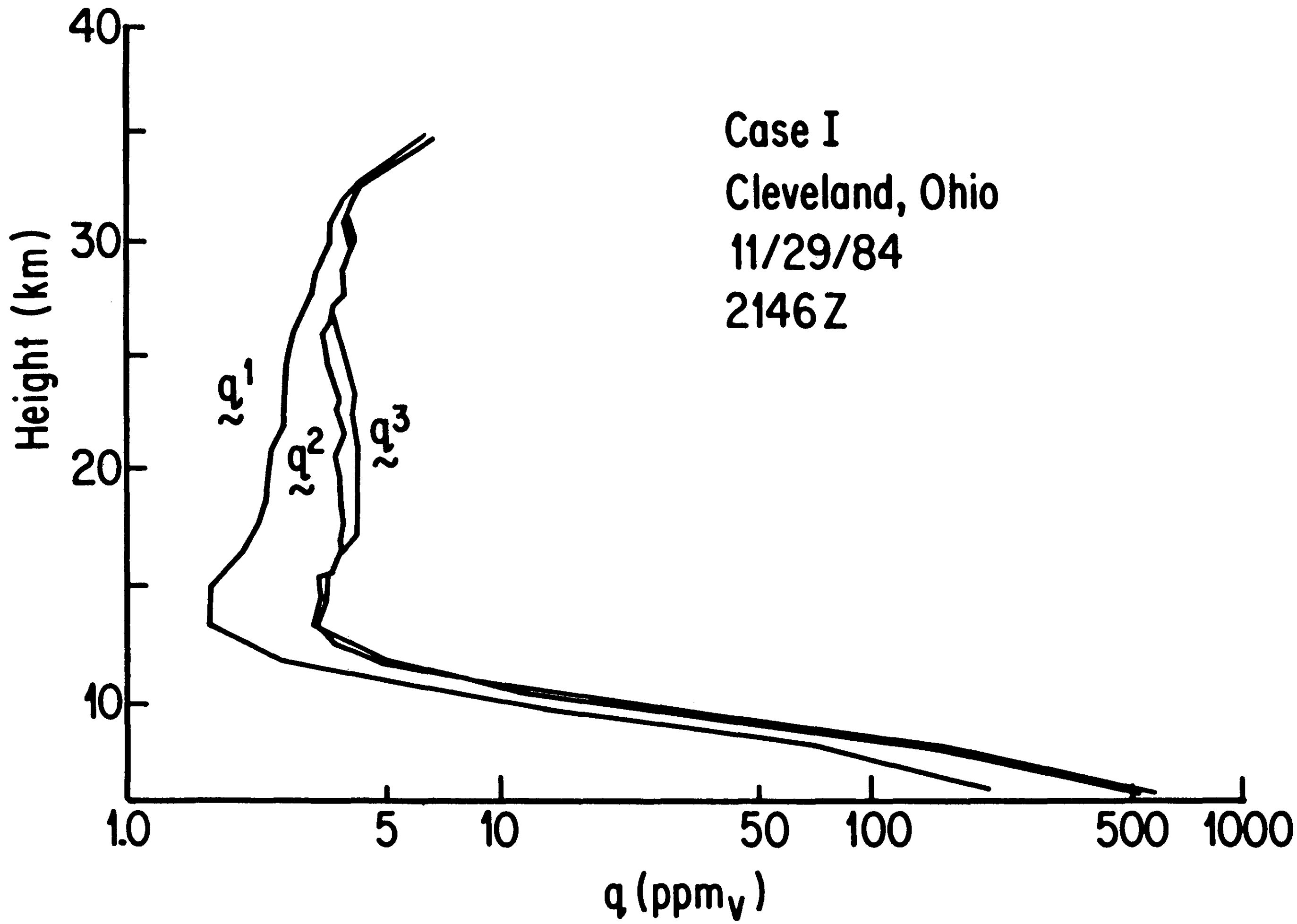

Figure 4.8. Iterative solutions to the case I set of measured effective optical depths for Cleveland, Ohio

measurements taken over Cleveland, Ohio on 11/29/84 at 2146Z and it can be seen that there is a rapid convergence to a steady solution. The solution $\tilde{q}^4$ is not plotted on Figure 4.8 simply because it could not be distinguished from $\tilde{q}^3$.

One of the favorable aspects of the iterative technique is the fact that neither the first guess values for path water vapor amount, $\tilde{u}^1$, or the values of $P_u(Z_m)$ play a decisive role in the final solution determined for the water vapor mixing ratio distribution. It might be expected that since both $\tilde{u}^1$ and $P_u(Z_m)$ were determined for particular atmospheric conditions that some biasing in the final solution might result if the true atmospheric conditions were significantly different. But the solution toward which the iterative solutions converge is unique and the process by which the progressive estimates for $\tilde{q}$ are determined only serves to govern the rapidity with which that solution is approached. The reason that the power law iteration was used is not because it adds any information to the reduction process but because it very rapidly converges toward the unique solution. In fact even under extreme atmospheric conditions, the progressive mixing ratio estimates rapidly converge.

Discussion

A method for the determination of the vertical water vapor distribution has now been developed. Given a set of limb transmittances as a function of path tangent height, there are factors which contribute to the uncertainty in the determined water vapor profiles.

Among the more important of these factors are horizontal homogeneity, random measurement errors, errors in the assumed atmospheric temperature distribution, the specification of α'_v, and the effect of any failure in the correlated absorption coefficient assumption.

By examining Equation 4.10 it can be seen that there is an implicit assumption that the atmosphere is horizontally homogeneous since S'_{0n}, α'_{vn} and q_n are considered to be independent of the horizontal location within the layer. Since the water vapor density decreases rapidly with height, an assumption that the atmosphere is horizontally homogeneous is not significant for the full depth of the atmosphere. It is instead found for a particular paths that a large fraction of the attenuation occurs within a relatively small vertical distance of the tangent height and horizontal homogeneity need be maintained only below this height. The fraction of optical depth originating below some height may be defined by

$$g_\tau(1) = 1. - \ln[T_1(u(Z_m))]/\ln[T_0(u(Z_m))] \tag{4.22}$$

where $T_1(u(Z_m))$ is given by

$$T_1(u(Z_m)) = \int_0^1 \exp[-\sum_{n=m+1}^{N} S'_{0n}h_n(g)\rho_n S_n(Z_m)]dg. \tag{4.23}$$

The value of $g_\tau(1)$ for standard atmospheric conditions and tangent height paths of 5, 15 and 25km is given in Figure 4.9. On average it is found that about 75% of the attenuation originates within 5km of the tangent height. This is very nearly the same thickness as was required for the ground based radiometer but due to path geometric

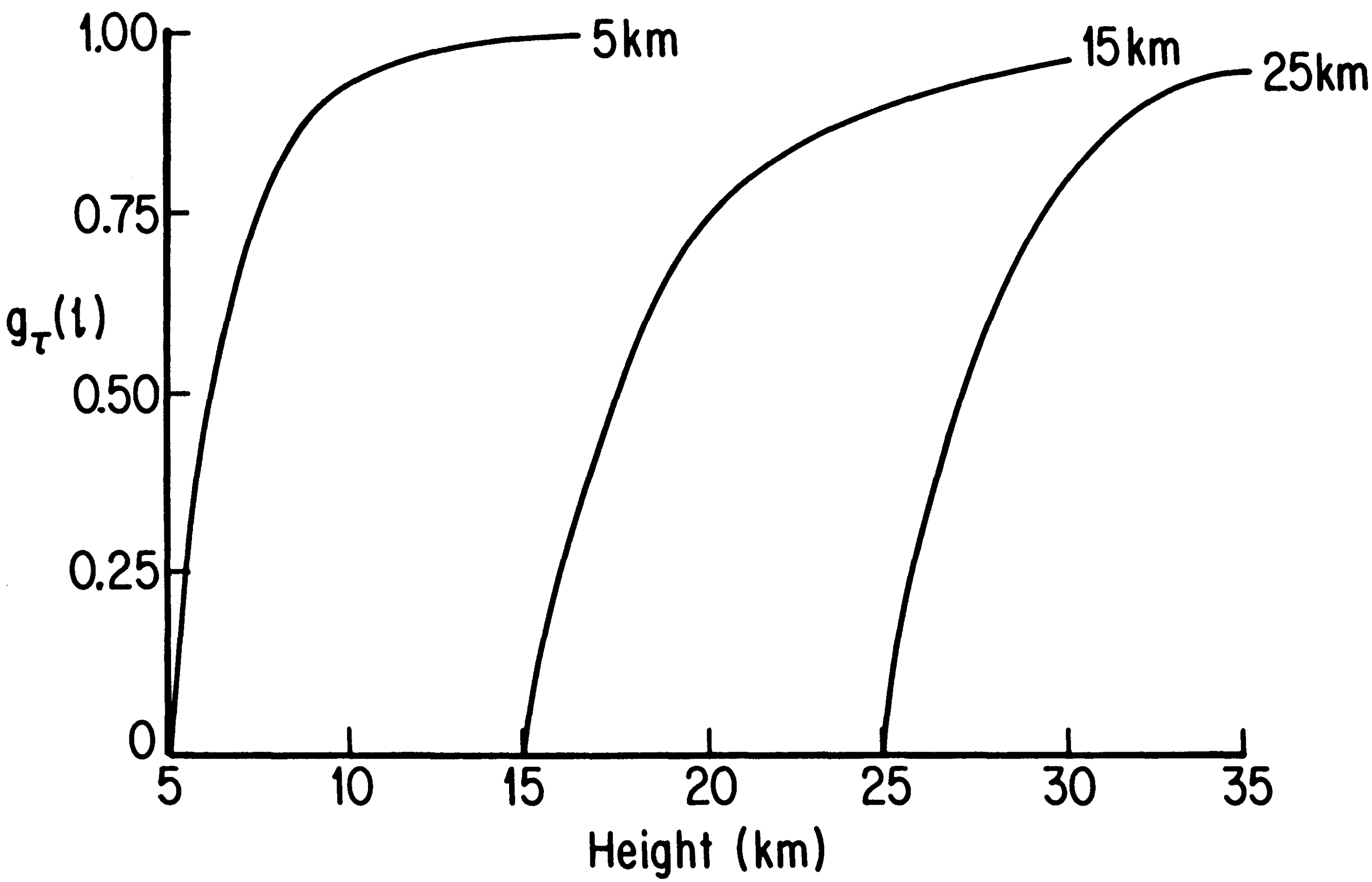

Figure 4.9. The function $g_\tau(1)$ as a function of height for selected tangent heights and standard atmospheric conditions

differences, a 5km height now implies a horizontal homogeneity requirement of about 500km. Below the tropopause assuming that the atmosphere is horizontally homogeneous on the scale of 500km is frequently not valid and it will often lead to a degradation of solution. Within the stratosphere, this range presents less of a problem as the stratosphere is more homogeneous than the troposphere (Ellsaesser, 1983). However, it still represents a significant difficulty in the interpretation of an estimated vertical water vapor distribution. Horizontal inhomogeneities within a particular layer cause the estimates of water vapor mixing ratios in layers within 3 to 4km of that layer to be in error.

The magnification of random errors in the effective optical depth to errors in the path water vapor has been discussed, and this error is not passed on unaffected to the vertical water vapor distribution estimate. It has been shown (Frieden, 1983) that for a least squares solution for $\underset{\sim}{q}$ as given in Equation 4.18, a covariance matrix, C, may be expressed as

$$C = \sigma_u^{\,2}(D^T D)^{-1} \tag{4.24}$$

where $\sigma_u^{\,2}$ is the variance of the uncertainty in the elements of the vector $\underset{\sim}{u}$. The fractional uncertainty in the solution element q_n is given by

$$\varepsilon_q = 2C^{\frac{1}{2}}_{nn}/q_n \tag{4.25}$$

and the normalized correlation between solution element q_n and q_m is given by

$$\rho(m,n) = C_{mn}/(C_{mm}C_{nn})^{\frac{1}{2}} \tag{4.26}$$

The covariance matrix was derived for additive noise of zero mean and for the case that the solution vector, $\underset{\sim}{q}$, is an unbiased estimator of the true solution. If σ_u^2 is not constant for each element of the path water vapor vector, $\underset{\sim}{u}$, then the covariance matrix is given by

$$C = (D^TD)^{-1}D^TVD(D^TD)^{-1} \tag{4.27}$$

where V is a diagonal matrix with elements of $\sigma_{u\,n}^2$ or the variance of the noise in each element of the path water vapor vector. In Figure 4.10 is shown a plot of ε_q for standard atmospheric conditions and a realistic value of σ_{un} which is 10% of the limb path water vapor amount u_n. The most important inference that can be made from this figure is that errors in the path water vapor amount are magnified by about a factor of 2.5 in mixing ratio estimates.

The correlation between the various layers seems to be fairly stationary through the full atmosphere. If Equation 4.26 is rewritten as

$$\rho(n,n+\Delta n) = \rho(n,m) \tag{4.28}$$

then it is found that the correlation is nearly independent of n and mainly dependent on the separation Δn. In Table 4.1 is shown the mean behavior of the correlation as a function of Δn. The value of ρ is negative and decreases rapidly as $|\Delta n|$ becomes large. The vertical resolution that this implies is on the order of 1 to 2km depending upon the size of the feature to be resolved.

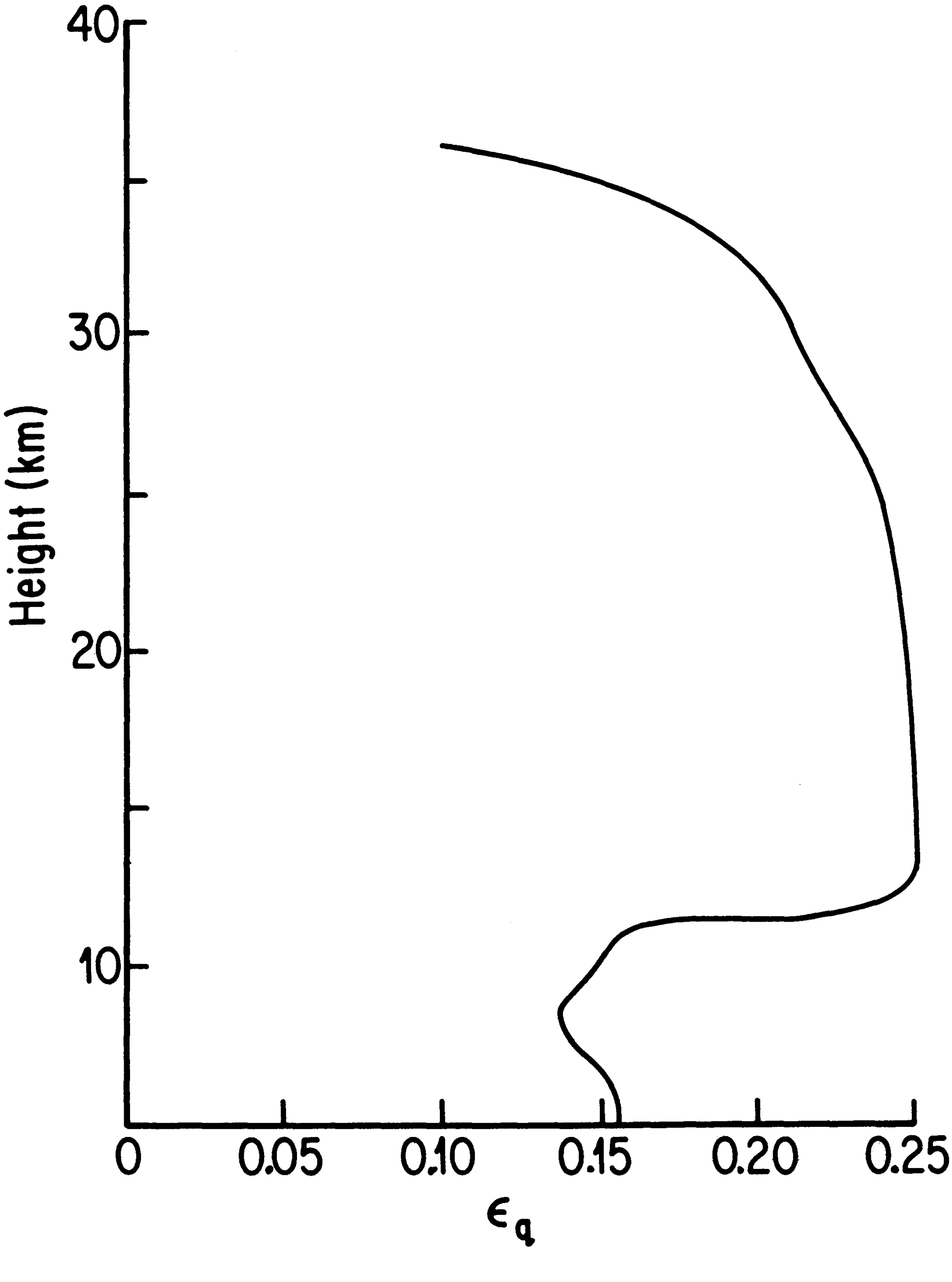

Figure 4.10. The fractional uncertainty, ε_q, in the estimated vertical water vapor distribution resulting from random measurement errors that have a standard deviation of 10% in $u(Z_T)$ at any given height

Table 4.1. The normalized correlation coefficient between the solution elements q_n and $q_{n+\Delta n}$ as a function of the separation between the layers n and n + Δn

$\|\Delta n\|$	$\rho(n,n+\Delta n)$
0	1.00
1	-0.32
2	-0.11
3	-0.03
4	-0.01

The reduction of limb transmission data to water vapor mixing ratio profiles is based upon the assumption that the thermal structure of the atmosphere is known. Since the temperature profile is usually determined by remote sensing techniques, there is a resulting uncertainty in the inferred temperature profile and ultimately in the inferred water vapor distribution. In Figure 4.11 is shown the error in the estimated water vapor mixing ratio at a particular height given a locally systematic error in the vertical temperature profile of ΔT. A typical 95% confidence limit in a remotely determined temperature profile is about $\pm 5°K$ and that corresponds to an uncertainty in q_n of about $\pm 4\%$. The magnitude of this uncertainty is relatively independent of height varying over the full atmosphere from $\pm 3\%$ to $\pm 5\%$.

The specification of α'_v is a source of biasing in the inference of vertical water vapor distributions just as in the ground based radiometer problem where the specification of α'_L was a source of biasing. The problem in this case, is in fact the problem in specifying α'_L which is incorporated into the determination of α'_v. As in the ground based problem, the uncertainty in α'_L is about 10% but the importance of it in the determination of α'_v decreases with increasing altitude so that uncertainty in α'_L has progressively less effect on the uncertainty in the water vapor mixing ratio. In Figure 4.12 the fractional uncertainty in the water vapor mixing ratio ε_q, due to the uncertainty in α'_v as a function of height is shown for standard atmospheric conditions. The value of ε_q represents a 95% confidence limit.

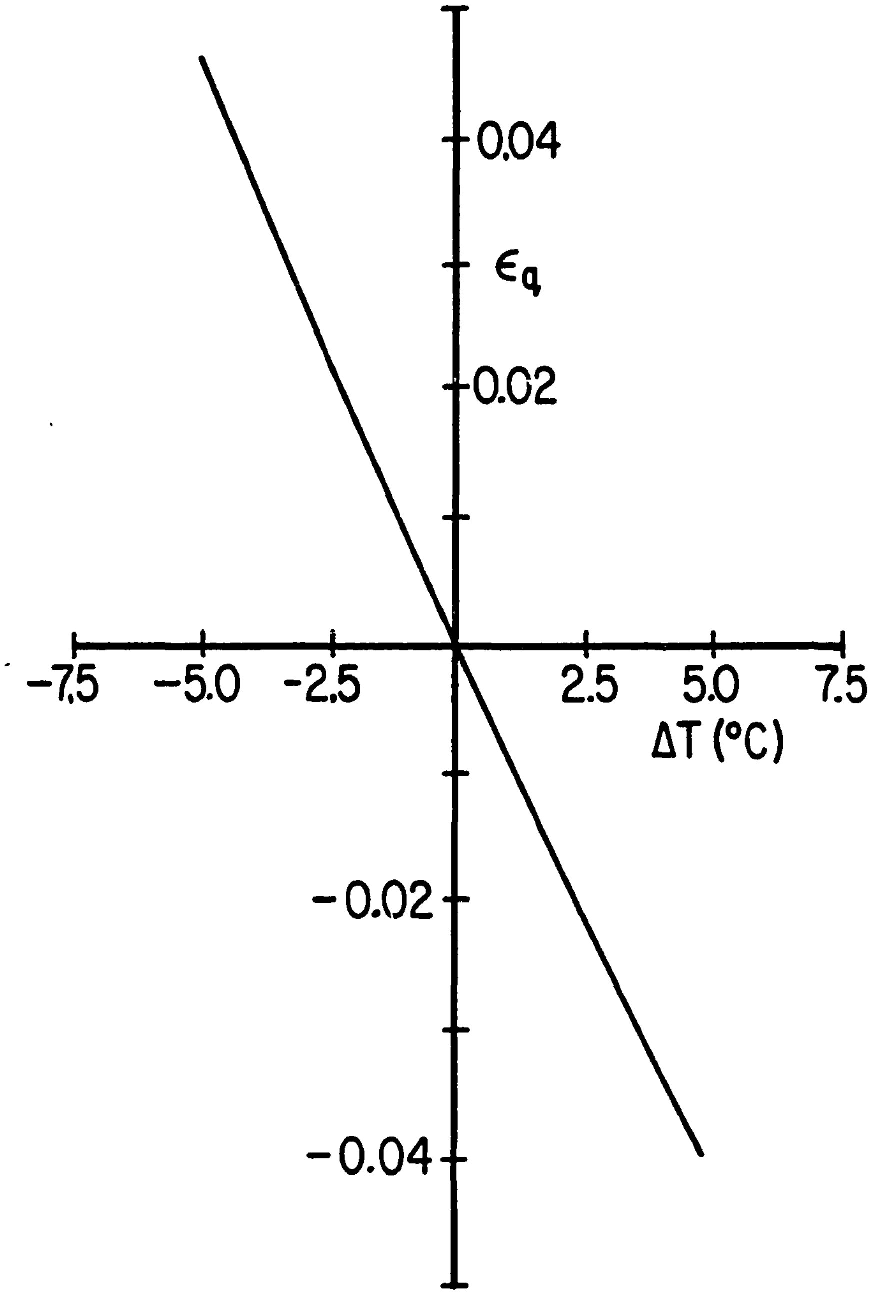

Figure 4.11. The fractional uncertainty, ε_q, in the estimated vertical water vapor distribution resulting from a locally systematic error in the estimated vertical temperature field. -- ΔT is positive when the estimated temperature is too high.

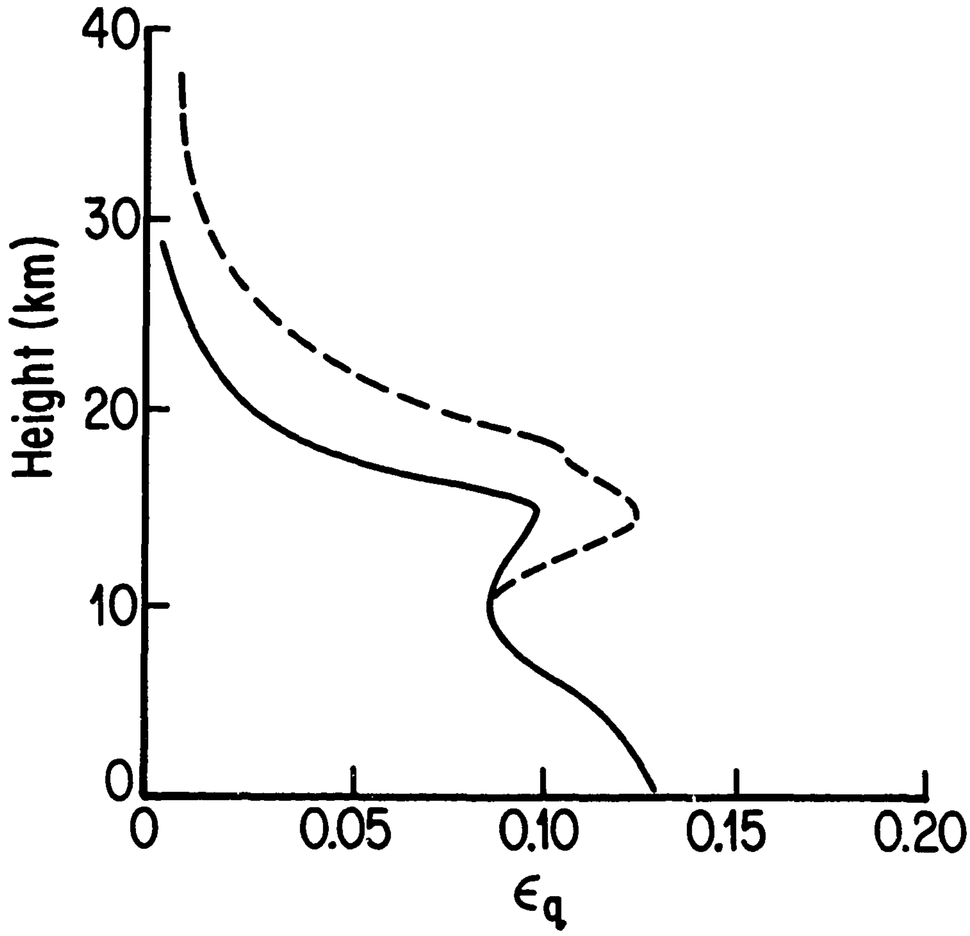

Figure 4.12. The fractional uncertainty, ε_q, in the estimated vertical water vapor distribution resulting from the uncertainty in the specification of α'_v (solid) and from all significant sources of model urcertainty (dashed)

Also in Figure 4.12 is shown the estimated maximum likely error associated with the model. This error includes the effect of the problem in the specification of α'_L and in specifying a single value of α'_v which forces the equivalent optical depth predicted by Equation 4.10 to be the same as that predicted by Equation 4.4.

It can be seen that the magnitude of the possible biasing due to the specification of α'_v is at worst comparable to and in general much less than the effect of realistic measurement errors shown in Figure 4.10. Based upon a comparison of Figures 4.10 and 4.12 it is reasonable to assert that within the stratosphere the model is effectively not biased.

The final possible source of error is in any failure in the correlated absorption coefficient assumption. The value of the RMS spreading of absorption coefficient rank, G, is shown in Figures 3.9a and 3.9b as a function height. Using a two layer model of the atmosphere and the transmission model of Equation 3.66 it was found that errors in the effective optical depth calculation for stratospheric conditions would be expected to be less than 1% throughout the stratosphere and less than 0.1% above 20km due to the above assumption. Therefore the uncertainty in the mixing ratio determination due to the assumption of the independence of the absorption coefficient rank on temperature and pressure is negligible.

Three sets of water vapor effective optical depth measurements have been acquired courtesy of NASA-Langley for 11/29/84 to 11/30/84 over Laramie, Wyoming and Cleveland, Ohio. These measurements, made as a function of tangent height in increments of 1km were made for a temperature and pressure distribution measured locally by radiosonde. Along with the measurements, estimates of the uncertainty in the effective optical depth were given as were solutions to the three data sets achieved by an independent inversion technique. The technique which NASA-Langley employed was the emissivity curve of growth method described by Weinreb and Neuendorffer (1973).

The results of the data reductions by the iterative method developed in this chapter are shown in Figures 4.13a, 4.13b and 4.13c along with the results from the emissivity curve of growth method as calculated by NASA (Chu, personal communication). There is a good overall agreement between the two models as the basic trends of the estimated water vapor profiles by both techniques are quite similar. Below 16km the two modes of estimation yield results that exhibit no systematic difference, however, above 16km the iterative reduction method yields water vapor mixing ratios that average about 10% less than those determined by the other method. This systematic disagreement indicates that either one or both of the techniques is moderately biased. The RMS difference between the two sets of solutions is about 8%.

In Figure 4.14 the uncertainty in q_n, ε_q, due to random measurement errors as determined by Equations 4.27 and 4.25 are shown for the three example cases. The results are somewhat disappointing in that the 95% confidence limits average to be 30% of the value of

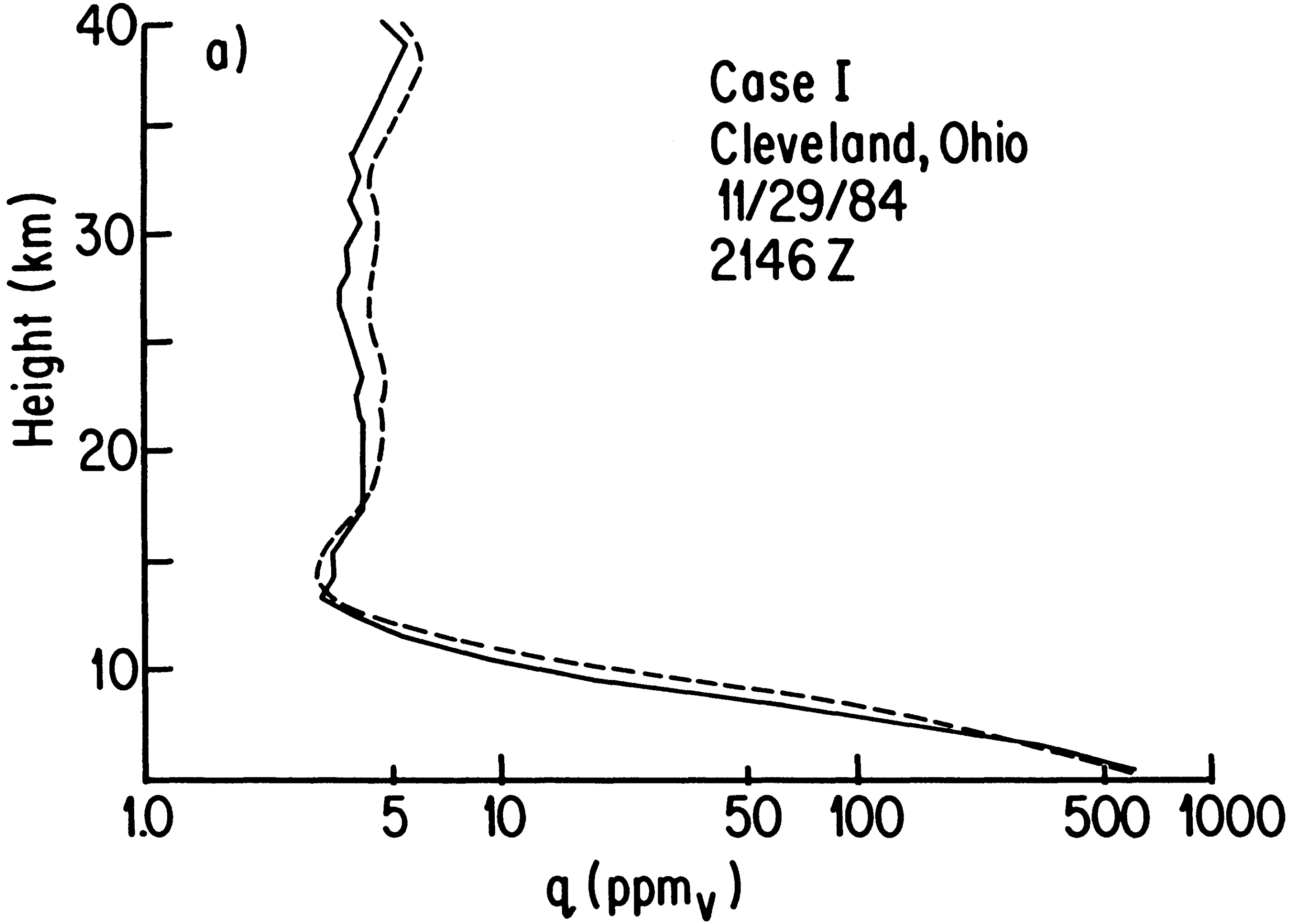

Figure 4.13a. Case I solution $\underset{\sim}{q}^3$ (solid) and the NASA-Langley solution (dashed)

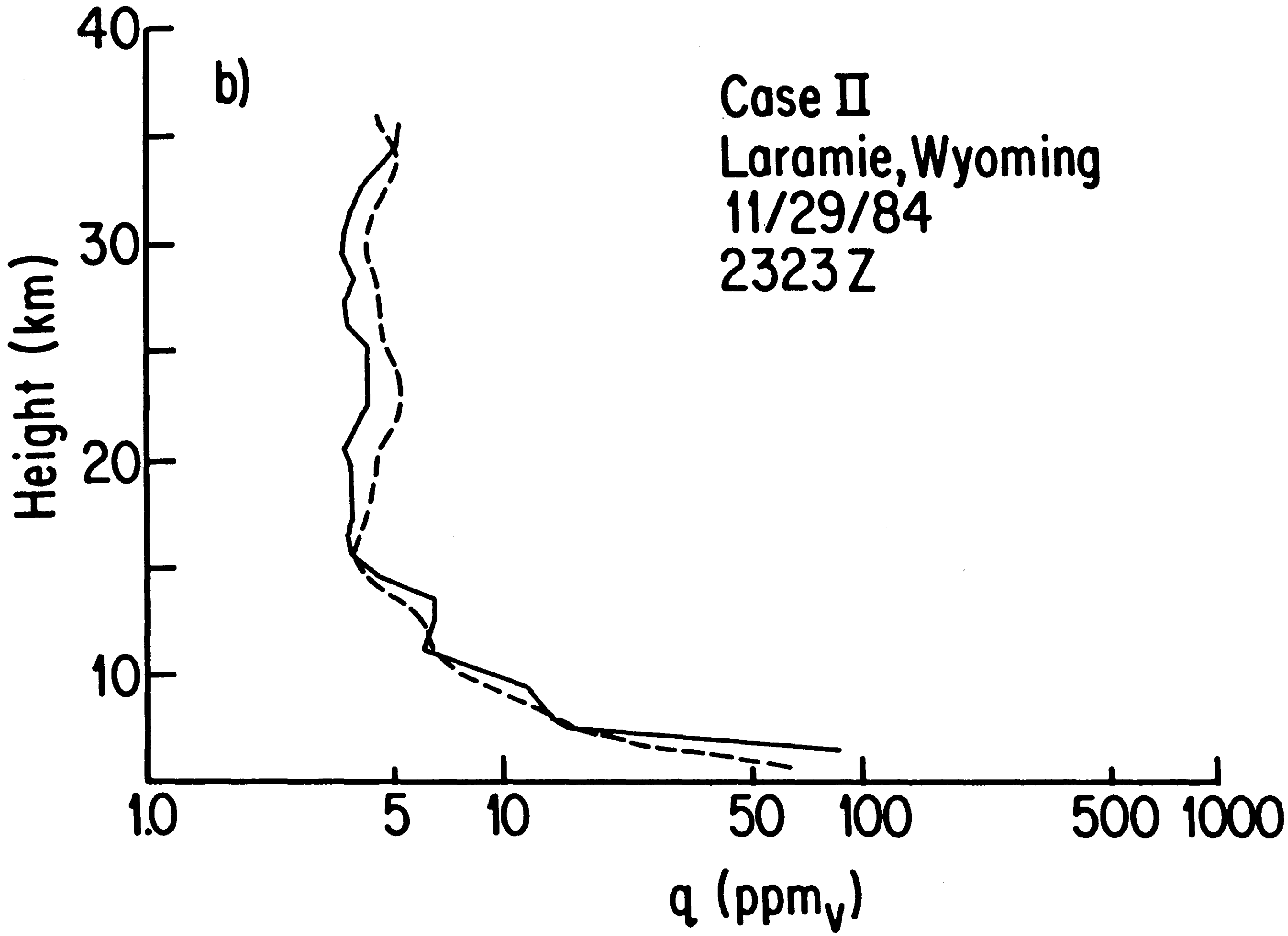

Figure 4.13b. Case II solution $\underset{\sim}{q}^3$ (solid) and the NASA-Langley solution (dashed)

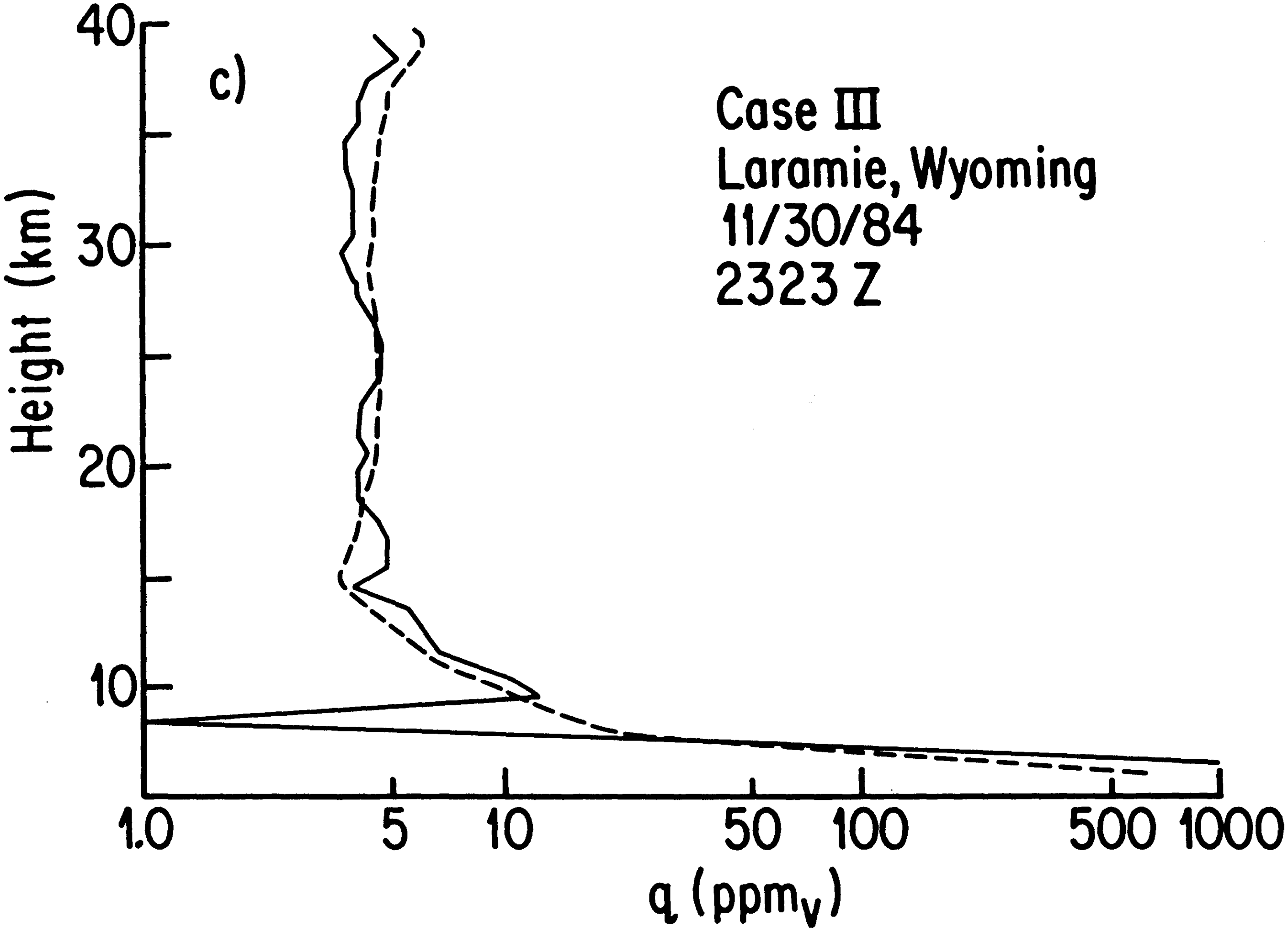

Figure 4.13c. Case III solution $\underset{\sim}{q}^3$ (solid) and the NASA-Langley solution (dashed)

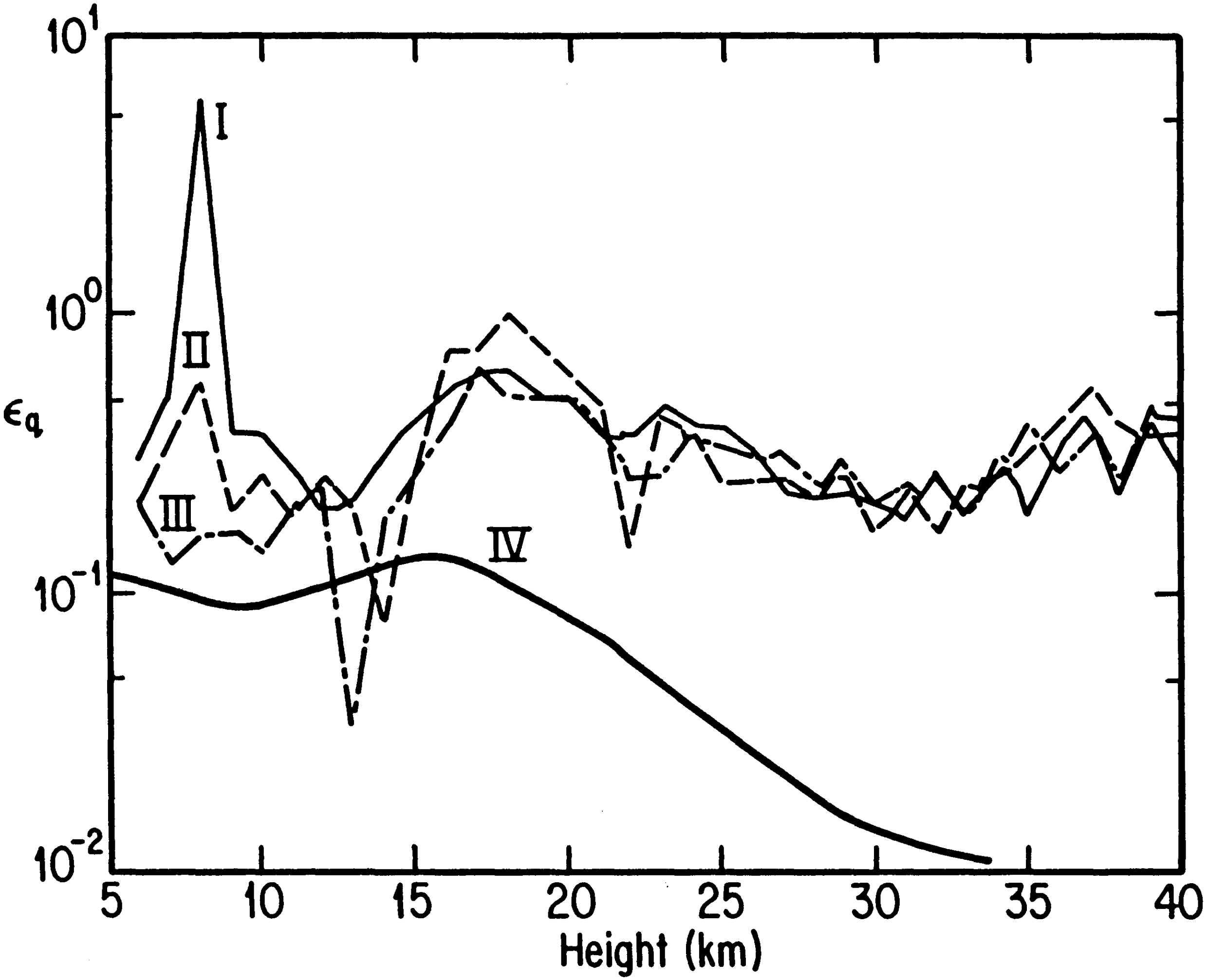

Figure 4.14. The fractional uncertainty, ε_q, due to random measurement errors as estimated by NASA-Langley for cases I, II, and III. -- Curve IV is the estimated model uncertainty as shown previously in Figure 4.12.

the mixing ratio and frequently are significantly larger. This is due mainly to problems in removing the effect of non-water vapor attenuations from the effective optical depth. Below 20km the problem is mainly in the removal of attenuation by aerosols; above 20km the main problem is the unanticipated presence of ozone absorption where its spectral absorptive properties are poorly known. As the RMS and systematic disagreements between the two techniques are less than 10%, it is apparent that, for the level of uncertainty due strictly to measurement uncertainty, the disagreement between the two approaches is unimportant.

The iterative method gives results that have a greater structure in the water vapor vertical distribution than does the method used by NASA. This is a result of the fact that while the reduction technique developed herein is unconstrained, the curve-of-growth method is usually constrained to exhibit a priori characteristics such as smoothness. This is perhaps best illustrated in case 3 at the 8km level, where examination of the transmission data seem to imply the presence of a very dry layer. The iterative technique indeed finds a very dry layer at that height but the curve-of-growth method does not indicate any significant departure of the water vapor mixing ratio at that height from the amount in adjacent layers. In many ways this lack of constraint is preferrable as it is usually desired that a reduction produce the structure implied by the measurements. On the other hand, the lack of constraint also means that it is possible that a feature may be created or exaggerated by the presence of measurement error. In the dry layer discussed above, it can be shown that the 95% confidence limit associated with the estimated measurement error at that height is about $\pm$600%. This indicates that it is likely that the extent of dryness in the layer is exaggerated by the iterative method; but this level of uncertainty still supports the presence of a substantially drier layer at this height than indicated by the curve-of-growth solution. It can be seen, however, that because of measurement uncertainties, many of the less pronounced features shown in Figures 4.13a, 4.13b, and 4.13c are not considered to be physically significant. A feature of the iterative model is that the decision of which features to give credence is left to the investigator and not to the computer.

In this chapter a transmission model suitable to stratospheric conditions and limb path geometry has been developed. The model has been incorporated into an iterative reduction technique for the determination of vertical water vapor distributions given effective water vapor optical depth as a function of the limb path tangent height.

The vertical resolution of the model is good to 1 to 2km but horizontal atmospheric homogeneity is assumed for 500km horizontal distances about the tangent point. The maximum likely errors to be associated with the model itself are 10 to 15% below 20km and decrease rapidly above 20km. Comparisons with an independent reduction technique show about a 10% systematic difference above 16km but, since the uncertainty due to the estimated measurement errors is about 30%, the difference is of little importance. The agreement between the two solution sets tends to validate each model on the 10 to 20% level.

Overall, the Stieltjes transmission model and the associated iterative reduction technique seem to fulfill the requirement of computational efficiency and accuracy. While the level of measurement uncertainty associated with the SAGE II data perhaps makes even this level of computational sophistication unjustified, the fundamental approach has been shown to yield reasonable results and to be a potentially powerful tool in remote sensing.

CHAPTER 5

SUMMARY AND CONCLUSIONS

A new technique for calculations transmission along inhomogeneous paths in spectral intervals dominated by molecular line absorption has been developed for remote sensing applications. It has been incorporated into a reduction technique that is numerically stable and which produces a unique solution to a set of measured effective optical depths. The method, as was required, has been shown to be computationally efficient and accurate.

The technique, which is called the Stieltjes method, has previously been applied only in an empirical fashion to flux divergence calculations which are substantially less sensitive calculations than the ones addressed in chapters III and IV. The first explicit derivation and formulization of the Stieltjes method has been presented. The first formal test of the correlated absorption coefficient assumption showed that the correlation between different heights in the atmosphere is quite low and this would imply that the model is invalid. From the derivation of the method, it was shown that the actual assumption made in the model is that the rank of the absorption coefficient at any wavenumber is independent of temperature and pressure. This assumption was shown to be reasonably valid as it was shown to cause errors no greater than 3% in precipitable water estimates and negligible errors in water vapor mixing ratio estimates for the stratosphere.

The numerical integration of the Stieltjes transmission equation can easily be performed with high precision for homogeneous and inhomogeneous atmospheres. To simplify the computational problem, model forms of the distribution of absorption coefficient were derived and a new technique for the determination of the model's significant parameters was introduced. While there was good overall agreement between the model g(k) and the true g(k), there was some degree of difference which found expression in the uncertainty in the specification of both α'_L and α'_V. The estimated maximum error in precipitable water estimates resulting from the use of a model form of g(k) is 8% while in the determination of the water vapor mixing ratio distribution, it was found to be between 0 and 15% depending on height. The maximum error estimated to result from model assumptions was shown to be no worse than comparable, and in general much less than, the uncertainty in the solutions introduced by measurement error. Overall, the technique is nicely capable of solving the two problems to which it has been applied.

For the current applications, there is little justification in further numerical intricacies. However, if the measurement errors are reduced or the method is applied to a different spectral applied to a different spectral interval, there are some further refinements that may be warranted. If the computational facilities allow, the creation and use of cumulative absorption coefficient distributions by the random-frequency-selection method would eliminate or greatly reduce the single largest source of error associated with the method. The other source of error associated with the model is the correlated absorption coefficient assumption which is a significant source of error only in the lower atmosphere. A band transmission function independent of any correlation assumption and for an inhomogeneous path may be written as

$$T_b(u) = \int_0^\infty \int_0^\infty \int_0^\infty \cdots \int_0^\infty \exp\left[-\sum_{n=1}^{N} k_n u_n\right] p(k_1, k_2, k_3 \ldots k_N) \, dk_1 dk_2 \ldots dk_N \tag{5.1}$$

where $p(k_1, k_2, k_3, \ldots k_N)$ is the joint distribution of absorption coefficient within layers 1 through N. The joint distribution of absorption coefficient may be written $p(\underset{\sim}{k})$ and $p(k_1, k_2, k_3, \ldots, k_N)$ $dk_1 dk_2 dk_3 \ldots dk_N$ is the probability that the absorption coefficient in layer 1 is between k_1 and $k_1 + dk_1$ and in layer 2 it is between k_2 and $k_2 + dk_2$ and so on through layer N. The correlated absorption coefficient assumption presumes that $p(\underset{\sim}{k})$ may be written as

$$p(\underset{\sim}{k}) = p(k_1)\delta(k_2 - f_2(k_1))\delta(k_3 - f_3(k)) \ldots \delta(k_N - f_N(k)), \tag{5.2}$$

where the function f_n is single valued. By substituting Equation 5.2 into Equation 5.1, the Stieltjes transmission equation as given in Equation 2.23 may be produced. It has been shown that the assumption of rank maintenance that underlies the joint distribution of absorption coefficient of Equation 5.2 is not completely valid.

It is possible that further study will yield at least an empirical coorection to $p(\underset{\sim}{k})$ that allows realistic variations of the rank of the absorption coefficient at a given wavenumber with height.

The main strength of the Stieltjes method is that it maintains many of the characteristics of a line-by-line transmission calculation. This allows a low cost means of simulating other more empirical transmission or inversion techniques in order to rigorously test their model assumptions and their overall applicability. For instance, the emissivity curve of growth method is derived for a monochromatic measurement and applied to fairly broad spectral interval measurement. If it's performance must be tested by line-by-line calculations then the test must be limited in scope but use of the Stieltjes method would allow thorough testing of the method even given limited computing facilities.

LIST OF REFERENCES

Box, M., 1981: Finite Bandwidth and Scattered Light Effects on the Radiometric Determination of Atmospheric Turbidity and the Dolar Constant. Appl. Opt., 20, 2215-2219.

Chandrasekhar, S., 1960: Radiative Transfer. Dover Publications, Inc., 393 pp.

Chou, S., and D. Atlas, 1982: Satellite Estimates of Ocean-Air Heat Fluxes During Cold Air Outbreaks. Mon, Wea. Rev., 110, 1434-1450.

Chu, W., 1983: Calculations of Atmospheric Refraction for Spacecraft Remote-Sensing Applications. Appl. Opt., 22, 721-725.

Clough, S., F. Kneizys, L. Rothman, and W. Gallery, 1981: Atmospheric Spectral Transmission and Radiance: FASCOD1B. SPIE, 277, 152-166.

Domoto, G. A., 1974: Frequency Integration for Radiative Transfer Problems Involving Homogeneous Non-Gray Gases: The Inverse Transmission Function. J. Quant. Spectrosc. Radiat. Transfer, 14, 935-942.

Ellsaesser, H., 1983: Stratospheric Water Vapor. J. Geophys, Res., 88, 3897-3906.

Frieden, B. R., 1983: Probability, Statistical Optics, and Data Testing: A Problem Solving Approach. Springer-Verlag, 404 pp.

Gille, J. and R. Ellingson, 1968: Correction of Random Exponential Band Transmissions for Doppler Effects. Appl. Opt., 7, 471-474.

Godson, W. L., 1955a: The Computation of Infrared Transmission by Atmospheric Water Vapor. J. Meteor., 12, 272-284.

Godson, W. L., 1955b: The Computation of Infrared Transmission by Atmospheric Water Vapor, Part II. J. Meteor., 12, 533-535.

Goody, R., 1964: Atmospheric Radiation, Theoretical Basis. Clarendon Press, 436 pp.

Goody R., 1952: A Statistical Model for Water Vapor Absorption. Quart. J. R. Meteor. Soc., 78, 165-169.

Gradshteyn, I. and I. Ryzhik, 1980: Table of Integrals, Series, and Products. Academic Press, 1160 pp.

Hansen, J., G. Russell, D. Rind, P. Stone, A. Lacis, S. Lebedeff, R. Ruedy, and L. Travis, 1983: Efficient Three-Dimensional Global Models for Climate Studies: Models I and II. Mon. Wea. Rev., 111, 609-662.

Heicklen, L., 1976: Atmospheric Chemistry. Academic Press, 406 pp.

Kondrat'yev, K. Ya., 1969: Radiation in the Atmosphere. Academic Press, 912 pp.

Kreyszig, E., 1979: Advanced Engineering Mathematics. John Wiley and Sons, 939 pp.

Lacis, A. A., and J. E. Hansen, 1979: A Parameterization for the Absorption of Solar Radiation in the Earth's Atmosphere. J. Atmos. Sci., 31, 118-133.

Liou, K., 1974: On the Radiative Properties of Cirrus in the Window Region and Their Influence on Remote Sensing of the Atmosphere. J. Atmos. Sci., 31, 522-532.

Malkmus, W., 1967: Random Lorentz Band Model with Exponential-Tailed S^{-1} Line Intensity Distribution Function. J. Opt. Sci. Amer., 51, 323-329.

Mankin, W. G., 1979: Fourier Transform Method for Calculating the Transmittance of Inhomogeneous Atmospheres. Appl. Opt., 18, 3426-3433.

McClatchey, R., W. Benedict, S. Clough, D. Furch, R. Calfis, K. Fox, L. Rothman, and J. Garing, 1973: AFCRL Atmospheric Absorption Line Parameters Compilation. Environ. Res. Pop. No. 434, AFCRL-TR-0096, 80 pp.

Rodgers, C. D., and C. D. Walshaw, 1966: The Computation of Infrared Cooling Rate in Planetary Atmospheres. Quart. J. R. Meteor; Soc., 92, 67-92.

Russell, J., J. Gille, E. Remsberg, L. Gordley, P. Bailey, H. Fischer, A. Girard, S. R. Drayson, W. Evans, and J. Harris, 1984: Validation of Water Vapor Results Measured by the Limb Infrared Monitor of the Stratosphere Experiment on NIMBUS 7. J. Geophys. Res., 89, 5115-5124.

Spencer-Gregory, H., and E. Rourke, 1957: Hygrometry. Pitman Publishing Corp., 254 pp.

Staelin, D., K. Kunzi, R. Pettyjohn, R. Poon, R. Wilcox, and J. Waters, 1976: Remote Sensing of Atmospheric Water Vapor and Liquid Water With the NIMBUS 5 Microwave Spectrometer. J. Appl. Meteor., 15, 1204-1214.

Stark, P., 1970: Introduction to Numerical Methods. MacMillan Publishing Co., Inc., 334 pp.

Taylor, A. and W. Mann, 1972: Advanced Calculus. John Wiley and Sons, 7?4 pp.

Thomason, L. W., B. M. Herman, R. M. Scotland, and J. A. Reagan, 1982: Extraterrestrial Solar Flux Measurement Limitations due to a Beer's Law Assumption and Uncertainty in Local Time. Appl. Opt., 21, 1191-1195.

Twomey, S., 1977: Introduction to the Mathematics of Inversion in Remote Sensing and Indirect Measurements. Elsevier Scientific Publishing Company, 243 pp.

U.S. Standard Atmosphere, 1976: NOAA-SIT 76-1562, U.S. Government Printing Office. 227 pp.

Wang, W., and P. B. Ryan, 1983: Overlapping Effect of Atmospheric H_2O, CO_2, and O_3 on the CO_2 Radiative Effect. Tellus, 358, 81-91.

Weinreb, M., and A. Neuendorffer, 1973: Method to Apply Homogeneous-Path Transmittance Models to Inhomogeneous Atmospheres. J. Atmos. Sci., 30, 662-666.